



• 5TH INTERNATIONAL
TSUNAMI FIELD
SYMPOSIUM



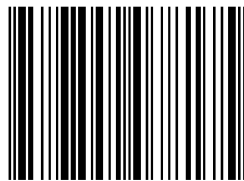
Field Trip Guide

EDITORS: *PEDRO J.M. COSTA, CÉSAR ANDRADE*



SEPTEMBER 2017

ISBN 978-989-20-7817-5



9 789892 078175

5th International
Tsunami Field Symposium

Field Trip Guide

Editors:

P.J.M. Costa

C. Andrade

September 2017

Contents

| | |
|--|----|
| Foreword..... | 7 |
| Pre-Meeting Field Trip..... | 9 |
| Boulder deposits in the Lisbon region..... | 9 |
| Introduction and objectives | 9 |
| Wave and tidal regime along the Portuguese west coast..... | 10 |
| Stop 1 - Coxos coastal reach and boulders | 13 |
| Geology and geomorphology – an overview | 13 |
| Boulder deposits | 17 |
| Boulder sources and entrainment | 18 |
| Scalar, vectorial and morphological properties | 19 |
| Chronology and origin of boulder emplacement..... | 22 |
| Stop 2 - Guincho – Cascais coastal reach and boulders | 25 |
| Geology and geomorphology – an overview | 25 |
| Boulder deposits | 33 |
| Site # 1..... | 33 |
| Site # 2..... | 38 |
| Site # 3..... | 41 |
| Post-Meeting Field Trip..... | 43 |
| Tsunami deposits in the Algarve coast of Portugal..... | 43 |
| Introduction and objectives | 43 |
| Geology and geomorphology – an overview | 44 |
| Wave and tidal regime along the Algarve coast | 46 |
| Coastal evolution throughout the Holocene..... | 47 |
| STOP 1 – Boca do Rio..... | 49 |
| STOP 2 – Martinhal..... | 58 |
| STOP 3 – Salgados | 65 |
| STOP 4 – Ria Formosa..... | 79 |
| References..... | 89 |
| Annex 1 - Lithostratigraphy of the windward sector of the Algarve..... | 97 |

Foreword

Bem-vindos!

The 5th International Tsunami Field Symposium (ITFS) is part of a series of successful meetings that started in the early 2000's. Previous meetings have covered a wide spectrum of disciplines keeping pace with developments in the study of high-energy single events of coastal inundation and related geological imprints. These symposia have been set up with strong focus on field observation of tsunami deposits and geomorphological signatures.

The 5th ITFS edition follows this tradition and has been organized to provide a broad perspective on Portuguese tsunami (and storm) case-studies. Besides indoor presentations, two field visits offer an opportunity to discuss the significance of high-energy deposits in the central-western and Algarve Portuguese coasts.

We wish us all a successful meeting and thank all field trip participants for their valuable discussions. We strongly believe that exchanging ideas and experiences is the best way to further the science and to drive progress in tsunami research.

The Editors

Pre-Meeting Field Trip

Boulder deposits in the Lisbon region

September 3, 2017

M. A. Oliveira, C. Andrade

maoliveira@fc.ul.pt; candrade@fc.ul.pt

Departamento de Geologia, Instituto Dom Luiz, Faculdade de Ciências da Universidade de Lisboa, Bloco C6, 3 piso, Campo Grande, 1749-016 Lisboa, Portugal

Introduction and objectives

Extreme marine flooding of coastlines by storms and tsunamis may result in the deposition of sediment onshore. In coastal cells where sediment is abundant, the onshore record of high-energy events is frequently represented by sand-sheets, which are found inter-bedded with low-energy materials accumulating in active low-lying depositional systems (e.g. estuaries, lagoons). In contrast, the signature of such events along sand-starved rocky and cliffed coasts usually consists of coarse particles, ranging from a few centimeters up to several meters in length. The literature reports observations of entrainment, transport and re-deposition of large boulders landward of the shoreline during both contemporaneous tsunamis and storms, but it has proved difficult to distinguish boulders deposited by storms from those produced by tsunami when addressing pre-historical events.

The west coast of mainland Portugal is exposed to intense North Atlantic storms, such as the January 2014 *Christina* event that generated damage in excess of 6M Euros along the Portuguese coast. According to Diogo et al. (2014), maximum significant wave height and period recorded during this storm exceeded 9 m and 13 s, respectively (Tp max. of 27 s). Other high-intensity storms impacted the Portuguese coast throughout the 20th century, such as the 15 February 1941 cyclone or the 28 February 1978 storm that partially destroyed the west jetty of Sines port (Daveau et al., 1978; Freitas and Dias, 2013). Portuguese coast is also not far from the Azores-Gibraltar plate-boundary. The tectonic framework of this region has the potential to generate high magnitude earthquakes capable of significantly disrupting the ocean floor and generating destructive tsunamis, such as the AD 1755 event, which is known to have had an immense potential of destruction.

In the west coast of Portugal, which is to a large extent rocky and sand starved, little is known regarding deposits from extreme marine events. Scheffers and Kelletat (2005) have identified boulder deposits near Lisbon (Cascais-Guincho) that they attributed to tsunami inundations;

Oliveira et al. (2011) addressed boulder transport by storm waves north of Praia das Mações (close to Ericeira); Pereira et al. (2016) reported large boulder deposits atop coastal cliffs in the SW coast, north of Vila Nova de Milfontes, which they relate to the AD 1755 event. In the south-facing coast of the western Algarve, Costa et al. (2011) found marine boulders emplaced by the AD 1755 tsunami in two coastal lowlands that locally interrupt the continuity of coastal cliffs.

Pre-meeting field trip will address two coastal boulder deposits located in the vicinity of Lisbon, along the Guincho-Cascais and Coxos reaches. The geological and geomorphological settings, together with high tidal amplitude, high-energy wave regime and a record of tsunamigenic flooding in the 18th century, combine to increase the difficulty of unequivocally assigning these occurrences to tsunamis or storms. Additional drawbacks are the difficulty of reconstructing chronologies for boulders' emplacement and of inferring directional data on incoming waves (using both vectorial and scalar attributes of single particles, or morphology of accumulations), which could eventually shed some light on the driving processes. We are certain that many of these difficulties have been experienced by researchers working on the broad issue of relating coastal boulder accumulations with extreme events all around the world's coastlines. Indeed, the debate on sedimentary signatures left by both tsunamis and extreme storms in coastal boulder accumulations is still going on.

The main objective of this field visit is to provide a contribution to this "work in progress", by presenting and discussing, in the field, morphological, sedimentological and chronological data obtained so far on both the Guincho-Cascais and Coxos boulder accumulations.

To the best of our knowledge, Sheffers and Kelletat (2005) and Oliveira et al. (2011) are the only studies published so far on coastal boulder deposits in the vicinity of Lisbon. Boulder deposits, including those reported in Sheffers and Kelletat (2005) as well as the Coxos accumulations, were object of further examination in the frame of the M. A. Oliveira PhD dissertation project (here cited as Oliveira, 2011) and thesis (that awaits viva examination at the University of Lisbon, scheduled to late September), herein cited as Oliveira (2017). Most of the ground work and summary compiled in this guide relies upon the afore-mentioned work, with contributions from other researchers of the RG3 group of Instituto Dom Luiz – University of Lisbon, and of University of Coimbra. This has been supported by projects GETS (FCT PTDC/CTE-GEX/65948/2006) and NEAREST (EU – 037 110_2008-2010).

Wave and tidal regime along the Portuguese west coast

The western coast of Portugal is a mixed energy, wave dominated coast. Tides are semi-diurnal with average amplitude of 2.2 m and the average maximum water level related to astronomical tides is about 1.9 m above mean sea level (msl).

The contribution of storm surge to sea-surface rise is relatively small. Surge-related increase in sea-level is less than 0.5 m in the central western coast, although values in excess of 1 m have been recorded at Viana do Castelo harbor, in the NW Portuguese coast (Taborda and Dias, 1992).

The characterization above indicates that storm effects along the Portuguese coast are essentially related with the impact of breaking or broken waves, rather than inundation caused by intense storm-related surges, the latter sharing more similarities, to some extent, with tsunami-induced flooding.

Wave regime is of high energy and essentially related with swell generated in the North Atlantic. Mean annual significant wave height (H_s) and peak period (T_p) are of 2m and 11 s. Storms are more frequent in the winter and essentially related with west to northwest waves (Esteves et al., 2010, Andrade et al., 2013), although southwesterly storms occasionally occur. On average, this coast is impacted by 12 storms per year, with a large inter-annual variability, ranging between four and nineteen (Almeida et al., 2009). $H_{s_{max}}$ of storm waves reaches 14 m and T_p is over 20 s (Almeida et al., 2009, Esteves et al., 2010).

Stop 1 - Coxos coastal reach and boulders

Geology and geomorphology – an overview

Coxos littoral area is located in the Atlantic central west-facing coast of Portugal, approximately 40 km NW of Lisbon and 5 km N of Ericeira (Figure 1).

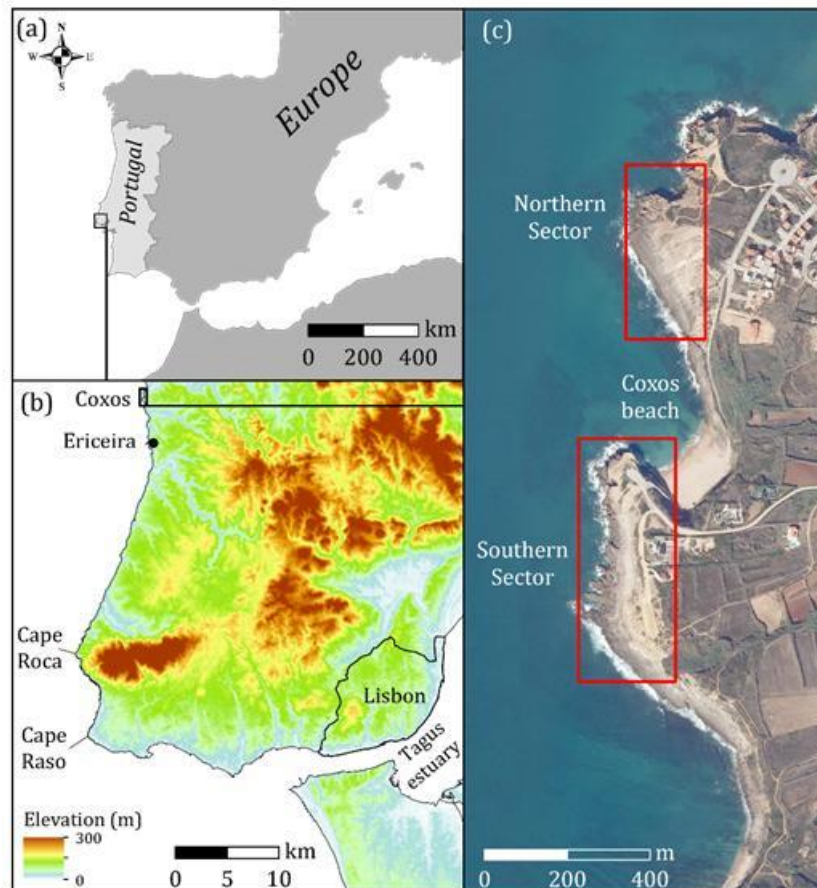


Figure 1. (a) Location of the field area in Europe and (b) in the broad Lisbon area (over ASTER Digital Elevation Model, METI and NASA -<http://reverb.echo.nasa.gov/reverb/>); (c) location of Coxos beach and rocky platforms over IGEO 2010 orthophotos. Northern and southern sectors framed in red. Modified after Oliveira (2017).

The Coxos area is a sediment-starved rocky coast, with an irregular coastline and N-S general trend, where 20-50 m-high cliffs alternate with pocket beaches and structurally controlled rocky platforms. The uppermost cliff edge limits a 10 km-wide plateau with maximum heights of 200 m, inland of the coast. There are only few shore platforms at the toe of the cliffs and they mostly correspond to plunging cliffs. These features allow for moderately high waves approaching the shoreline to preserve most of their energy until breaking or surging at the cliff face.

Both cliffs and platforms are cut in lower Cretaceous sediments consisting of claystone, sandstone, marl and limestone layers. The Cretaceous layers gently tilt toward SSW and are intercepted by faults, magmatic intrusions and, more frequently, open joints with metric spacing (Figure 2, Figure 3).

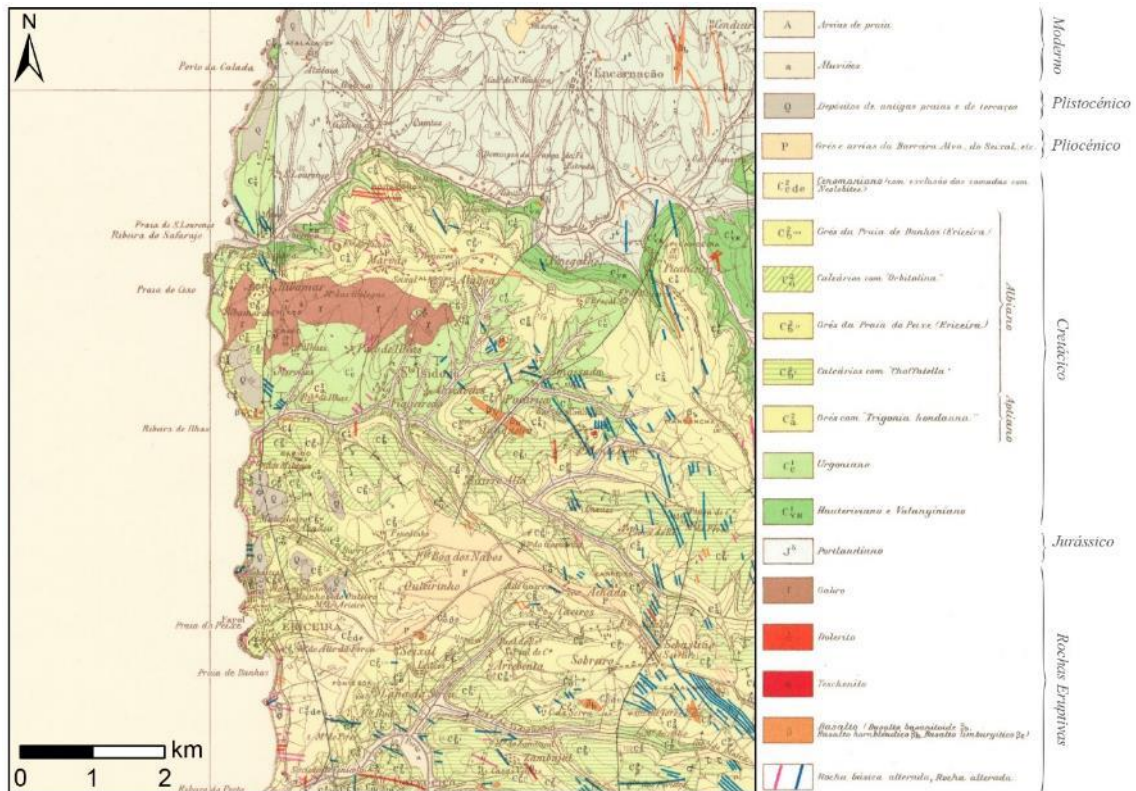


Figure 2. Geologic map of Ericeira-Coxos region (fragment of the 1:50000 30-C Torres Vedras geological map, Zbyszewski et al., 1955. Image not to scale).

The lateral continuity of cliffs is interrupted in this location by a pocket beach (Coxos beach), consisting of a thin veneer of sand resting over a rocky platform. The beach is encased in a U-shaped fault-controlled embayment. The southern steep-sloping wall corresponds with a vertical, NW-SE trending fault that rose the southern Cretaceous block in relation to the northern block (vertical offset of about 20 m), and this generated repetition of the stratigraphic sequence north and south of the beach. In addition, a number of NNE-SSW secondary faults and flexures (visible from the car park and looking towards the northern sector) generated smaller, metric-sized, and more localized offsets.

The field visit will address the southern sector of the Coxos area.

The coastal profile is influenced by outcropping lithology, fracture spacing and orientation, and bed thickness and attitude. Thick sets of hard limestone and sandstone layers develop subtidal to supratidal platforms limited by vertical scarps that evolve by rock fall. In places where more resistant layers are inter-bedded with softer sandstones, marls or mudstones, the cliff face undergoes differential erosion and develops an irregular profile with overhangs, benches, visors and pseudo-notches as well as stepped structurally-controlled surfaces (Figure 3). The tread of stepped surfaces slopes west and southward (seaward) in agreement with the dip of the strata. The rise of the steps corresponds to WNW-ESE to N-S near-vertical fractures showing metric spacing, and is inherited from the thickness (0.5–1 m) of the harder layers.



Figure 3. (a) Northward views of Coxos area showing irregular and stepped profiles with overhangs, vertical scarps and structural notches and (b) stepped supratidal structural platforms. Scale is 3 m long. Modified after Oliveira (2017).

Low-sloping cliffs ($<40^\circ$) develop in thick sequences of marls and claystones. These low-angle surfaces essentially correspond to the upper section of the cliff and mainly evolve by sheet erosion, gullying and mass wasting instead of marine-related processes.

The Cretaceous sequence outcropping in this location is described in Zbyszewski (1955, see also reference to previous work therein). Rey (2007) and Rey et al. (2003, 2009) conducted detailed litho and bio-stratigraphical investigations and concluded that it formed during a marine transgressive-regressive second-order cycle dated from the lower Cretaceous (Upper Valanginian-Upper Hauterivian). This cycle comprises a number of third-order complete depositional sequences, separated by evidences of exposure, erosion or interruption of sedimentation.

Five main lithostratigraphic units (Units A to E) were defined by Oliveira (2017) based on stratigraphical sets described by Rey (2007) and geomorphological aspects. Upper and lower boundaries of each unit (herein named surfaces S I to S IV) correspond to structural surfaces and benches developed by differential erosion, some of which corresponding to *hardground* surfaces (Figure 4).

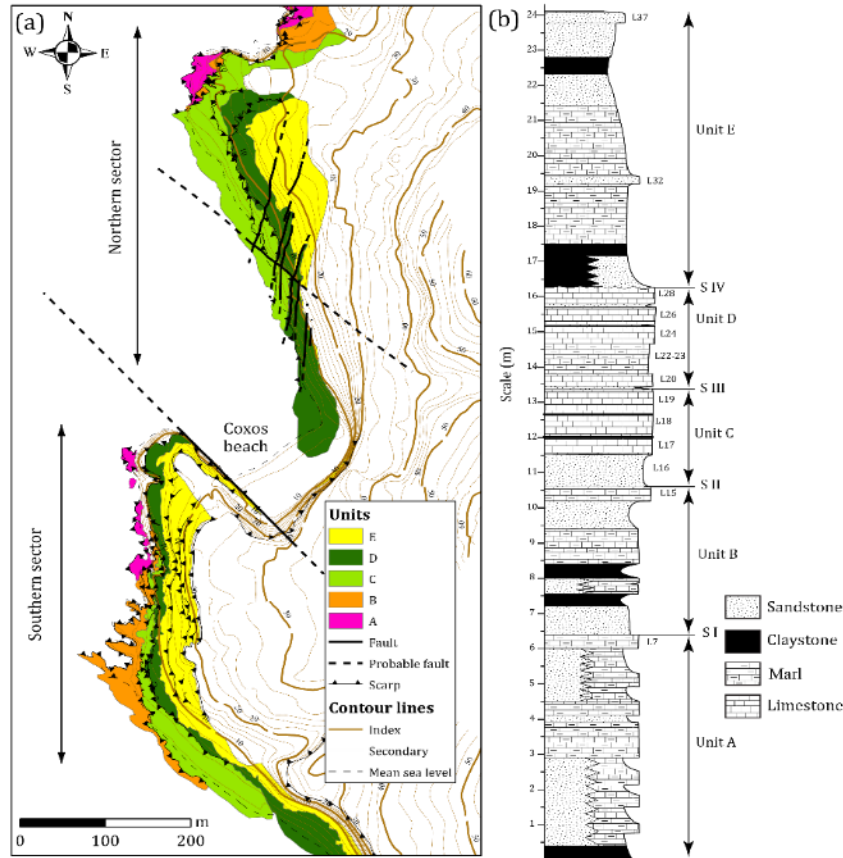


Figure 4. Map and summary log of main lithostratigraphic units (Unit A to Unit E) and structural surfaces (S I to S IV). Modified after Oliveira (2017).

Unit A outcrops at the very base of the cliffs. It consists essentially of sandstones inter-bedded with sandy limestones. The outcrops locate in the intertidal domain and are seldom accessible. A hard limestone layer at the top of the unit controlled the development of the lower S I surface.

Unit B is made of fine sandstones inter-bedded with claystones and intensively bioturbated sandy limestones. They outcrop in the lower section of the cliffs of the southern sector. Differential erosion of layers within this unit generated an extremely irregular coastline with narrow and elongated headlands alternating with deeply encased and funneled embayments, limited by steep walls. Joint sets affecting this unit preferably develop NNW-SSE with about 3 m spacing, in agreement with, and controlling the plan shape development of the shoreline. Unit B is topped by a Cretaceous *hardground*, which developed in resistant sandy limestone and gave rise to the wide structural surface S II.

Unit C consists of calcarenites (detritic limestone) and, secondarily, sandy limestones, upon which rests a thick and resistant crystalline limestone layer. The top of this limestone favored the development of structural surface S III. This unit shows larger bed thickness and lower joint frequency in comparison with other lithostratigraphic units.

Unit D is composed of three crystalline limestone layers interbedded with soft marls and thin siltstones, the mechanical resistance increasing towards the top. The topmost limestone layer controls the development of surface S IV and the whole set forms a pronounced step along the southern sector. Transition from Unit D to Unit E is locally made by a lenticular body of silty, very

fine micaceous sand of fluvial facies, indicating a brief regressive episode that allowed for the development of a fingered detrital fan than invaded the otherwise shallow carbonate marine platform.

Unit E contrasts in mechanical resistance, lithology and bed thickness with all the underlying units. It is composed of inter-bedded thin layers of soft claystones and marls, and thin hard (though densely fractured) sandstones. This unit outcrops inland of the underlying units, due to differential erosion and faster retreat of the cliff face affecting the softer Unit E sediments, exposing the rocky structural platform S IV. The cliff face also adopts a smaller angle, in relation with prevailing terrestrial erosion processes. Surface run-off and mass-wasting originate colluvium deposits consisting of clay and silt with some sand, cobbles and boulders that accumulate at the base of this slope, covering S IV. The horizontal (seaward) extension of the colluvium over S IV is variable in space and limited by frequent outwashing promoted by rain and wave swash.

Boulder deposits

The deposits of Praia dos Coxos consists of over 1600 boulders bearing evidence of transport against gravity and landward, which accumulated in two subsets, north and south of Coxos beach. The northern subset consists of only 34 boulders, standing at 4-11 m (mean sea level - msl), a small number in comparison with the 1580 found, examined, measured and geo-referenced in the southern sector. The field visit develops in the southern sector along structural surface S IV and starts at the southern end of the boulder deposit.

In this sector the vast majority of boulders consist of massive limestone ranging in mass from 3 kg to 30 ton. The predominant source layers (unequivocally identified in 409 out of 1579 boulders) are the resistant beds topping Unit C (boulders accumulated over S III) and Unit D (boulders over S IV) (Figure 4 and Figure 5), added by less frequent and smaller particles sourced from underlying units. In cases where the specific source layer could not be precisely identified, lithological, paleontological and morphological criteria allowed reducing the possibilities to a few top layers within each of the units mentioned above. The upward and landward distances travelled by boulders are small. Vertical distances are in the order of 1-2 m and horizontal pure cross-shore displacement is in the order of the width of the platform, or less. Oblique displacement, including both cross shore (landward) and longshore components (the latter in favor of the platform slope) are larger, reaching tenths of meters.

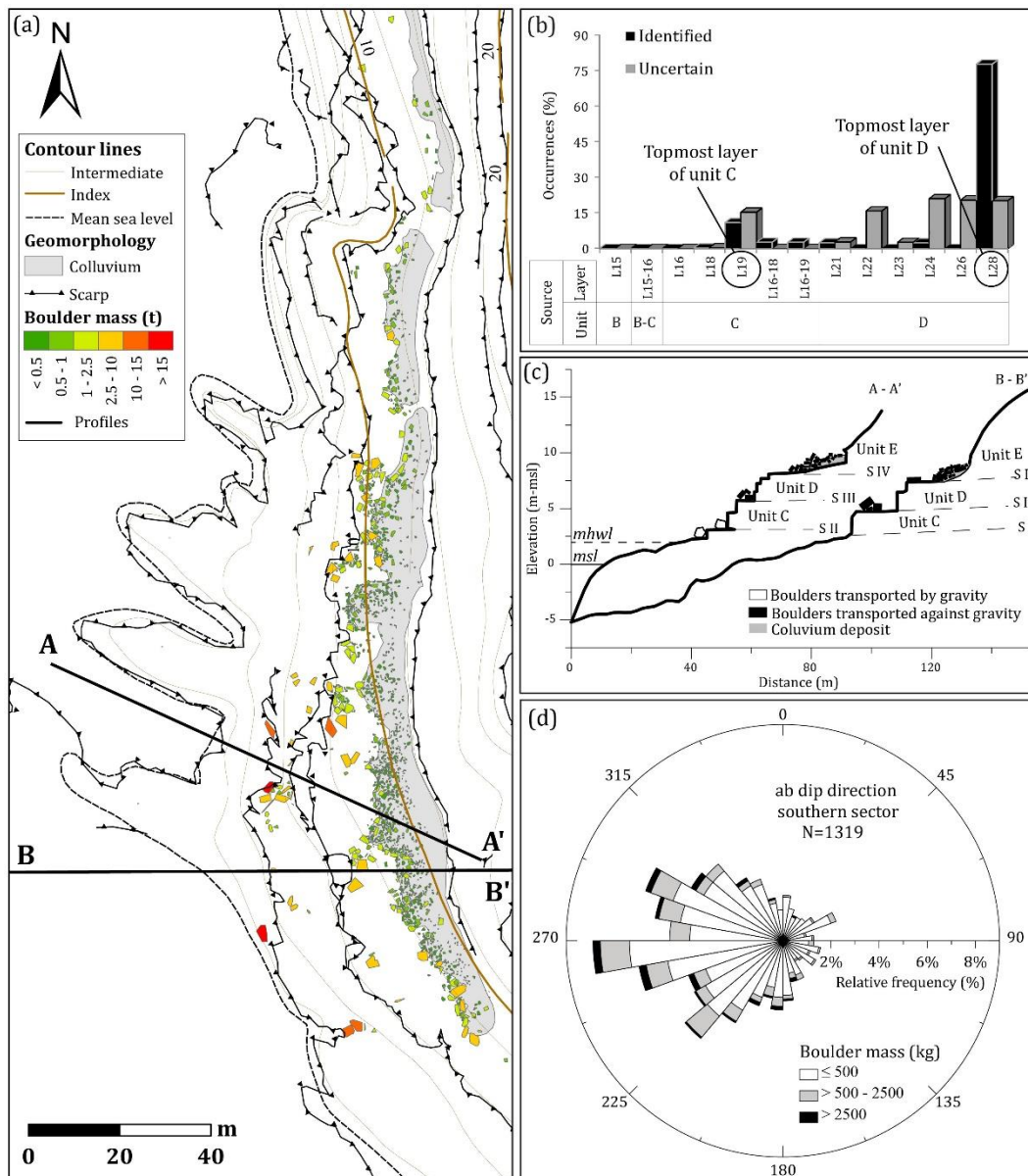


Figure 5. (a) Spatial distribution of boulder size in the southern sector; (b) Frequency distribution of boulders by source layer; (c) Profiles of the field site (profiles locations shown in (a)); (d) Rose diagram showing frequency distribution of the ab surface dip of disk-, bladed- and rod-shaped boulders. Modified after Oliveira (2017).

Boulder sources and entrainment

The description above indicates that, regardless of associating to storms or tsunamis, the waves responsible for the present day deposit mostly picked boulders from the upper region of each steep-sloped reach of the stepped cliffs, and especially from their uppermost edges, rather than sweeping and nourishing on loosened rock masses along the whole cliff face.

Moreover, in cases where unequivocal socket-deposit relationship was established, field observations show that the width of displaced boulders often exceeds the width of the rock surface originally underlying the displaced blocks, and that became exposed at their sockets. This indicates that, at least in part, these boulders correspond to former overhangs, and in many

cases the bedding plane separating the underlying layer from the (overlying) source layers is deeply karstified and exhumed. Altogether, these observations suggest that the mechanical effects of incoming waves and wave ability to entrain and displace large *in situ* rock pieces could have been substantially raised by both water wedge effects and momentum increase of flow-induced forces acting upon the basal surface of overhangs.

Similar processes may occur elsewhere along the cliff face where overhangs and under-excavation features exist at lower altitudes. However, if a suitable accommodation space (a structural platform or bench) is not present in the vicinity and at a short distance above the source, these particles will move upwards for a brief time interval after plucked from the cliff face and eventually fall down, adding to the toe deposits.

Both differential erosion and karst features vary in expression along the study area, and are relevant in determining which compartment of the study area offers ideal geomorphological settings (as described above) to promote the entrainment of boulders when impacted by a high-energy event. Once the cliff surface is leveled from crest to toe, its reactivation becomes more difficult, regardless of the frequency distribution of extreme events. It is reasonable to assume that weathering and erosion will produce in due time a new set of irregularities, favoring cliff reactivation and boulder production. This implies that boulder entrainment and deposition on top of S III, and especially SIV, is discontinuous in time and space.

Scalar, vectorial and morphological properties

Figure 5 shows the spatial distribution of boulder mass across surfaces S III and S IV. The height of emplacement of boulders resting upon surface S IV is about 6 to 13 m above msl, the elevation increasing northward in agreement with the general slope of the structural surface. In addition, a general northward decreasing trend of both boulder density per unit area and of boulder mass is apparent, despite pronounced irregularity in size-distribution at smaller spatial scales. Boulder size also depicts a general landward size-grading trend.

At first glance, the spatial distribution of boulders' mass and frequency depicted in Figure 5 may suggest that this deposit could have been emplaced by a single, extreme inundation event, capable of engulfing and sweeping this coastal ribbon, the flow progressing towards north. This hypothesis is compatible with the impact of a high-intensity tsunami with source located southwest of the study area, the AD 1755 event arising as a plausible candidate. The irregularities in size distribution found at more local scales could be interpreted as an artifact of the small duration of the inundation event (minutes), precluding more effective and inclusive size-grading of the boulders.

However, a more detailed investigation of the parameters of the AD 1755 tsunami and of the geomorphology of the boulder accumulations makes this hypothesis implausible, despite this particular tsunami meeting the required propagation direction, and the overwhelming destruction it caused.

Actually, the boulders are not randomly nor simply scattered by size across surfaces S III and S IV. Surface S III is more frequently reached than S IV by storm waves, especially during spring high-tide, and presents the largest boulders (> 10 ton) found in the southern sector (Figure 6). These boulders lean against or straddle the bench-edge topped by surface S III, showing minimum horizontal and vertical displacements, which mostly fail to exceed the boulder's long axis length. The size of the largest particles relates with higher thickness and lower joint frequency of their source layers in unit C. Other boulders sitting on this surface (2.5 to 10 ton) are arranged in clusters showing imbrication (Figure 6a).



Figure 6. (a) 10-15 ton imbricated boulders originated from unit C (layers L18-19) standing on surface S III and leaning against the scarp between S III and S II; (b) Parallelepiped boulders (mass up to 10 ton) located next to, and landward of the edge of surface S IV, and respective socket in topmost layers of Unit D (Photos by T. Silveira).

The directional distribution of elongated and platy boulders sitting on surfaces S III and S IV (Figure 5) (that could shed some light on flow direction) reveals three directional modes (NW, W and SW) and not a SW unimodal distribution, an expectable pattern in the case of only one inundation episode related with an extreme southwesterly event having been responsible for the setting of the deposit. The rose diagram in Figure 7 retains only directional data from stacks of imbricated boulders in surface S IV. The SW directional mode is strongly attenuated, whereas the westerly and northwesterly modes remain (the latter rotated a few degrees clockwise) and a north to NNW mode is added to the previous diagram.

Actually, boulders sitting over surface S IV can be grouped in three subpopulations based on mass, source layer, location in the surface and morphology of the accumulation (Figure 7).

One set includes boulders sitting near the bench edge of S IV. They were sourced in layer L28 (topmost layer of unit D), show straight and sharp edges and parallelepiped shape. They occur either isolated or in clusters of a few individuals, their mass ranging from 2.5 to 10 ton (Figure

6b and Figure 7). They are generally located near their sockets and the transport was mainly cross-shore (eventually added by a smaller longshore component matching the slope of the structural surface), the travelled distance being equal or smaller than the size of the boulder. Northward decrease in boulder size and boulder frequency observed in these cases is interpreted as resulting from increasing elevation of the cliff edge and larger fracture spacing in the same direction. Isolated and flatter boulders directly lying upon over structural surface S IV rest on their ab surface and thus tilt in agreement with the general attitude of that surface.

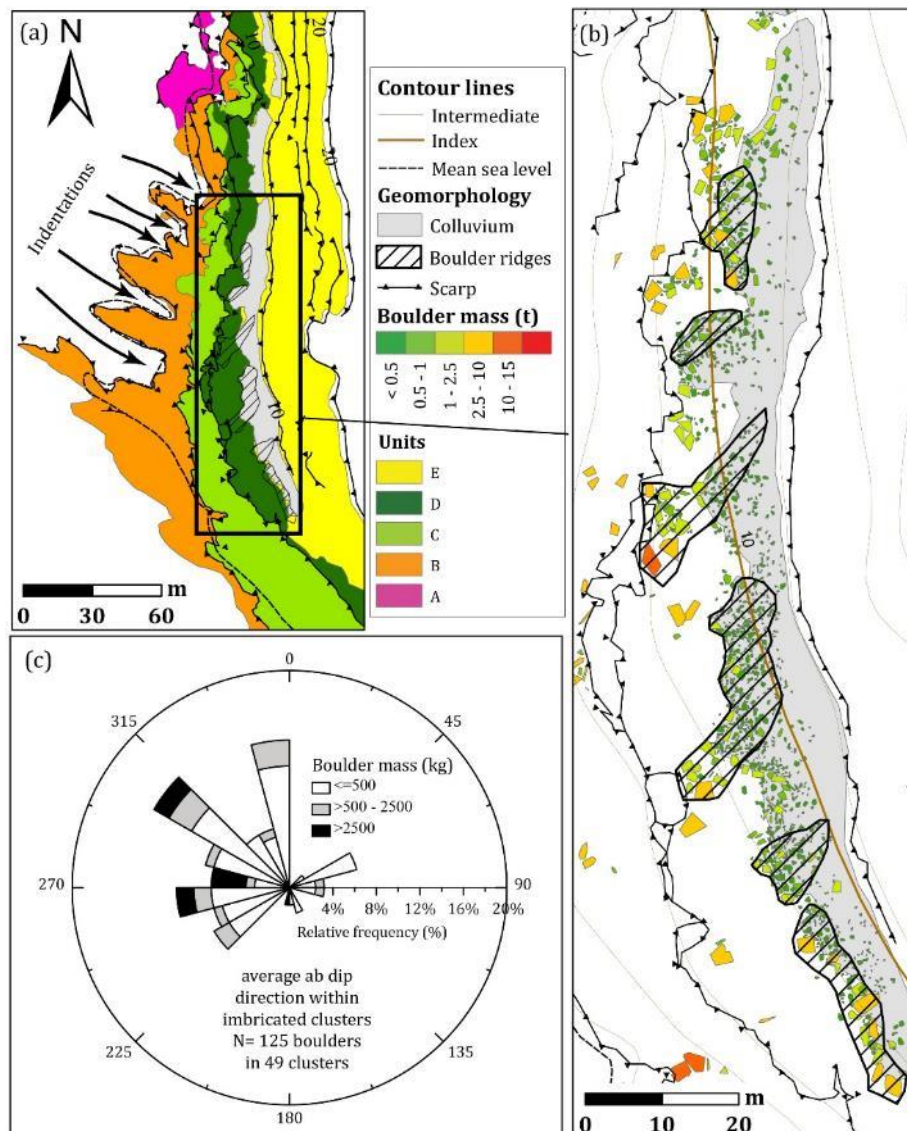


Figure 7. (a) Lithostratigraphical units and Indentations on the lower structural platform and cliff face. Arrows illustrate funneling and directional effects of steep-sided and deep corridors over incoming wave bores and relations with boulder ridges over S IV; (b) Detail of (a) showing boulder ridges and spatial variation of boulder mass over S IV and within the ridges; (c) Rose diagram showing distribution of up-current directions as inferred from stacks of boulders showing imbrication. Modified after Oliveira (2017).

A second set corresponds to elongated accumulations over S IV and were categorized as boulder ridges (Figure 7 and Figure 8). These accumulations consist of heterometric boulders (always less than 1 ton and including cobbles) exhibiting varied shapes, in cases showing rounded edges. In many cases the source materials could not be unequivocally identified but in every other case

they were sourced in topmost layers of Unit D. Ridges attach at their landward tip to the colluviums blanketing the toe of the cliff developed in Unit E materials, and the lateral contact between both deposits is inter-fingered – an indication of alternation between slope mass movements and marine-induced input of boulders, compatible with continued construction and dismantling of the ridges. The boulder ridges are roughly aligned N-S to NE-SW, and show poorly defined, seaward sloping crest, the robustness of the accumulations also decreasing seaward (Figure 7b).

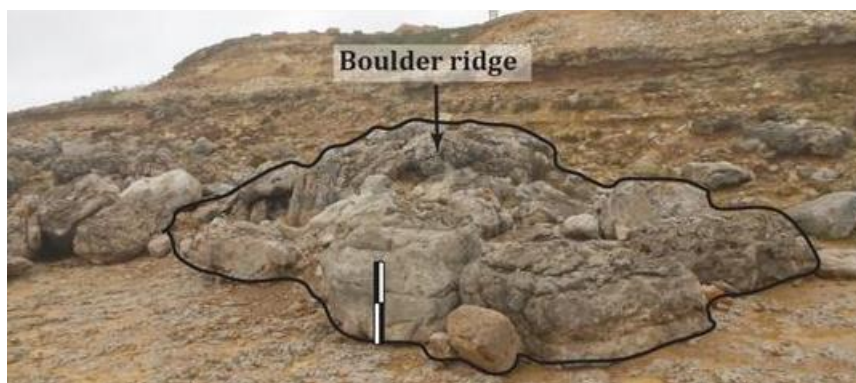


Figure 8. Landward view of a NW-SW aligned boulder ridge. The view is approximately parallel to the ridge crest. Modified after Oliveira (2017).

Imbrication of boulders in ridges was found correlated with ridge growth and is well represented by the rose diagram in Figure 7c. It relates with boulders moved from either the nearby bench edge and across the structural surface, or from more northern locations over the same platform, their movement having been stopped by immobile larger particles or by the ridge itself. Landward-tilting boulders were found at the landward surface of ridges and are interpreted as corresponding to particles that were thrown over the ridge crest and came to rest over its lee slope. Ridges occur landward of and spatially related with deeply incised and steep-sloped excavations (referred to as indentations in Figure 7a) affecting lithostratigraphic Unit B and, to some extent, the lower layers of Unit C. Canelas et al. (2014) tested the ability of these indentations to modulate incoming waves and concluded that they were able to concentrate high-energy flow, increasing its ability to entrain and transport large boulders.

A third set includes boulders ranging in mass between 1 and 10 ton that align along and armor the colluviums front, locally merging with the ridges. They act as a barrier, hindering colluvium washing out by rain and wave swash. In locations where the rocky bench surface S IV is wider, the boulder sets above are separated by a barren ribbon where boulder frequency is very low to null.

Chronology and origin of boulder emplacement

Besides comparing aerial photographs from 1948 onwards, age estimations of boulders' emplacement in the southern sector of Coxos were undertaken using Optically stimulated luminescence (OSL) (over two samples of marine sand underneath boulders preserved within the colluvium materials - Figure 9), downwearing rates of the exposed surface of a Cretaceous

detritic layer where a ledge developed by differential erosion underneath one boulder, measured by MEM (micro erosion meters) (Figure 10), and lichenometry (*Opegrapha durieui* living and dead specimens colonizing 24 boulders in the southern sector, out of 35 in both sectors, Figure 11) (see Oliveira, 2017 for methods and results). In addition, recent storms (such as the winter 2014 *Christina* and *Nadja* storms) provided a unique opportunity to observe and measure boulder movement by storm waves.



Figure 9. Marine sand mixed with, and supporting, floating boulders. Image obtained from an excavation to sample sand for OSL. Modified after Oliveira (2017).



Figure 10. Limestone boulders sitting on top of a Cretaceous very fine sandstone. The sandstone exposed surface is downwearing and protection afforded by boulder B 1509 (on the left) allowed for the development of a ledge. Vertical arrows indicate location of MEM measurements. Vertical scale is 1 m long. Modified after Oliveira (2017).



Figure 11. *Opegrapha durieui* growing on the surface of a limestone boulder. Photo by M.A. Oliveira.

Chronology results obtained from different methods are mutually consistent and allowed the identification of asynchronous periods of boulder accumulation, extending back in time to ca. 500 years. Aerial photography show that boulder movement has occurred in the last 60 years, although not affecting all mapped and surveyed boulders. Larger particles tend to be less reworked than smaller particles, as expected. Large morphological features, such as boulder ridges, are persistent through time in aerial imagery, although there are evidences of individual particles having been added to the ridges and others removed. In fact, addition and removal of boulders over the whole of the study site are continued processes, and the vast majority of particles at present populating the structural surfaces has been or will be affected by them.

Lichen growth data allows concluding that the absolute majority of boulders were emplaced from the last quarter of the 19th century onwards and more than half in the past 65 years. Curiously, the time window of 1740 to 1875 (that includes the time of the 1755 tsunami) is represented by a minimum in frequency (2 cases, one of which corroborated by MEM measurements) and older ages, in the time-interval of ca. 1560 to 1740, were obtained from only 5 boulders.

Altogether, the data above strongly suggest that flow responsible for the entrainment and relocation of boulders essentially relates with powerful storm waves and not the AD 1755 tsunami. And yet, the OSL ages obtained from sand beneath and above boulders, found in the middle section of the southern sector provided ages of 230 ± 20 and 290 ± 50 years that are compatible with that tsunami. However, the OSL dated sand corresponds to a unique occurrence, because it is the only mixture of a large volume of marine sand involving and supporting boulders found so far in this area, both materials having been preserved *in situ* by mass waste capping. Observed storms essentially mobilize large-sized particles and little sand is carried along onshore, no observation of a similar mixture having been recorded so far.

The uniqueness of this deposit and the age results above suggest that the 1755 tsunami effectively affected this area, but rather than contributing to increase the number of boulders in the accumulation coeval of that inundation, it must have been most effective in winnowing the rocky substrate from pre-existing boulders. This would have allowed for resetting the age of the overall accumulation, explaining the near-absence of particles older than the middle 18th century. Throughout the last 260 years, storm waves reconstructed the accumulation pattern pre-dating the 1755 tsunami, and the time interval of ca. 65 – 135 years may represent the average time interval of boulder residence on the upper structural platform.

Stop 2 - Guincho – Cascais coastal reach and boulders

Geology and geomorphology – an overview

The broad coastal area to the NW of Lisbon shows two main geomorphological features: the Sintra range and the Cascais platform.

The Sintra range corresponds to a residual relief that largely coincides with the cropping out of a sub-volcanic intrusion dated from the Late Cretaceous, the entirety of which is classified by UNESCO as a World Heritage Cultural Landscape (Figure 12). It comprehends an inner granite mass surrounded by syenites and gabbros that together with a dense network of radial and ring-dykes intruded Mesozoic sediments (see Ramalho et al., 2001, Kullberg and Kullberg, 2005, and references therein, for details and previous work). The landscape associated to this range evolved by differential erosion and it stands out in the present-day landscape, its highest elevation reaching about 500 m above mean sea level.

The Cascais platform is a polygenic erosion surface carved mostly on lower Cretaceous rocks, though it affects Jurassic beds closer to the Sintra range. The Cretaceous beds essentially consist of inner shelf fossiliferous carbonates, including reefs, together with few sandstone and marl layers, representing occasional return to more littoral facies, always related with shallow, carbonate-rich peri-littoral environments (see Rey, 2007 and Rey et al., 2009, for details on lithostratigraphy and palaeogeographic reconstructions). These sedimentary rocks have been subjected to extensive dolomitization that partially obliterated original textural, lithological and paleontological features.

In broad terms, the Mesozoic sequence gently tilts towards S and SSW (with some small-scale open-folds), the dip angle increasing south of cape Raso. Cretaceous layers are densely fractured and faulted and intruded by dykes, most of which exploited dextral strike-slip faults trending N30°W. At present, these dykes frequently correspond to “matacães” (the Portuguese word equivalent to the French “calanque”) where they meet the coastline: elongated differential erosion excavations limited by vertical walls, developed by combined action of weathering and marine erosion, added by roof collapse of endokarst features.

The same directional family of fractures, which typically correspond to open fissures lacking infill, controlled to a large extent the development of main karst linear features. Actually, the whole of the limestone platform has been subjected to karst denudation and solution processes testified by abundant surface, and endokarst features, such as lapiés (karren), sinkholes and galleries.

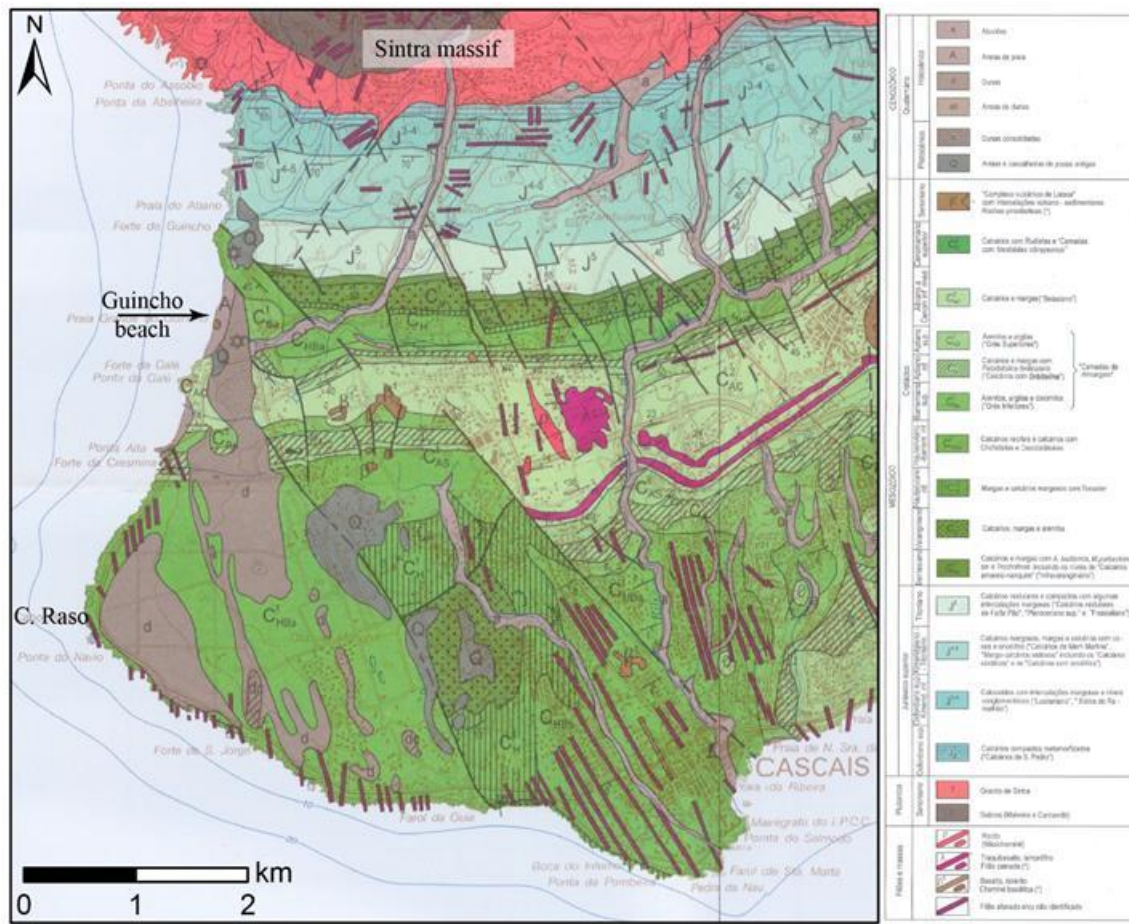


Figure 12. Geologic map of Sintra-Cascais region (adapted from the 1:50000 34-C Cascais geological map, Ramalho et al., 2001). Image not to scale.

At smaller spatial scales, the morphology of karren features varies between layers reflecting textural and compositional controls: dolomites typically show well-developed and thin clints, crystalline limestones develop large solution pits, grooves and channels, sandy or marly limestones preferably show microkarren features such as centimetric-sized pits, and bioturbated limestone present a distinctive weathering pattern associated with the protrusion of resistant burrows (Figure 13). Additionally, intense pitting of the rock surface can be observed along a belt with some 10 m width along the coastline.

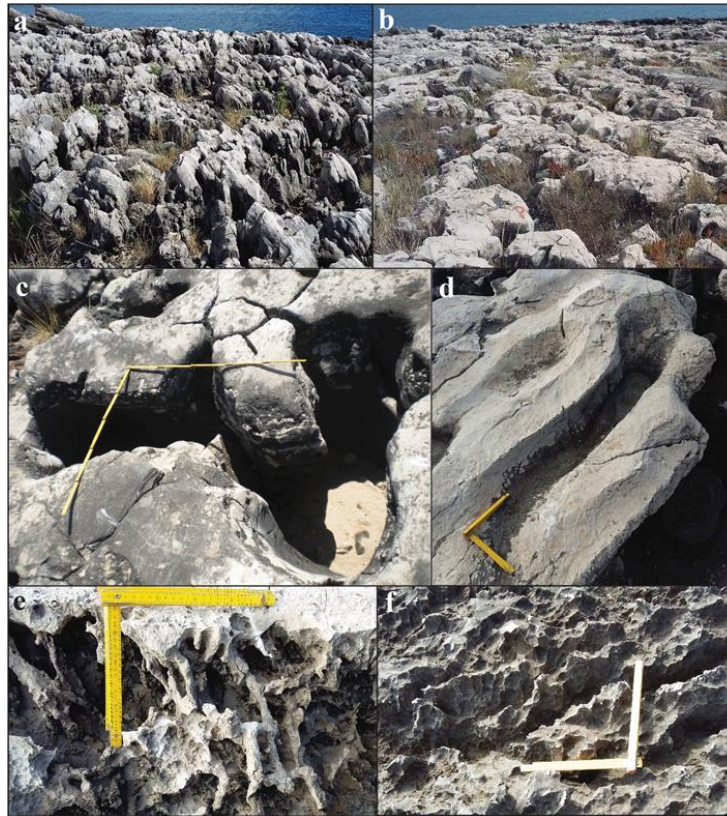


Figure 13: Karren features in the Cascais platform: (a) field of lapiés with interconnected solution pits); (b) well-developed grikes and clints in dolomite; (c) detail of connected solution pits; (d) meandering channel; (e) distinctive weathering pattern of bioturbated limestone layers; (f) pitting in coastal karren. Photos by M.A. Oliveira.

As referred above the Cascais platform is an essentially erosive surface developing from ca. 80 m above msl inland and gently sloping (about 8°) towards Cape Raso (SW), where it ends at the top of plunging cliffs, which also border this surface along its southern edge (Figure 14). The width of the platform is small in the regions of Cascais and Guincho beach and it widens considerably landward of Cape Raso.



Figure 14: Image of the gently sloping Cascais platform close to the coastline and limiting plunging cliffs. Photos by M.A. Oliveira.

This platform comprises a staircase of poorly preserved Pleistocene marine terraces that developed in relation with marine high-stand episodes (see Ramalho et al., 2001, Duarte et al., 2014, Cunha et al., 2015 and references therein for previous work and discussion of morphology and age of marine terraces). North of Guincho beach, the terraces still preserve remnants of marine pebbles and sand, but further south they essentially correspond to erosive features (Figure 15 and Figure 16), despite some patches of marine sand and pebbles. Correlations between terraces north and south of Guincho beach has been tentatively proposed using altitude, morphology and slope-breaks as main criteria.

The field visit runs along a coastal reach containing traces of marine terrace T3 (Duarte et al., 2014, Figure 16) whose inner edge stands ca. 20 m above msl. This surface cuts the Cretaceous limestone and degrades progressively seawards, in tune with the increase in intensity of present-day karst processes and quarrying of limestone slabs, the latter mechanism favoring the exposure of structural surfaces. Ramalho et al. (2001) report the existence of a lower terrace, preserved in discontinuous patches at 4 to 6 m above msl, locally covered by well cemented shelly marine gravel. The latter feature (terrace T4 in Figure 16) may represent stage MIS 5e, during which sea level remained about 4 to 6 m higher than present (Siddall et al., 2006), although Duarte et al. (2014) propose the same stage as responsible for the setting of T3. Ramalho et al. (2001) report numerous evidences of human occupation since the Paleolithic and extending up to modern times in relation with marine terraces, including worked pebbles, quartzite tools, remnants of cooking fireplaces together with accumulations of marine shells, and pottery.

The inner edge of terrace T3, as well as most of the surface of the adjacent older terrace T2, is blanketed by Holocene aeolian sand, which corresponds to vegetated sand sheets and parabolic dunes. Close to Oitavos (just north of Site #2, north of the road, see below) the remnants of a Pleistocene consolidated dune (the Oitavos dune) outcrops from the Holocene sand and are known to sit over an organic-rich paleosoil. In turn, the paleosoil fills karst hollows affecting the Cretaceous rocks. The soil contains abundant shells of pulmonate gastropod *Helix* sp. and ¹⁴C dating of organic matter and shells in the soil yielded ages in the range of 16.4 to 34 kyr BP (Pereira and Angelucci, 2004, Soares et al., 2006, Prudêncio et al., 2007). The radiocarbon age of about 30 kyr BP is thus a minimum age for the development of the karst and a maximum age for the setting of the aeolian cover.



Figure 15. Wave-cut surface truncating Cretaceous beds and corresponding to terrace T3 (from Duarte et al., 2014).

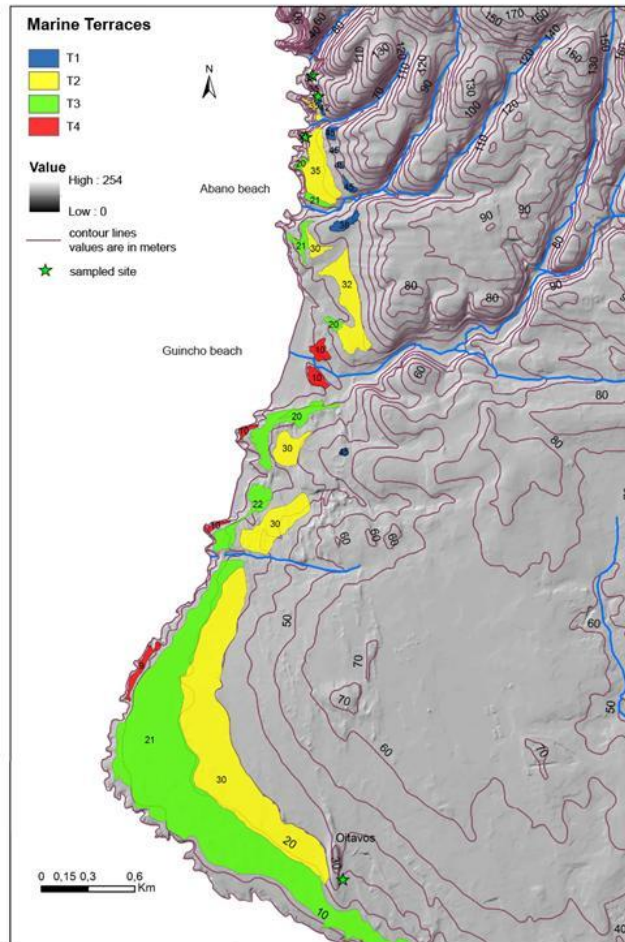


Figure 16. Marine terraces recognized along the Guincho-Cascais coastal reach. Modified after Cunha et al. (2015a).

Aeolian activity across the Cascais platform has thus been persistent since the late Pleistocene and is still relevant at present, as shown by the volumes of sand that every summer are blown across the road from the Guincho beach to nourish and maintain the Guincho and Cresmina bare dunes, which steadily migrate inland. The present-day rate of sand transfer by wind from the beaches of Cresmina and Guincho to these dunes was estimated by Rebêlo et al. (2002) in $1.2 \times 10^4 \text{ m}^3 \text{ yr}^{-1}$.

The general wind direction, as inferred from foresets in the Pleistocene aeolianites and morphology of Holocene parabolic dunes is N to NNW, in broad agreement with the present-day wind-regime and migration trend of the Guincho and Cresmina dunes (Figure 17 and Figure 18).



Figure 17. Oblique aerial view of Cresmina beach and foredune and Guincho-Cresmina active dunes. Note vegetated dunes on the far right of the image and sand retention structures at the centre-right of image. Guincho beach (not shown) is to the left of image. Prevailing wind blows towards the upper right corner of image (SSE). Aerial photo from Google Maps.

According to Rebêlo (2004, in Santos, 2006) the Guincho and Cresmina dunes are located at the upwind edge, and integrate a transgressive dune system, nourished by sand supplied from both Cresmina and Guincho beaches. This system forms an aeolian corridor (about 4 km long and slightly less than 1 km wide), roughly aligned $N25^{\circ}W - S25^{\circ}E$, which connects the beaches of Cresmina and Guincho (at its NW tip) to the coastal reach extending between Oitavos and the Guia lighthouse (farther SE) (Figure 18). Together with the cartographic expression of Holocene aeolian sand patches (Figure 12), these data indicate the existence of intense and intermittent wind-driven sand movement across the Cascais platform throughout the last several millennia. This is further evidenced by the widespread presence of aeolian grooves and polishing of limestone outcrops which indicates abrasion by northerly winds (Figure 19). The directional spread of ventifacts is narrow, in the range of $N10^{\circ} - 25^{\circ}W$. Scheffers and Kelletat (2005) attributed to intense aeolian sand blasting (sharing the same direction) the asymmetrical shape observed in clints of the lapiés.

Aerial photographs dated from the early 1940's clearly show a blanket of aeolian sand covering a large portion of the rocky platform addressed in this field trip (Figure 20). The sand cover has been since then removed by wind deflation and surface run-off and only a few sand patches remain captured in lapiés grikes and hollows on the karst-sculptured surface.

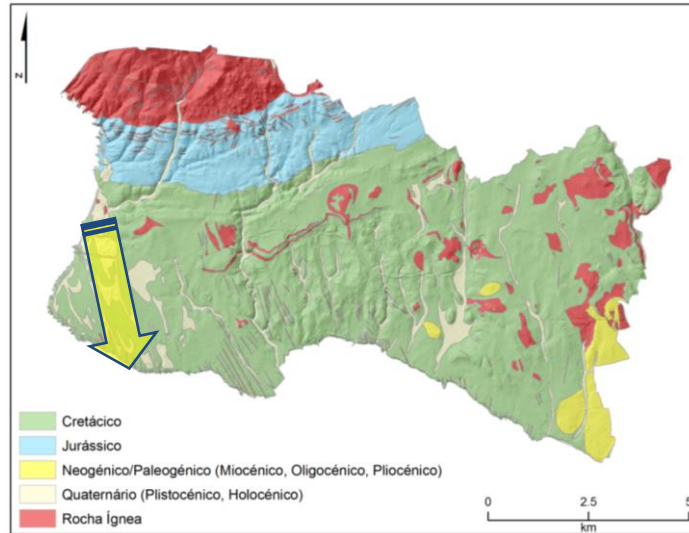


Figure 18. Geological sketch of Cascais municipality with indication of the aeolian corridor connecting Cresmina and Guincho beaches to the southern rocky coast (adapted from Taborda et al., 2010).



Figure 19: (a) Aeolian grooves on limestone outcrops; (b) asymmetrical clints in lapiés (wind-re-sculptured?).

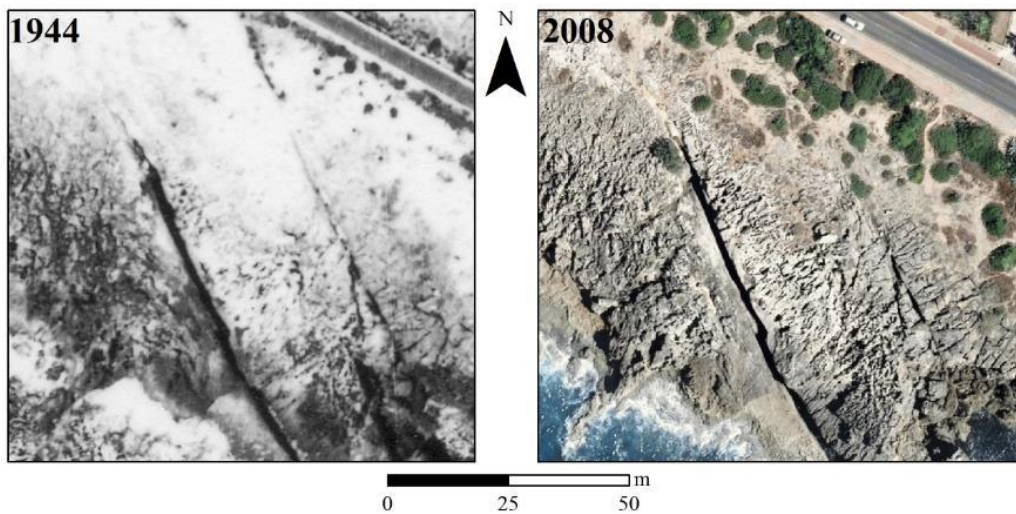


Figure 20. Aerial photographs taken in 1944 (DGOT) and 2008 (DGOT) showing effective wind deflation over a thin aeolian sand sheet that covered about half of the rocky platform in the 1940's.

South of the Sintra range, the coast is cliffed and sediment-starved, the cliffs affecting Jurassic and Cretaceous limestones, with only a few pocket-beaches (e.g. Ursa, Guincho, Cresmina). Beaches correspond with the mouths of structurally-controlled valleys or locations where differential erosion of the rocky coast provided localized sheltering, allowing for the accumulation of thin veneers of sand or shingle over limestone substrate.

The Tagus estuary is not a relevant sand source for the coast extending northward and southward of the inlet channel, including the Cascais – Guincho reach. The rate of sand supply from sources external to the coastal system (cliff erosion and rivers) developing between Peniche (a non-bypassed headland at the northern boundary of the coastal cell containing the Guincho – Cascais reach) and cape Roca was estimated in ca. $10^4 \text{ m}^3\text{yr}^{-1}$ (see Ribeiro et al., 2014 and references therein), an amount that broadly corresponds with the intensity of the Cresmina dune sink and one order of magnitude lower than the potential southward net littoral drift in this coastal stretch (Ribeiro et al., 2014).

Sand driven by longshore currents bypasses cape Roca but not cape Raso (the southern boundary of the coastal cell referred above), and wind-blown sand bypassing cape Raso may play an important role in supplying sand to the coast extending to the east of the Guia lighthouse. This sand is distributed further eastward by littoral drift up to São Julião da Barra Fort and headland, very close to the northern margin of the Tagus inlet channel. North and east of cape Raso the wave energy is markedly different due to sheltering and refraction of incoming waves (Figure 21).

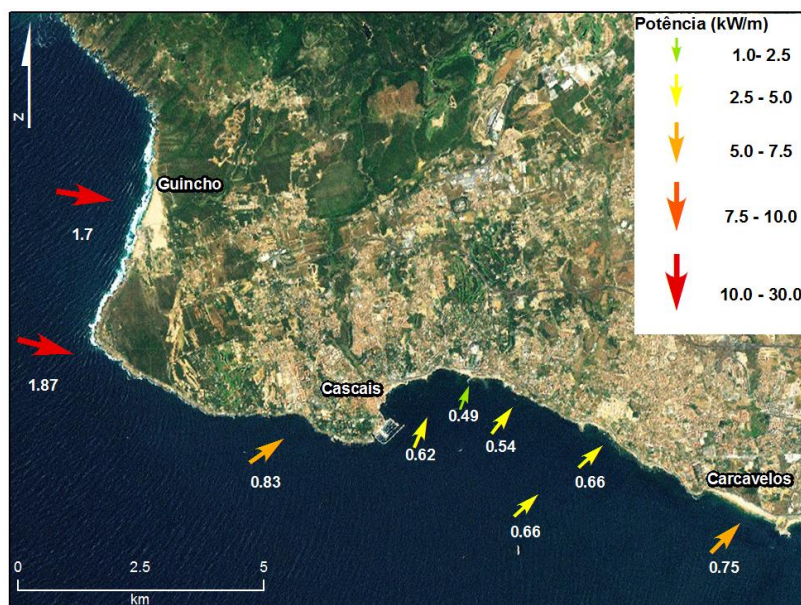


Figure 21. Longshore distribution of mean annual wave power (inset), significant wave height and wave direction (colored arrows in image and white numbers) (adapted from Taborda et al., 2010).

Boulder deposits

The field visit addresses a number of stops along the southward-facing reach of the Cascais - Guincho coast. Here, the attitude of the Cretaceous strata (pending 15-20°SW) and slope of the marine terrace surface (pending 8°SW) combine to create a particular geometric arrangement, in which younger layers topping the sedimentary sequence outcrop seaward, and at lower altitudes (Figure 22). This increases the difficulty to distinguish boulders unequivocally transported upward or landward from others that have been transported downslope in favor of gravity or just remained in situ and represent relicts of the source layer.

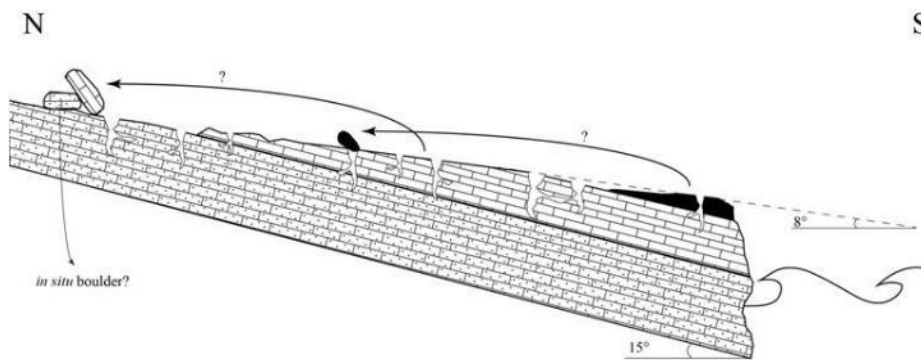


Figure 22. Boulders sitting on top of gently seaward-sloping terrace surface affecting layers that also dip seaward but at a slightly higher angle. In the absence of clear source-sink criteria other than lithology (e.g. microkarst sculpturing) it may be difficult to distinguish among in-situ boulders, representing relicts of an almost completely worn out source layer, from boulders transported seaward by gravity and boulders transported landward by extreme wave events. Modified after Oliveira et al. (2017).

Site # 1

This site is located 1300 m SE of cape Raso. Here, the coast trends WNW-ESE and corresponds to a gently seaward sloping rock platform exhibiting a deeply crenulated edge. The platform is structurally controlled and ends at the top of low (< 5m) plunging cliffs, though locally the sloping surface extends into the submarine domain producing a natural ramp (Figure 23).

This site allows for the observation of a typical boulder ridge at the western region and also of the largest boulder that Scheffers and Kelletat (2005) refer to have found in this area, and that they indicate as excluding any other emplacement mechanism different from a tsunami (East region).



Figure 23. Site 1, showing location of ridge and boulder E6B1 (aerial photo, Google maps).

West region

The boulder ridge aligns NW-SE and stands at approximately 6 m msl. Other ridges and clusters comprising scattered boulders can be observed elsewhere along the same coastal reach and at higher elevations, above 10 m msl. Here, a thick sand deposit (aeolian sand resting on top of marine coarse sand and small rounded pebbles) may be seen south of the road and decreasing in thickness and losing spatial continuity seawards. Aerial photographs of the early 1940's show about half or more of the rocky platform width covered by windblown sand that has been subjected to deflation and washing out since then (Figure 20).

The ridge mostly comprises fracture-bounded platy boulders 1 to 2 m long, together with a number of smaller and well rounded, spherical to prolate boulders (Figure 24). Some of the platy boulders show imbrication, indicating landward transport perpendicular to the trend of the coastline and paralleling the dip direction of the ramp. In a number of cases, the source layer is easily recognized showing that these particles have been quarried from the seaward region of the sloping platform and pushed upwards and landwards for less than 30 m. The ridge and surrounding areas are frequently overtopped by storm waves and the Civil Protection Authority placed a warning sign to elucidate coast users and people looking for the angling spot at the platform tip. Detailed mapping of smaller boulders at a short distance from the ridge shows that these are frequently re-entrained during winter, some being returned to the sea, others moving across and along the ramp and others being emplaced and adding to the total boulder population.

Lichens of *Opegrapha durieui* species, competing with at least two other lichen forms, colonize some of the boulders. Lichenometry provided minimum age of emplacement for 4 boulders colonized by *Opegrapha durieui* in the range of 100 – 500 years.

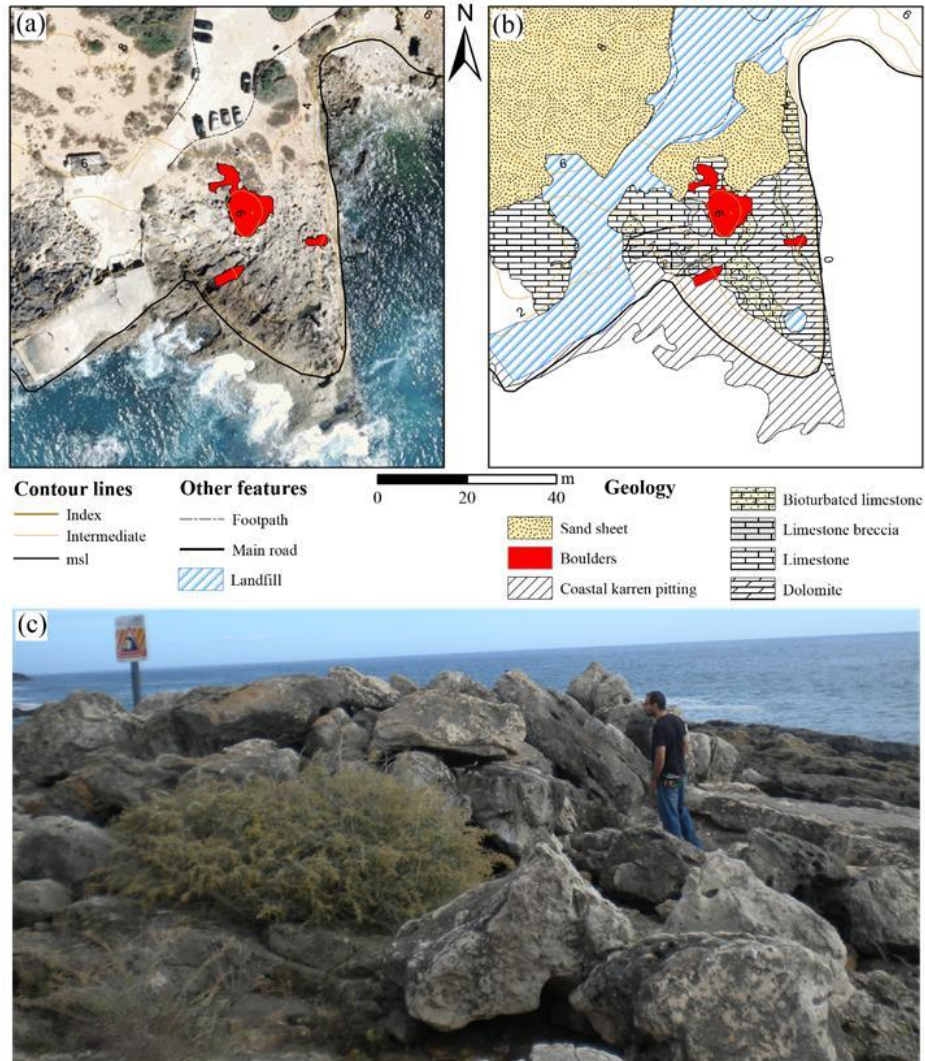


Figure 24: Western section of site #1. (a) Orthophoto showing the location of boulder ridge over the platform; (b) Geological map; (c) View of the boulder ridge towards SE. Note imbrication, structural surface exposed in the right far region of the picture and warning sign. Modified after Oliveira (2011).

East region

About 200 m ESE of the ridge rests boulder E6B1, the largest and heaviest boulder (over 100 ton) identified in this region by Scheffers and Kelletat's (2005) study, together with a number of smaller elements (E6B2 to E6B5) scattered across the structural rocky platform (Figure 25).

In this area, the rocky platform is about 50 m wide and somewhat lower than elsewhere in this visit, reaching a maximum elevation of 8 m msl inland and ramping seaward into the ocean. At its inner edge, the platform is topped by a sand blanket, comprising well rounded coarse marine sand and grit (at the base), which grades upwards to dune sand. The Cretaceous sequence comprises marls, limestone, dolomitic limestone and bioturbated sandy limestones, among which a >2.5 m-thick dolomitic limestone layer stands out (Figure 25). To the East, the sequence and platform are interrupted by a N30W fault and dyke. Most of the fault breccias and igneous mass were eroded, generating a wide matacão. The floor of this steep sided valley is covered by cobbles and boulders actively reworked by waves, as illustrated by the varying degrees of rounding.

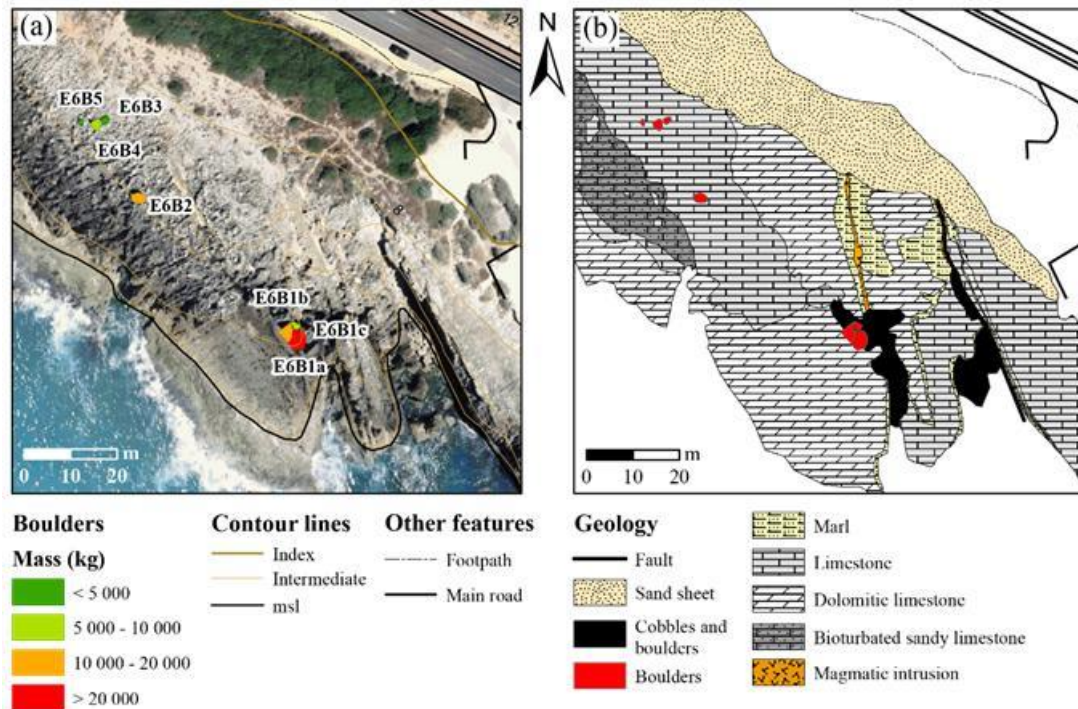


Figure 25: Eastern section of site #1. (a) Orthophoto showing the location of boulders over the platform; (b) Geological map. Modified after Oliveira (2011).

The mass of boulders E6B2 to E6B5 was estimated to less than 6 ton and they rest below 7 m msl, about 20 m landward and NE of their presumed sockets and outcropping layers.

The spatial distribution of mass suggests that smaller particles are preferably located farther inland from the coastline and this is also compatible with prevailing flow from SW. Age estimation of the transport and deposition of these particles was limited to the comparison of 1944 aerial photographs with 2008 orthophotos; the largest boulders of this set (B2, B3 and B4) are clearly visible in the oldest photograph and thus their transport pre-dates 1944. The extension of sand coverage of the rocky surface in the 1940's photographs precluded clear identification of E6B5.

Boulder E6B1 sits very close to the shoreline at about 5m msl on top of a structural surface that ramps into the sea (Figure 26) and it has been standing in the same location since, at least, 1944. Sheffers and Kelletat (2005) noted it was broken into four pieces and estimated the mass of the largest piece to about 100 tons and the whole rock mass to near 200 tons. Three fragments of the original mass are indicated in Figure 25 as E6B1a, E6B1b and E6B1c (E6B1b shows further cracking but failing to achieve full breakage), and smaller fragments may be found close-by. These rock pieces consist of dolomitized limestone. E6B1 displays normal polarity. Under macroscopical observation the rock is quite similar to the carbonate beds that outcrop in the immediate vicinity and that make the only set with layer thickness compatible with the height of E6B1 (about 3 m). This is evident from the karst features at the top (large and deeply incised well developed solution pools) that match in size and pattern the solution features found atop the in situ massif just next to the detached fragments.



Figure 26: View to SW of boulder E6B1 (Photo and comments M. A. Oliveira).

The larger elements originally making boulder E6B1 are aligned N50W making an angle of about 20° with the trend of the fault controlling the elongation of the steep sided valley and other dominant and long open fractures affecting the rock platform. The aligned boulders (especially E6B1a) also display open fractures bearing the same alignment (N50°W). They sit at the edge of the matacão southern wall and are tilted towards the valley's bottom, the landward (horizontal) displacement of the rocks increasing to SE up to a few meters. Furthermore, a triangle-shaped section of the in situ rock surface immediately adjacent to the base of E6B1 (its edge pointing NW) is virtually free of marine corrosion features, in contrast with intense pitting of the same surface beyond the polygon's borders. A similar feature can be observed a few meters seaward, at the exposed surface of the rocky platform, indicating recent removal of one other rock slab.

Altogether, these evidences suggest that E6B1 fell into the valley once differential erosion of underlying marls progressed to such an extent that the rock mass became unstable and finally collapsed. Full topple was inhibited by the small vertical offset between the bottom of the valley and the base of the moving rock mass, in comparison with its width. Collapse was also accompanied by leftward rotation, justifying the angular offset between equivalent linear features found in the displaced masses and bedrock, its weight, twist and sudden impact with the floor facilitating further breakage. Exposure of rock surface corresponding to the top of the layer initially covered by the displaced rock mass is recent, but up to date no quantification of the time interval involved was possible.

We could not find evidence of upward dislocation or landward transport, and though a push by wave action cannot be excluded, gravity must be invoked as the main driver of the displacement.

Site # 2

This site comprises a section of the coast 1.7 km west of Guia lighthouse, limited by two deeply incised matacões trending N 25°-30° W in association to strike-slip faults that were intruded by dykes (Figure 27).

An intensely fractured and weathered narrow (80 m wide) platform can be observed, gently pending seawards. The landward region corresponds to an erosive surface cutting the carbonate strata (which also dip seaward but with a slightly higher angle); further seaward the platform slope increases and the surface develops in agreement with bedding, thus grading into a structural surface that is in general limited by low plunging cliffs. Sand remains of marine facies may be found across the platform, their lateral continuity and thickness increasing northward and showing maximum development close to the road.

The sedimentary sequence comprises a lower unit consisting of bioturbated sandy limestone (herein interpreted as representing back-reef lagoonal materials) that grades upwards into an intermediate unit made of crystalline coral and rudist-rich reef-facies limestone – the reef frame (containing intra-formational breccias at its seaward façade – forereef zone?); transition from the lower unit to the reef-frame sediment is gradual. The upper unit on top of the previous materials consists of secondary dolomite (Figure 27).

The lithological and textural contrasts between sediments in the different units controlled the development of different surface and endokarst features in each of the sediment units above, and, together with lithology, were used as main criteria to correlate displaced boulders to respective source areas and layers (Oliveira, 2011).

In addition to karst, aeolian grooves indicating sand blasting by N10° – 25°W wind are numerous and widely scattered.

About ten boulders of variable mass (mostly under 2.5 ton) have been found within a 30 m- wide area, up to 11 – 12 m msl, their source layers located seaward and at lower elevations, indicating prevailing transport to the northeast. Among these, boulder E1B1 stands out by its size, its mass having been estimated to 18 tons. E1B1 is turned upside down, as demonstrated by aeolian grooves and pronounced karst sculpturing together with upward narrowing clefts at its bottom face, which are in contrast with the smoothness of the top, exposed surface.

E1B1 makes the outermost element of a stack of imbricated boulders sitting at 11 m above msl. Imbrication suggests flow incoming from 165° but reconstruction of the displacement path by connecting the boulder to its source area indicates 220°. The angular difference resulting from the two criteria may be due to multiple entrainment episodes or, more probably, to adjustment of the boulder's attitude when it came to rest against E1B2. The same applies to other and smaller boulders in this region that adapted their attitude to karst irregularities.

Using vectorial relations between flow direction and trend of long axis, E1B2 indicates eastward displacement, whereas the broad imbrication pattern indicates NE; E1B10 could have travelled westward and E1B3 in the opposite direction. Source to sink spatial relations in the latter case actually suggest flow from 220°-230° as most probable. This illustrates uncertainties in

reconstructing flow direction using only attitude of a small number of particles dispersed over an irregular substrate.

The oldest available aerial photographs of this area show that half of these boulders have been emplaced prior to the early 1940's and that they remained immobile since then (the extension of the aeolian sand cover in those photographs precluded identification of the remaining particles).

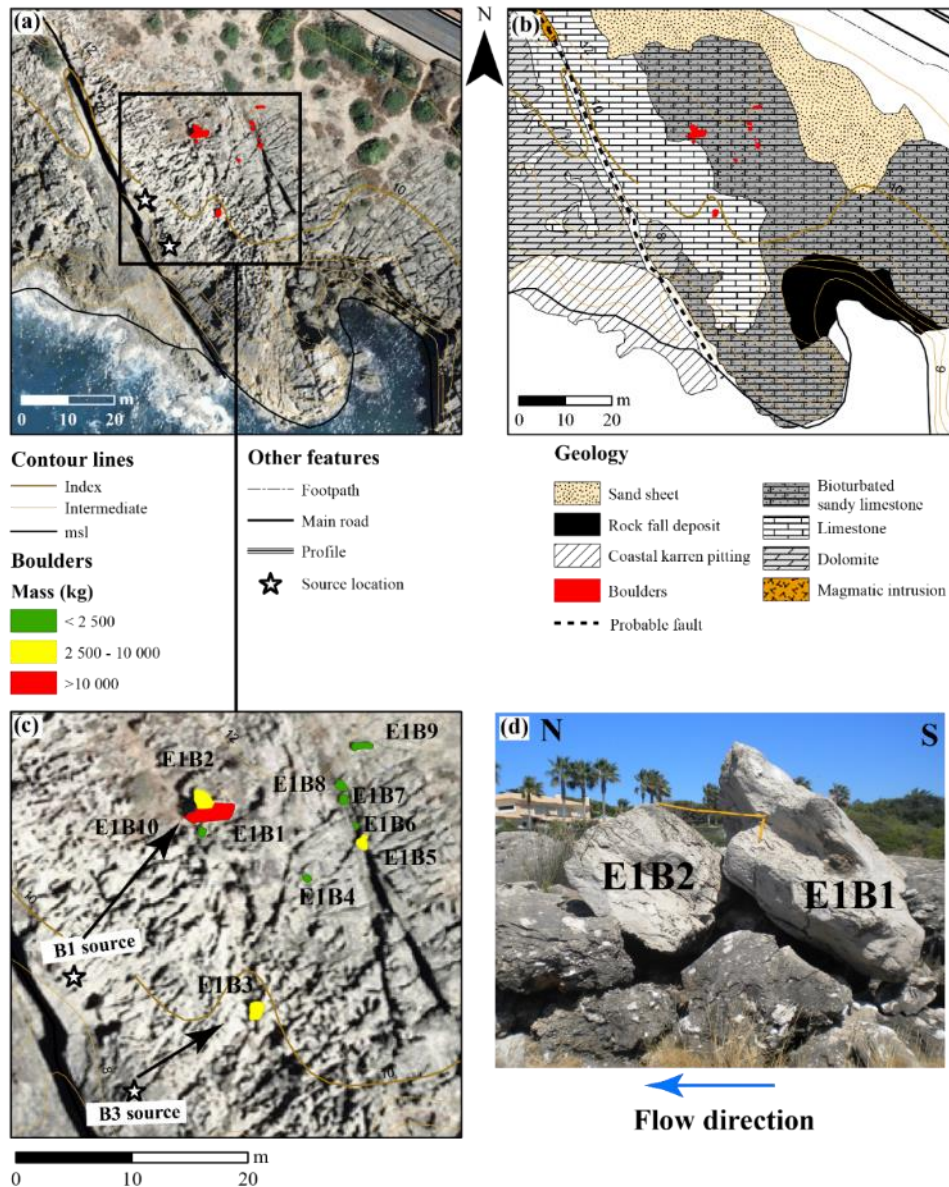


Figure 27. (a) Orthophoto of region at site # 2 showing the location of boulders over the platform and probable source areas; (b) geological map; (c) boulders' location, mass and flow direction inferred from a-axis direction and source location; (d) photograph showing imbrication and inferred flow direction. Modified after Oliveira (2011).

An additional effort to further constrain the time of boulder emplacement was attempted by installing a microerosion meter measurement station on a small dissolution pool affecting the upper surface of E1B1; the dissolution feature apparently developed after E1B1 came to rest in

its present location and position. Two measurements acquired 5 years apart yielded 0.0179 mm for the average total downwearing of the pool's bottom (rate of 0.0036 mm.yr⁻¹), which is lower than the magnitude of uncertainty, and thus not significant. It is also one order of magnitude lower than the minimum value indicated by Scheffers and Kelletat (2005) as representative of karst downwearing rates in limestone substrate. It was not possible until present to further constrain the chronology of emplacement of the boulders or to find evidence of successive re-entrainment episodes.

One interesting additional feature may be observed in this particular location, and relates with the widespread occurrence of well cemented and hard, iron-rich, and black to brown sediment infilling or coating the walls of karst hollows, especially at the seaward region of the rocky platform. The precise age of formation of those infills is unknown but they should correspond to Late Pliocene or Pleistocene paleo-karst deposits. Close to the possible socket of E1B1, karst galleries were exhumed and expose these materials, which are overlain by a mat of well-rounded very coarse quartz sand of marine facies, including gritt, occasional small and rounded, disk-shaped quartz pebbles, and marine shell fragments. The elevation of this particular occurrence was measured to about 7 m above msl. Taking into account the Pleistocene sea-level history and terraces affecting this coast, together with the accommodation volume and permeability offered by endokarst features, it is reasonable to consider that during Pleistocene (and earlier?) higher-than-present sea level stands, the lowest part of the presently exposed rock surface should have been submerged. This would have allowed marine sediment to invade the endokarst and accumulate up to some distance above the coeval sea-level. This hypothesis implies that the ancient coastline would have been located more landward than at the present. In this case, the distances separating boulders from ancient coastlines would have been much smaller and they could just represent geological signatures of Pleistocene storms.

This hypothesis would also solve the difficulty in devising the mechanism by which a large and heavy boulder, such as E1B1, could have been transported more than 20 m landward (and about 3 m upward) across an extremely rugged surface, where multiple large hollows and ridges and scarps could have easily stopped it.

Field observations of the endokarst deposits, though not exhaustive, indicate that paleo-karst infills can be traced up-platform to about 9.5 m above msl but the rounding, size and composition of the sand changes with increasing altitude. At higher elevations, the cemented sand includes about 1/3 of sub-angular to sub-rounded quartz particles, and sorting is less effective; the biogenic contribution increases and is similar in size, preservation and diversity to the biogenic component observed in Holocene sand deposits at the inner edge of the rocky platform and nearby colluvium. This may indicate mixture of ancient beach sand with materials sourced further inland and later transported by wind and run-off, which eventually infiltrate the endokarst adding an additional complication to the working hypothesis above.

Site # 3

This site is located 1 km west of the Guia lighthouse at the western scarp of a steep-sided and narrow valley (matacão) related with a N20°W fracture and dyke, both having been extensively exhumed by weathering and marine abrasion (Figure 28). The surface of the platform gently slopes seaward, in agreement with the general dip of strata (SW), until it meets a low (5 m-high) plunging cliff at the interface with the sea. The platform surface is structural at its seaward end, and exhibits abundant scars of quarrying. Sand patches including shell fragments occur confined to karst depressions in the northern half of the platform and linear aeolian abrasion grooves (ventifacts, trending N 30-35° W) re-sculpturing limestone and dolomite outcrops are widespread.

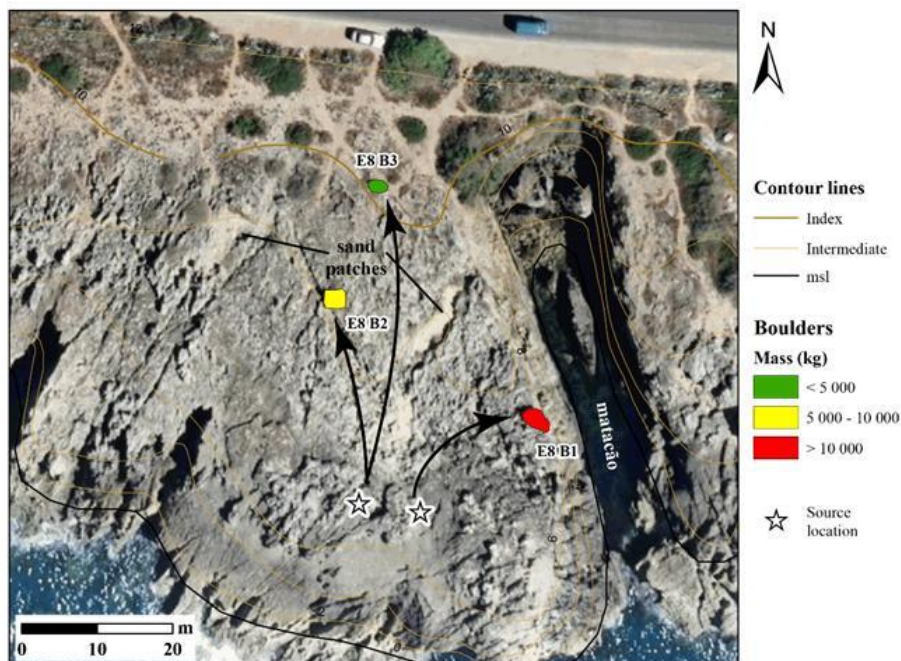


Figure 28. Vertical image of the coast at site 3 showing location of boulders and features referred in text. Arrows show Inferred directions of boulder transport and source areas are represented by stars.

A number of metric-sized boulders can be found scattered across the rock platform at this location up to 10 m above msl. The northern boulders (E8B2 and E8 B3 in Figure 28) are platy in shape and much smaller than E8B1. Each boulder encompasses two layers of dolomitic limestone. They have been pushed across the rocky platform up to about 55 m landward of their source area, which were determined using lithostratigraphy and karst sculpturing of the top layer as location criteria. No indication of the age of their emplacement could be found, nor if it was achieved by one single stroke or by accumulation of shorter dislocations.

Boulder E8B1 sits close to the edge of the western slope of the matacão, at about 8 m msl and its mass was estimated to about 15 ton (Figure 29).



Figure 29. Photograph of boulder E8B1, consisting of three layers (landward view). The steep wall limiting the matacão and the paved path covered by the boulder are visible at the right and center-up region, respectively.
Photo by M.A. Oliveira.

This platy boulder rests with normal polarity and is tilted towards the valley. It consists of a fracture-bounded piece of dolomitic limestone where three layers can be distinguished. Its source area is located 20 m to the SW and was found using lithological, stratigraphical and micromorphological criteria. Just like the other boulders in this location and elsewhere in this coastal stretch, there is no evidence allowing to resolve if the dislocation occurred by single or multiple strokes. One interesting aspect of this boulder is that it sits on top of a path used to access an angling spot and the path is paved with 20th century construction materials, thus ruling out tsunamis as drivers of entrainment, transport and re-deposition. This boulder was captured by the 1940's aerial photograph in its present location and thus the time elapsed since it was emplaced is small. However it was not yet possible to further constrain this time window and to relate its emplacement with any particular storm event. Just like in the previous observation spot (site #2), it is difficult to envisage the storm wave mechanism allowing for the displacement of E8B1 across an extremely irregular and rugged topographic surface such as the one separating the source and emplacement locations, even if cumulative effects of succeeding waves of the same storm are invoked.

Post-Meeting Field Trip

Tsunami deposits in the Algarve coast of Portugal

September 6 and 7, 2017

C. Andrade, P. J. M. Costa

candrade@fc.ul.pt, ppcosta@fc.ul.pt

Departamento de Geologia, Instituto Dom Luiz, Faculdade de Ciências da Universidade de Lisboa, Bloco C6, 3 piso, Campo Grande, 1749-016 Lisboa, Portugal

Introduction and objectives

The Algarve south-facing coast of Portugal was extensively impacted by the AD 1755 earthquake and tsunami (cf. Costa, 2005 and references therein for documentary sources and description of damages and social impacts). The extension and intensity of the 1755 marine flooding of this coastal area was unprecedented in historical times. Some authors suggested that pre-historic (likely) tsunamis of very high magnitude may also have affected this coast (e.g. Schneider et al., 2010, Trog et al., 2013, 2015). However, the available body of evidence forwarded in these studies is insufficient to discard alternative and more plausible drivers for the sedimentological and palaeoecological signatures supporting the single-event interpretations therein (see Andrade et al., 2016 for a discussion).

In contrast with the western-facing coast of Portugal, the Algarve coast has been thoroughly surveyed and investigated since the 1990's for sedimentary and geomorphological signatures of past tsunamis. Moreover, Andrade et al. (2016) compared and cross-correlated the data set retrieved from geological approaches with the documentary database, extending back in time to Roman times, and estimated in >3.5 kyrs the average time window separating two consecutive high intensity regional tsunamis, capable of extensively inundating coastal regions along the whole Algarve shoreline. This result is in agreement with return periods of 3.6 to 7.2 kyrs forwarded by Matias et al. (2013) for a Mw=8 tsunami-triggering submarine earthquake sourced in the wide Gulf of Cadiz.

This extremely large return period and pronounced contrast between the inundation potential of storms and of the 1755 event makes the Algarve coastal lowlands ideal to investigate the sedimentary signature of that tsunami. Work undertaken so far allowed contributing to the ongoing debate on using the sedimentary record for unequivocal signatures of tsunamis (versus storms). It made use of a varied suite of proxies (describing texture, structure, stratigraphy of deposits, geomorphology, composition, SEM-based grain micromorphology, paleoecology,

geochemistry, magnetic properties of the sediments, OSL, radiocarbon and stable-isotope dating) to address and reconstruct aspects of the inundation processes, such as inland extension of inundation, height of tsunami waves when crossing the shoreline, run-up, distinguishing between inundation pulses and between inrush and backwash flows, source of the sediment and volumes of sediment involved in tsunami inundations, quantification of tsunami-induced erosion, and mechanisms of sediment transport in relation with flow patterns.

Post-meeting field trip will address four sites along the Algarve coast, ranging between the sediment starved and cliffed coast of the western Algarve to the sand-abundant barrier coast of the eastern Algarve. The main objective of this field visit is to provide an opportunity to discuss work undertaken (though still ongoing) on essentially sandy deposits related with the 1755 tsunami by presenting and discussing, in the field, interpretations of morphological, sedimentological and chronological data obtained so far in coastal lowlands of the Algarve, some of which became now “classical” examples of tsunami investigation in Earth Sciences.

Most of the ground work and summary compiled in this guide was developed under projects GETS (FCT PTDC/CTE-GEX/65948/2006) and NEAREST (EU – 037 110_2008-2010).

Geology and geomorphology – an overview

The Algarve coast locates at the western tip of the broad Gulf of Cadiz, in the SW margin of Iberia (Figure 30) and comprises the easternmost segment of the Azores–Gibraltar fracture zone, which is interpreted as the Atlantic Africa–Eurasia plate boundary. This boundary is considered responsible for most of the large magnitude seismic and tsunami activity affecting the Portuguese margin.

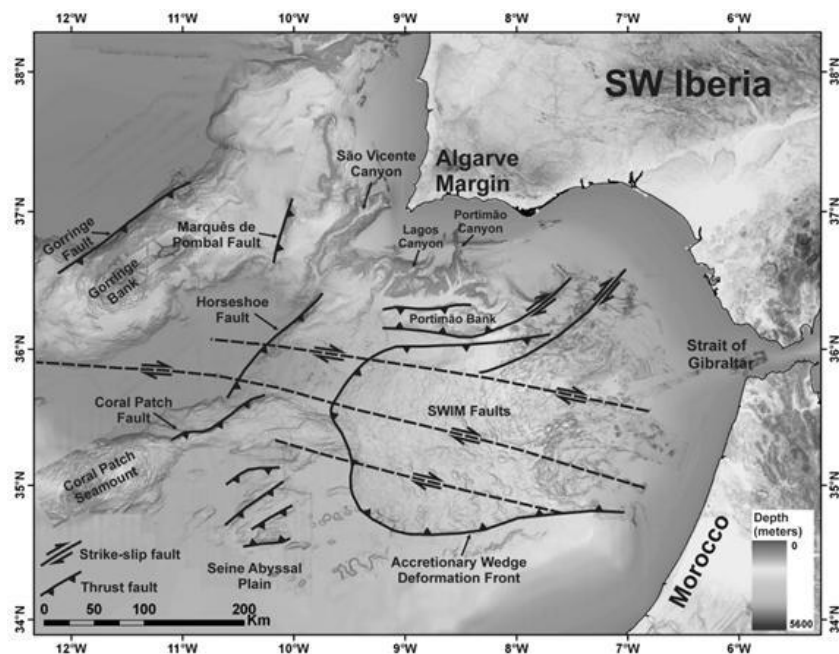


Figure 30. The broad Gulf of Cadiz, morphology of the ocean floor and major tectonic features related with the Azores-Gibraltar plate boundary (adapted from Duarte et al., 2011).

The southern Portuguese coastline presents a high degree of morphological asymmetry mainly due to differences in the local geology (Figure 31 and Figure 32).

In its westernmost section, the coastline is strongly irregular, developing in resistant Mesozoic limestone, the geotectonic setting favoring the development of high (ca. 70 m above msl) and steep (at times, plunging) cliffs, occasionally interrupted by small pocket beaches. These beaches accumulate thin veneers of sand over gravel and occur in relation with deep and narrow embayments at the outlet of small intermittent streams, which run through deeply incised, tectonically controlled, canyons. The streams drain small drainage basins and the sand input to the coast is very small.

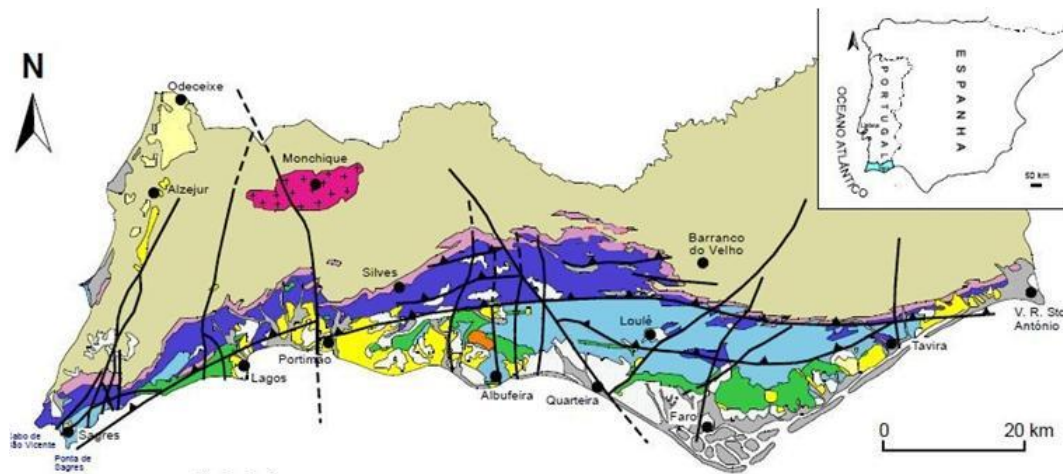


Figure 31. Geological sketch of Algarve (modified after <https://blacksmoker.files.wordpress.com/2010/09/algarv2.jpg>) (for details on E Algarve locations see Figure 79).

Central Algarve coast is cut in intensely karstified detritic limestones and poorly consolidated silty-sandstone of Miocene age. The coast is in general cliffed, with steep slopes and pocket beaches. Lithological contrast of outcropping rocks and an inherited endokarst, at present experiencing exhumation, favored the development of a strongly crenulated coastline featuring abundant points and coves, sea stacks, caves and arches. Sand supply is moderate and ensured by streams, small rivers and cliff erosion. Streams and rivers present larger drainage basins and outlet in lagoons, barred estuaries and wide bays with sandy beaches frequently backed by cliffs and, in cases, by dunes.

In contrast, the eastern Algarve coast shows higher abundance in sand and comprises only depositional forms, such as the barrier-lagoon system of Ria Formosa. The easternmost barrier root merges with the Manta Rota beach and foredunes, that together make the seaward edge of a ridge-and-swale prograding coastal plain limited eastward by the Guadiana estuary.

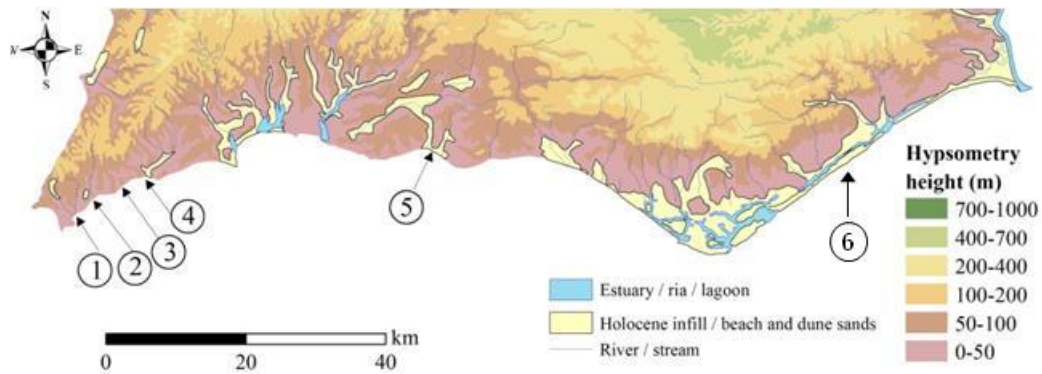


Figure 32. Algarve hypsometry, with location of main rivers, estuaries and lagoons and lowlands with sedimentary record of the AD 1755 tsunami: 1. Martinhal; 2. Barranco; 3. Furnas; 4. Boca do Rio; 5. Alcantarilha and Salgados; 6. Tavira barrier. Modified from Costa et al., 2016

Wave and tidal regime along the Algarve coast

The south facing coast of Algarve is a mixed energy, tide-dominated (Hayes, 1979) coast. Tides are semi-diurnal and range between 2.8 m (spring) and 1.3 m (neap) with maximum tidal range of 3.5 m (i.e. reaching 1.8 m above msl). Just like along the western coast, the contribution of storm surges to sea surface elevation is relatively small. Taborda and Dias (1992) indicate a typical value of + 0.42 m for the Lagos tide gauge but higher values were measured in the Ria Formosa lagoon in relation with spring tide and severe storm conditions (Esaguy, 1984).

According to Pessanha and Pires (1981) this coast is dominated by a low-energy wave regime with mean annual significant wave heights (H_s) slightly below 1 m and mean period of 5 s, with average T_p of 7 s (Costa, 1994, Costa et al., 2001). Calm sea ($H_s < 0.5$ m) represents about 1/3 of sea state observations. Conversely, H_s of storm-generated waves approaching from the SW during winter commonly reach values of about 3-4 m and period of 7-8 s. Southeasterly waves of lower heights and periods are generated by strong easterly winds blowing in the Gibraltar straight region. These short-period waves (sea) occur throughout the year and raise moderate storms with decreasing intensity westwards. According to Costa et al. (1994) the frequency of storms ($H_s > 3$ m, essentially south-westerlies) impacting this coast is about 9, on yearly average. Maximum significant wave height measured at the wave buoy moored in deep water offshore Faro was 7.5m and the return period of a 6 m H_s wave was estimated in 30–50 years (Pessanha and Pires, 1981, Filipe et al., 2000).

The nearshore and coastal mild wave regimes reflect significant attenuation of waves generated far in the north Atlantic when approaching an essentially west-east elongated coast. Just like in the western coast, the impact of storms along the Algarve coast is related to breaking or broken waves, rather than inundation caused by intense storm-related surges.

Littoral drift along the Algarve coast is dominated by southwesterly waves and predominately directed eastwards. The magnitude of potential net drift was estimated to $10^4 - 10^5$ m³year⁻¹ using an energy flux approach and quantification of geomorphological changes in barrier islands (Andrade, 1990a). Sand sources are essentially related to cliff erosion of Miocene and

Pleistocene materials in the central Algarve coastal ribbon, added by limited contribution of streams and retreating cliffs cutting Miocene sand and sandy limestone.

Coastal evolution throughout the Holocene

Lowlands of the southern Algarve coast evolved throughout the Holocene in three fundamental stages (Allen, 2003, Freitas et al., 2003a, 2003b, Dinis et al., 2006, Schneider et al., 2010, Trog et al., 2013, 2015), and this evolution was to a large extent influenced by relative sea-level changes (Figure 33).

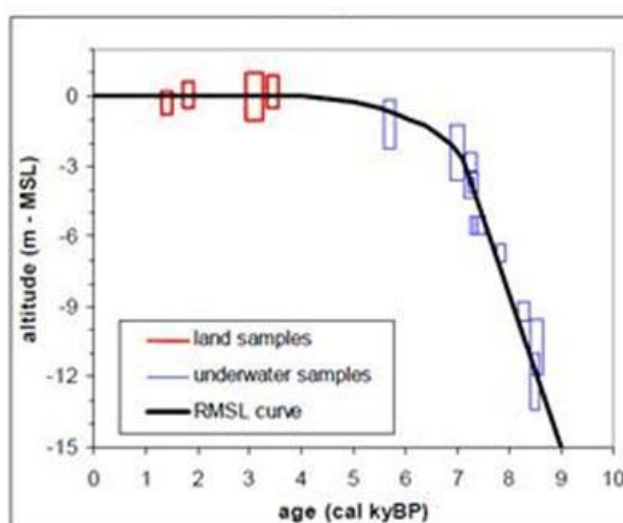


Figure 33. Holocene relative sea-level curve for the Algarve coastal region according to Teixeira et al. (2005).

The first stage corresponds to the marine inundation of topographic surfaces that were deeply dissected during Pleistocene low-stands of the ocean. The rapid rise in sea level characterizing the onset of the Holocene transgression originated an irregular, drowned coastal landscape, allowing the inland penetration of marine influence and promoting the infill of valleys and morphological lows.

The second stage starts with the transgressive maximum at 7.5–7 ka cal BP (Freitas et al., 2003a, Vis et al., 2008) when sea level rise rate dropped pronouncedly and later almost stabilized close to the present-day level (about 5 ky cal BP, cf. Teixeira et al., 2005). This allowed barriers to develop diachronically along this coast, between ca. 4.5 and 1.35 ky cal BP (Dawson et al., 1995, Costa et al., 2012, Trog et al., 2013), enclosing estuaries and lagoons that acted as depocenters for both marine and land-sourced sediment, the latter increasing in expression with the reduction of the tidal prism motivated by persistent siltation.

The third stage occurred during the last millennia, when marine and terrestrial sediment promoted partial to complete infilling of these depositional environments. The general pattern of change experienced by the Algarve lowlands in the Late Holocene was partly driven by human

influence and consists of shallowing and surface reduction of confined transitional water bodies, configuring a forced regression (Freitas et al., 2010).

The regional Holocene lithostratigraphy, the geochemical and paleoecological contents of the sediment infill of the lowlands correspond to depositional episodes reflecting each stage above. However, they set up diachronically in space in function of local differences in sediment input and morphological development of each basin.

The lower sedimentary unit, Unit A, essentially consisting of coarse detritic materials bearing marine signature and predating the formation of the barriers, represents the high energy open environment developed in tune with the drowning of the previous landscape. These sediments rest directly upon the dissected bedrock or cover Late Pleistocene – Early Holocene fluvial materials. Unit A is covered by alluvial, estuarine, or lagoonal muds and sands of Unit B, which accumulated in progressively shallower, low energy, and restricted depositional environments developed after the barriers developed. Unit C, the upper sediment unit (representing the present-day depositional system) essentially consists of (1) organic sand and mud and marginal peat, in alluvial plains or floodplains; (2) sand and mud where fluvial or stream-driven bay-head deltas accreted or prograded over former lagoonal or estuarine expansions. These sediments represent the final stages of evolution of coastal lowlands affected by an inexorable trend towards terrestrialization.

STOP 1 – Boca do Rio

Context

Boca do Rio is located between S. Vicente Cape and Lagos (Figure 34). It is a small flat-floored and sediment filled lowland located within the otherwise high-cliff coastline of the western Algarve (Figure 35 to Figure 38). The lowland area consists of a supratidal floodplain that is periodically subject to extensive river flooding. The Cretaceous limestone and marly limestone cliffs that limit the Boca do Rio beach reach heights of *ca.* 40 m above msl close to the inlet (Figure 39). The alluvial plain presents an average height of 1.7 m above msl and reaching 3m above msl to the north of the plain. The area is separated from the sea by a storm gravel and sand ridge and by a rock spur that together form a barrier to wave overtopping during storms (Hindson *et al.*, 1996). A high dune at *ca.* 8-10m above msl existed in Boca do Rio at the time of the AD 1755 tsunami (Pereira de Sousa, 1919) but the natural system failed to rebuild a robust dune or beach since then (Oliveira *et al.*, 2009). The beach is 200 m long and 115 m wide and the beach berm rests at 2.1m above msl. The drainage basin develops along *ca.* 80 km² in Palaeozoic schist and greywacke, claystone, Triassic siltstone and sandstone, Jurassic and Lower Cretaceous limestone and marls and Plio-Pleistocene sand and sandstone.

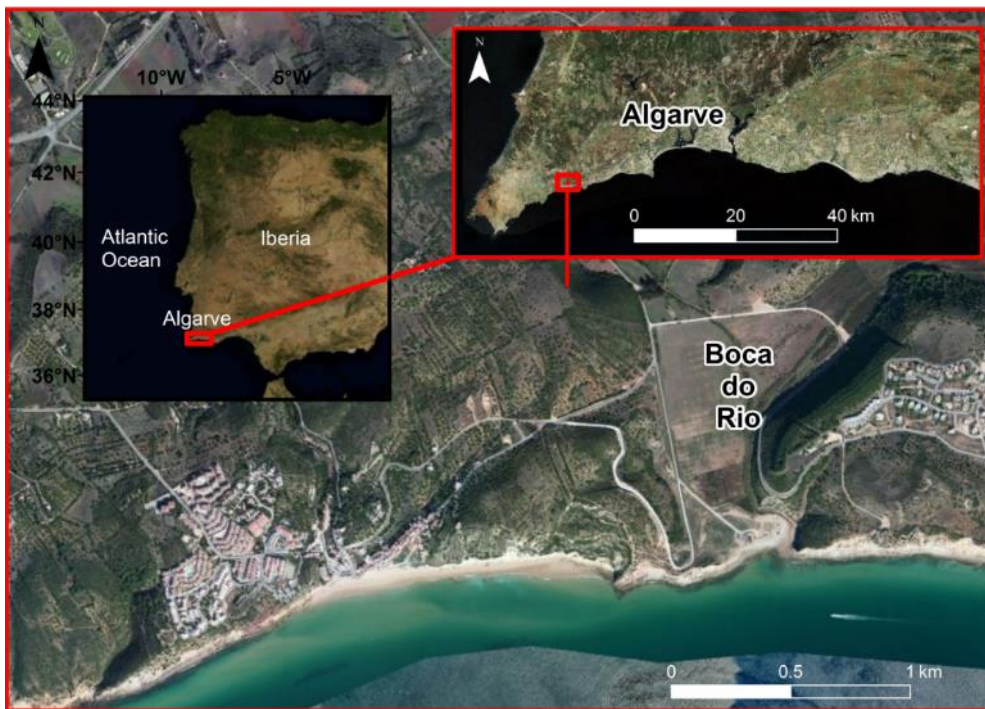


Figure 34. Location map of Boca do Rio. Modified from Costa (2012).

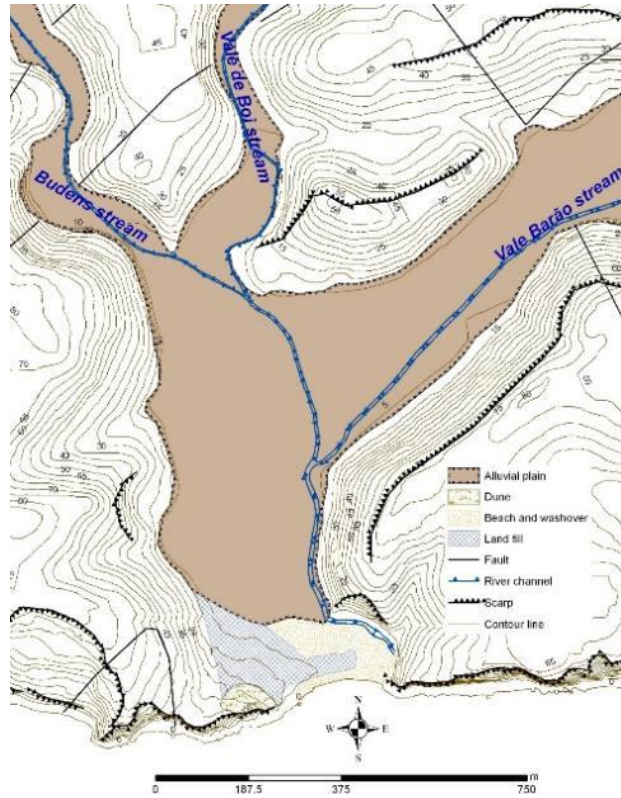


Figure 35. Geomorphological sketch of Boca do Rio (adapted from Andrade et al., 2010b and Costa et al., 2015).



Figure 36. View to the Boca do Rio alluvial plain and beach (photo facing the East). Photo by M.C. Freitas.



Figure 37. View to the west at Boca do Rio beach during winter (no sand can be observed contrary to the summer beach). Photo by M.C. Freitas.

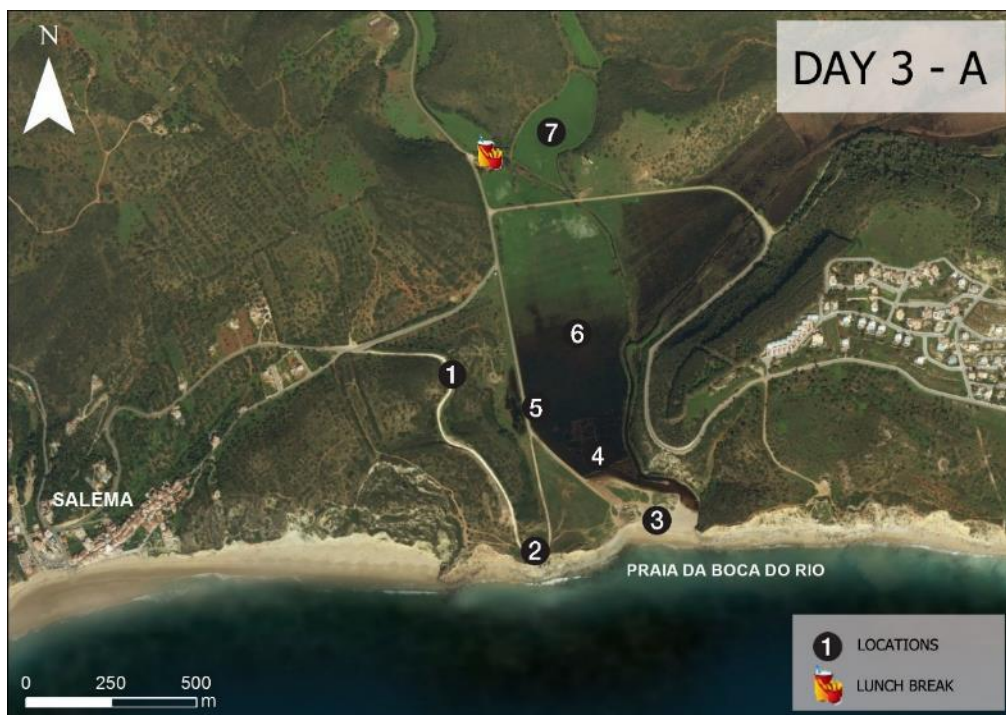


Figure 38. Points of observation (1 to 7) during the 5th ITFS Post-Meeting Field trip. Aerial image from ArGIS TM database.

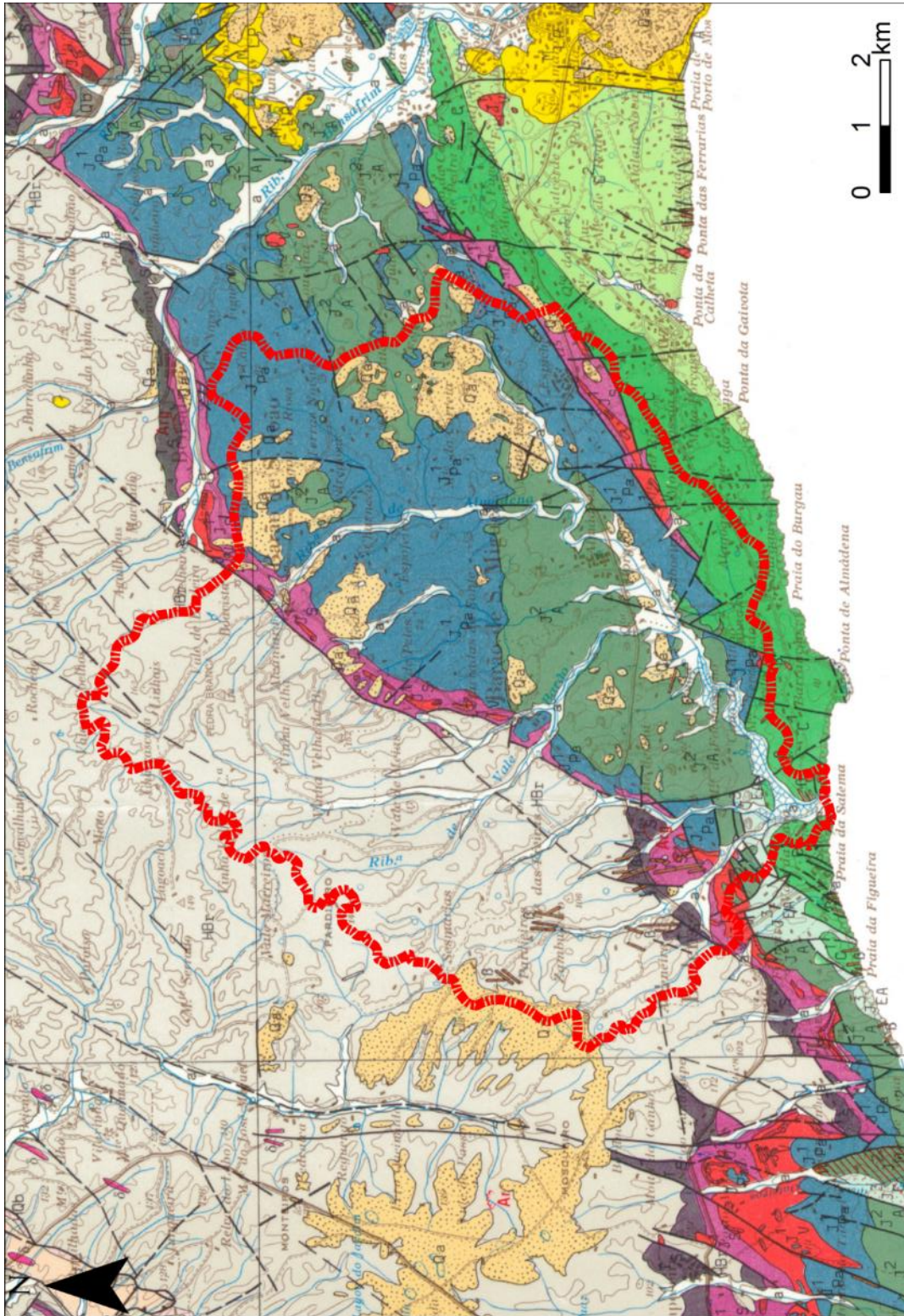


Figure 39. Drainage basin of Budens, Vale de Boi and Vale de Barão streams that drain to Boca do Rio alluvial plain (east of Praia da Salema). Modified from Manuppella (1992). Legend is in Annex 1.

Late Holocene stratigraphy

Four lithostratigraphic units represent the Late Holocene infill of Boca do Rio lowland.

Basal Unit 4 consists of medium sand and gravel with marine shell fragments representing deposition in drowned estuarine environments open to marine influence, predating the barriers, which formed diachronically between 2180 and 1360 yrs cal BP in the western and central Algarve (Dawson et al., 2005, Hindson et al. 1999, Kortekaas and Dawson, 2007, Costa et al., 2012).

Unit 3 consists of alluvial/estuarine muds, with few sand layers towards the base, representing low energy sedimentation in a restricted environment that followed barrier formation (Figure 40).

Unit 2 corresponds to a widespread layer of marine sand with shell fragments, which rises and thins inland. Muddy rip-up clasts are frequent and floating limestone boulders may exist at its base, which is erosional, reflecting the high energy deposit of the AD1755 tsunami inundation.

Unit 1 caps the sequence and atop represents the present-day depositional system. It consists of alluvial muds with freshwater molluscs and abundant fermented plant remnants.

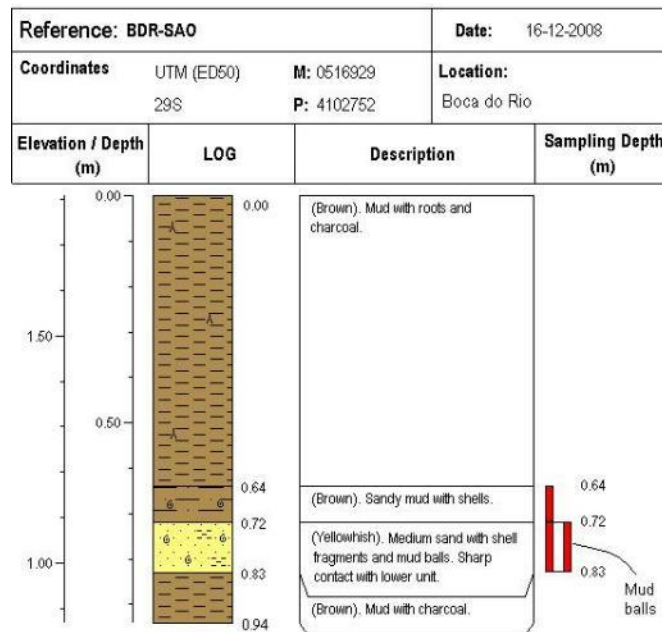


Figure 40. Macroscopic lithostratigraphic log description of sample-core SAO that roughly corresponds to the schematic lithostratigraphy of the alluvial plain topmost meter showing Units 1 to 3 (Costa, 2012).

The AD 1755 tsunami deposit

In Boca do Rio, according to coeval sources (Pereira de Sousa, 1919), the tsunami waves overtopped a large foredune and reached 11-13 m above msl. A detailed description of the effects of the backwash was also made, referring to the uncovering of Roman ruins in the beach

area that have been hidden for a very long time under aeolian sand. Since AD 1755, the coastal system has not been capable of rebuilding a robust foredune.

The tsunami deposits of AD 1755 that accumulated in Boca do Rio mostly consist of a laterally extensive layer of shell-rich sand displaying an erosive base and a gradual and irregular upper boundary. The tsunami layer ramps and thins landwards. In some locations, the tsunami deposit is entirely composed of sand. In other areas of the alluvial plain, it is characterized by sand sheets containing isolated (also referred to as “floating”) cobbles (Figure 41 and Figure 42).

The sandy tsunami layer in Boca do Rio consists of distinct sub-units that vary greatly in texture both vertically and horizontally. This unit is in contrast with the mud-dominated sedimentation, of terrestrial source, observed in the under and overlying units. The highly variable nature of the sandy horizon appears to be due to rapid variation in the hydrodynamic characteristics of the depositional event (inundation, backwash and periods mediating both processes where mud could settle) and diversity in source materials. The tsunami deposit detectable at ca. 0.80 m below the surface wedges out and becomes discontinuous landward, but it can be traced for more than 1.3 km inland (Figure 43 and Figure 44).



Figure 41. Trench wall (app. 1 m high) with yellowish sandy tsunami unit visible and clearly identifiable with cobbles at its base. Photo by M.C. Freitas.



Figure 42. Left image - detail of cobbles within (at the base of) the tsunami deposit. Right image – Vermetids, perforations and endolithic bivalves in cobbles. Photos by M.C. Freitas.



Figure 43. Sandy tsunami deposit at Boca do Rio. Left image shows the thickness of the overlying muddy unit (trench wall is app. 1m high). Right image displays the tsunami massive character in this trench. Photos by M.C. Freitas.



Figure 44. Contrast between under and overlying muddy units and the yellowish massive sandy tsunami deposit. Photos by M.C. Freitas (left) and M.A. Oliveira (right).

The likely source of the tsunami deposit has been discussed by several authors (Hindson et al., 1996, Hindson and Andrade 1999, Costa, 2012, Costa et al., 2012, Costa et al., 2015) using spatial, grain-size, micropaleontology, micromorphological, microtextural and heavy mineral analyses (e.g. Figure 45 and Figure 46) and all implied the beach and the dune as the main sedimentary contributors for the tsunami deposit and that the offshore/nearshore was the unlikeliest source.

In the establishment of provenance relationships, microtextural analysis revealed that tsunami sediments present very high results for fresh surfaces (similar to beach samples) and the highest value for percussion marks (also very high in dune samples) – Figure 47.

The heavy mineral assemblage analysed in the inner areas of the alluvial plain might suggest incorporation of backwash material in the tsunami deposit, although the massive facet of the deposit constrained the clear identification of sub-units that could reinforce that conclusion.

Calcareous nannoplankton, foraminifera and ostracoda assemblages in the tsunami deposit are diverse, containing a variety of predominantly marine species (Hindson et al., 1996; Hindson and Andrade, 1999), which is in contrast with the assemblages observed for the under and overlying

units, which are dominated by a small number of species that were able to tolerate the variable salinity conditions typical of estuarine and salt marsh environments.

The hydrodynamic behaviour in the alluvial plain was complex and it is reflected in textural, compositional and structural features of the tsunami deposit. For example, sand content in the tsunami deposit decreases with distance inland. A more complex behaviour is observed when median grain-size of total sediment is analysed. This more variable trend is interpreted as a result of local topographic effects, incorporation of variable amounts of mud and, in the inland-most areas, interference of backwash.



Figure 45. Sampling map in Boca do Rio (Andrade et al., 2010b).

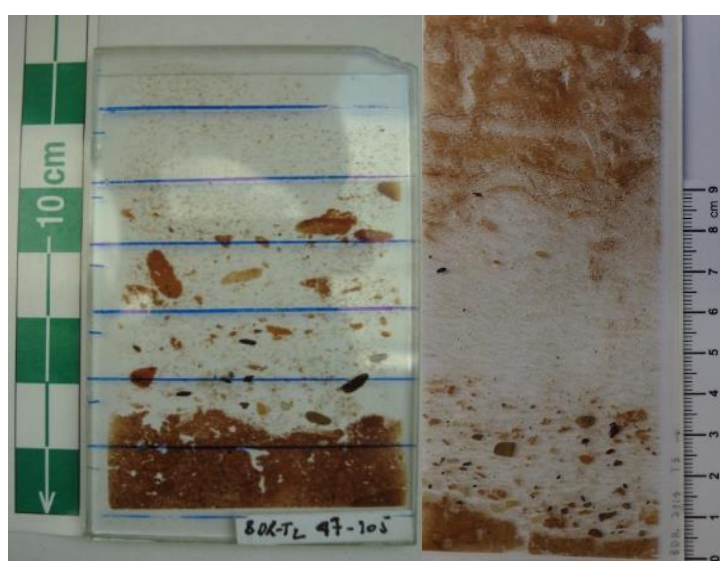


Figure 46. Image of very large thin sections from the tsunamigenic layer and underlying mud in Boca do Rio (Costa, 2012). Note the presence of rip-up clasts and coarse grains in the lower-part of the thin section.

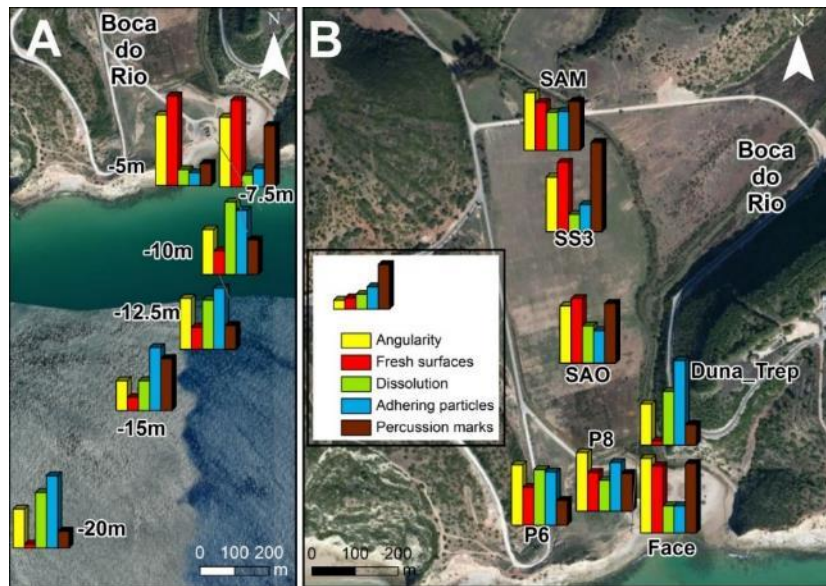


Figure 47. Microtextural results and their spatial distribution in Boca do Rio. A- Nearshore samples. B- Beach, dune and tsunami samples (Costa et al., 2012).

In terms of sedimentary structures, Boca do Rio deposit is very rich presenting basal erosional contacts, rip-up clasts, sigmoidal features, floating boulders/cobbles, etc. Some are particularly visible in the inland-most area (like sigmoid structures – Figure 48), others are more visible closer to the coast. Again, this richness and variability confirms the unique relevance of Boca do Rio deposit in tsunami geosciences.

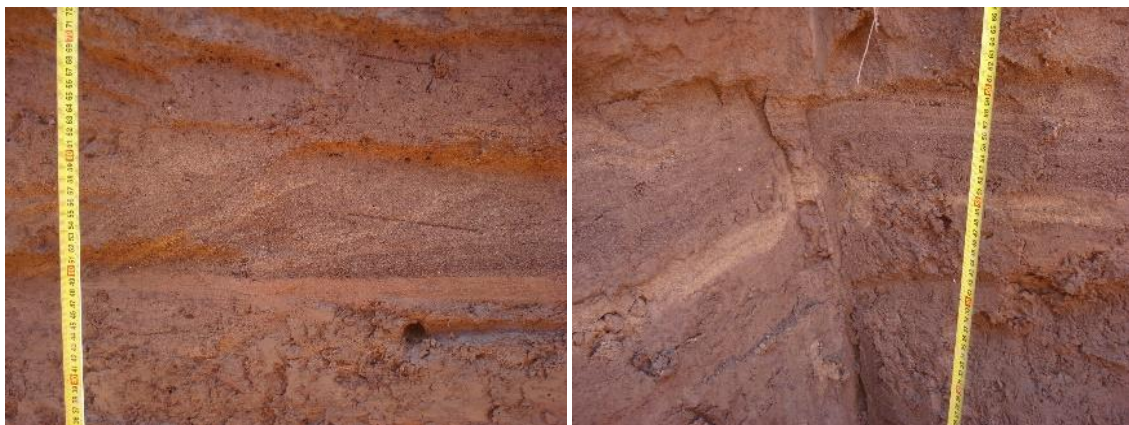


Figure 48. Details of sedimentary structures, namely sigmoidal structures above a massive yellowish sandy layer – sign of a backwash composed of fluvial sand? Photos by M.C. Freitas

STOP 2 – Martinhal

Context

Martinhal lowland is a small flat-floored valley which corresponds to the outlet of the Mós stream (Figure 49 to Figure 52). It cuts Middle and Upper Jurassic limestones, dolomitic limestones and marly limestones. The alluvial plain is located immediately to the east of Sagres (Figure 53). The lowland is roughly triangular in shape and is separated from the sea by a sandy barrier formed by a beach/(small) foredune ridge system (Andrade et al., 1997). During storms the barrier may be breached and marine water floods the lowland.



Figure 49. Location Map. Martinhal, visited on Day 2, is located in the B sector of the right-hand image. Aerial image from ArGIS TM database.



Figure 50. Points of observation in Martinhal during the 5th ITFS Post-Meeting Field trip. Aerial image from ArGIS TM database.



Figure 51. Martinhal beach and view to the west (Sagres). Photo by M.C. Freitas.

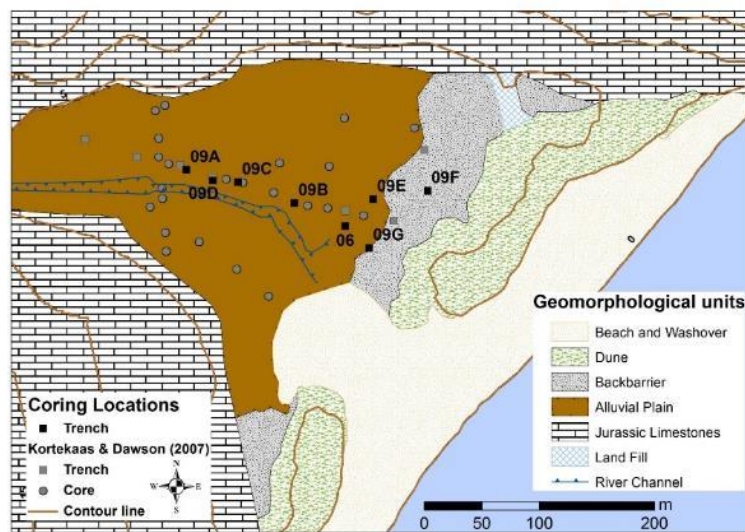


Figure 52. Geomorphological map of Martinhal (Cunha et al., 2015).

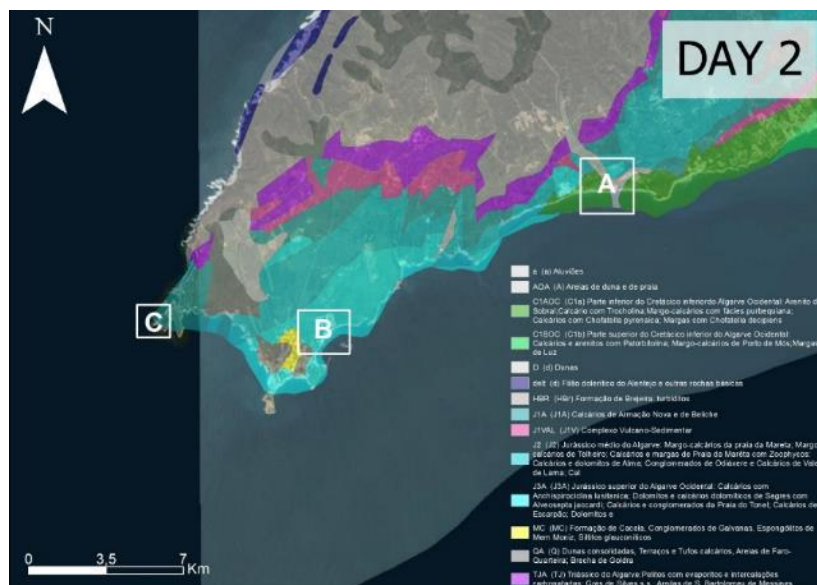


Figure 53. Schematic geological map of the SW Algarve. Martinhal is located in B.

Late Holocene stratigraphy

The lithostratigraphy of sediment-infill at Martinhal shares many similarities with other alluvial plains in the region (e.g. Boca do Rio). Earlier studies (Kortekaas, 2002; Costa, 2006; Kortekaas and Dawson, 2007; Andrade et al., 2010a) identified four major units in this sedimentary infill, which are also summarized in Cunha et al. (2015) and are the base of the descriptions below – Figure 54 to Figure 56.

Typically, grey shell-rich medium sand constitutes the basal unit (corresponding to *ria* or drowned estuarine environments fully open to the sea), pre-dating the establishment of the barrier. This is followed by thick brown clayish units representing monotonous low-energy sedimentation within a brackish lagoon or barred estuarine environment. This succession testifies the progressive infilling of a small estuary, coeval of the increase in efficiency of the sandy barrier. OSL dating (Cunha et al., 2015) indicates that this environment persisted until, at least, ca. AD 1300-1650 and has been interrupted by the AD 1755 tsunami inundation that may have eroded part of the sedimentary column. The tsunami deposit wedges out inland and is composed of very coarse to coarse sand, occasionally gravel, with many shell fragments and rip-up clasts together with small limestone cobbles, especially at the seaward region of the lowland (Kortekaas and Dawson, 2007) (Figure 54 to Figure 56).

Besides the event-layer, the most distinctive aspect of Martinhal's late Holocene stratigraphy is its topmost lithostratigraphic unit that represents sedimentation from the middle 18th century until present. In the seaward region of the lowland it consists of alternating and inter-fingering marine whitish sand and brown mud laminae (Figure 54B). The coarser laminae correspond to overwash episodes (eventually aeolian), whereas the mud was deposited in low-energy barred estuarine sedimentation regime. Farther landward the top unit is more similar to other Algarve lowlands and may reduce to alluvial mud, although in places the stratigraphy may be more complex due to post-tsunami reworking of coarser materials.

The presence of both storm and major tsunami event-layers in such a restricted and small alluvial plain is very rare. Even more so, when both types of event-sediments were deposited just within three centuries. This context provides unique conditions to investigate similarities and differences between tsunami and storm deposits.

Moreover, the overwash deposits are constricted to a narrow time-window post-dating the AD 1755 tsunami and without equivalent signatures in the estuarine sediments underlying the tsunami layer. This suggests that the barrier protecting the estuarine domain was destroyed by the AD 1755 tsunami waves and was never totally rebuild or able to offer the same level of protection regarding storm overwashes.

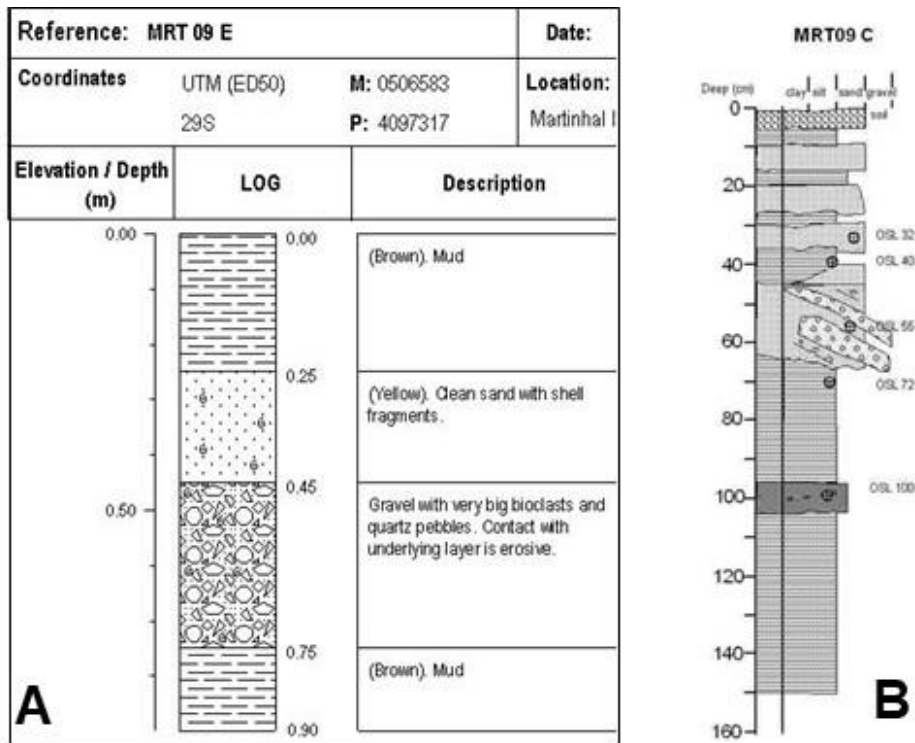


Figure 54. Example of Martinhal's top-meter lithostratigraphy. A - Note textural vertical changes in the tsunami deposit (0.25 to 0.75 m below surface) (Andrade et al., 2010b). B- Note the tsunami layer (45-65 cm below surface) and the alternating coarse and fine laminae in the top-unit (0-45 cm below surface) (Cunha et al., 2015).

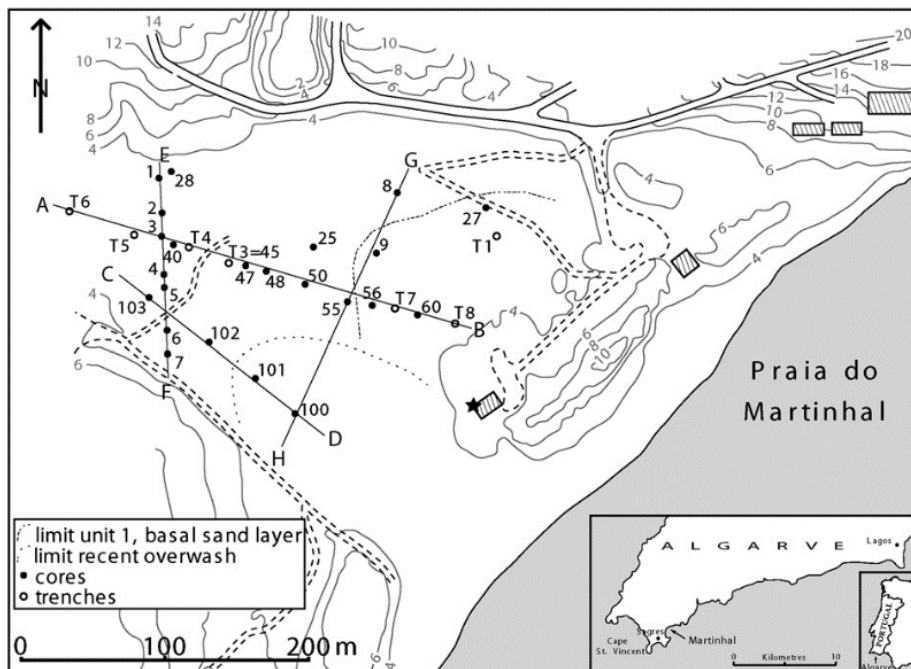


Figure 55. Location of cores and trenches studied by Kortekaas and Dawson (2007).

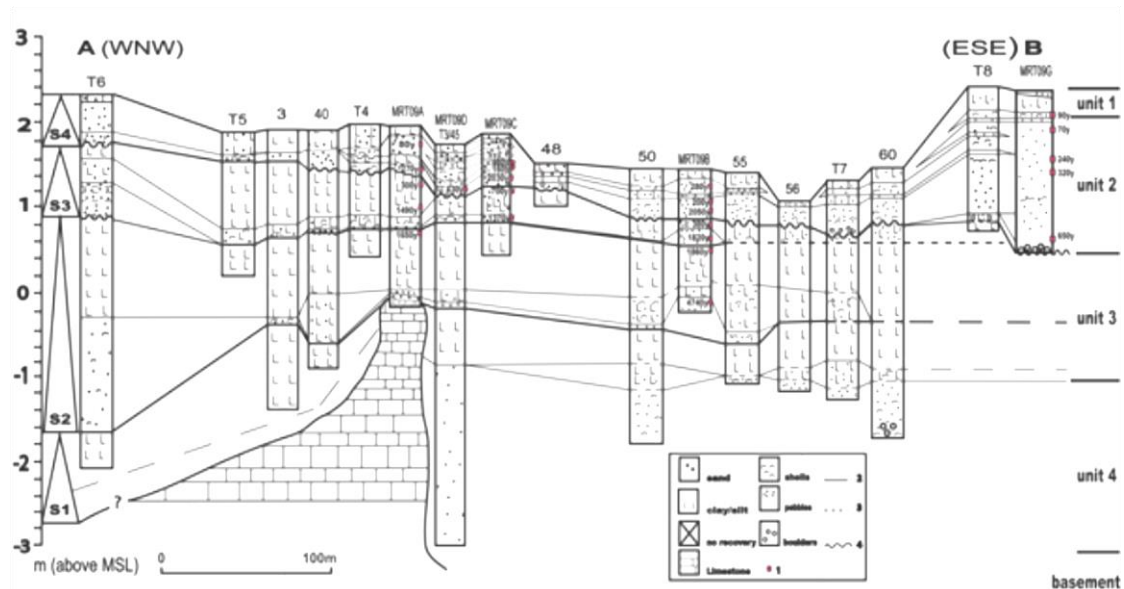


Figure 56. - Detailed stratigraphic correlation along the A-B profile shown in Figure 55 (modified from Kortekaas and Dawson, 2007) in Cunha et al., 2015.

The AD 1755 Tsunami deposit

The historical description in Martinhal is one of the most vivid descriptions regarding the AD 1755 tsunami sedimentological impact. *“The sea flooded a beach called ‘Mortinhal’, facing eastwards, by about 1/2 league (circa 2 km), ripping off vineyards and leaving the land as if it was a beach, covered by several types of fish and big ‘penedias’ (large boulders) of which one, weighing more than 300 ‘arrobas’ (circa 4500 kg), showed many shellfish stuck on its surface. Three times the sea struck and withdrew, the first wave being the largest.”* (Lopes, 1841, translation in Kortekaas and Dawson, 2007).

The AD 1755 tsunami deposit is located between the lower mud and the top layered unit and occurs as a widespread layer of coarse to very coarse sand with many shell fragments, sand-armed mud balls and limestone pebbles (Figure 57 to Figure 60). Grain size characteristics of the sediments, shell and foraminiferal contents and also the presence/absence of rip-up clasts and exotic pebbles, were used to reconstruct distinct sedimentary sub-environments and to distinguish between coarser materials deposited by either tsunamis or storms within the more recent section of the sequence (see references above).

An older episode of coarse sedimentation is embedded in the lower mud unit (Figure 54B and Figure 56). The corresponding sediments are ubiquitous along the lowland and with an extension similar to the tsunami sand sheet, but do not share neither compositional nor textural similarities with both the AD 1755 tsunami-sand and the present-day sediments accumulating within this lowland and in the beach-dune confining system.

Recent observations and interpretations of the depositional architecture suggest a more complex picture for the sedimentation of the sandy units resting upon the lower mud unit, namely due to emphatic lateral changes in facies between trenches located at short distances.

In the most seaward trench (MRT09G - Figure 56), dug in the back-barrier area, the marine deposits correlated with the tsunami unit exhibit only seaward dipping high angle planar lamination, indicating post-tsunami beach accretion by reworking of the sand originally input by the high-energy marine inundation (Cunha et al., 2015). Further inland, several wedging out sand units and small-scale sedimentary structures (lamination) suggest post-depositional reactivation of the tsunami deposit. Such remobilization is associated either to marine-processes acting in the onshore direction, or backwash activity as indicated by seaward directional features. Field observations also suggest that the landward limit of the tsunami deposit was most probably located farther inland than inferred from previous biostratigraphical and lithostratigraphical studies. The AD1755 inundation invaded the small canyons outletting in the lowland and fluvial and colluvial sediments were moved into the lowland, by retreating water, mixing with low-energy alluvial mud.



Figure 57. Details of the AD 1755 deposit and the overlying sandy unit. Photos by M.C. Freitas.



Figure 58. Details of Rip-up clast (within the deposit – right image). Photos by M.C. Freitas.

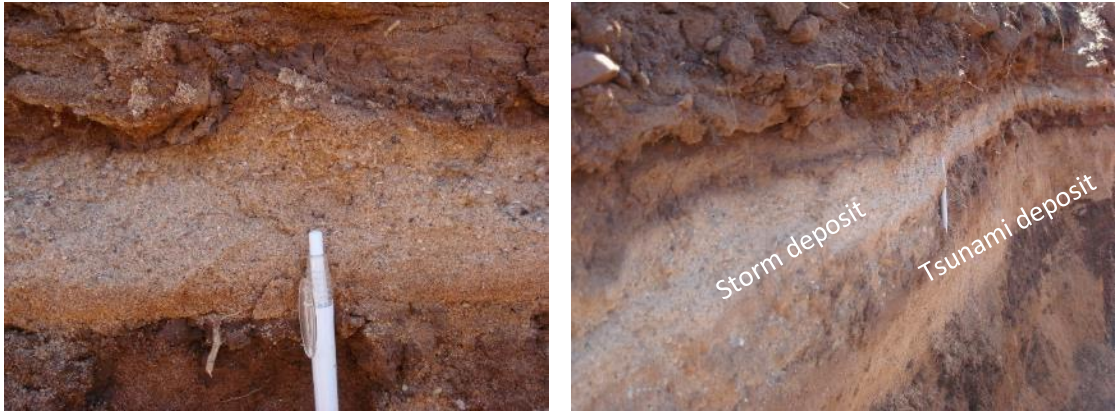


Figure 59. Detail of the sandy storm deposits (left image) and tsunami (below) and storm deposits (right image).
Photos by M.C. Freitas.



Figure 60. Left image – Cobble embedded in the tsunami deposit. Right image - tsunami (below) and storm deposits.
Photos by M.C. Freitas.

STOP 3 – Salgados

Context

The Alcantarilha and Salgados lowlands are located in the central Algarve coast between Armação de Pêra and Galé and are connected by a 6 km-long sand barrier (Figure 61 to Figure 63). The continuity of the sand barrier is interrupted by ephemeral inlets at both the Alcantarilha and Salgados lowlands. These are related to the hinterland valleys and meet the ocean as outlets of intermittent streams: The Alcantarilha and Espiche rivers drain 204 and 41 km² catchments, respectively, mostly developed over limestones, siltstones and sandstones (Manupella, 1992) - Figure 64. Nowadays, both lowlands are extensively silted up and their landward margins are occupied for agricultural and touristic purposes.

The barrier consists of a reflective-intermediate sand beach and foredunes that reach a maximum elevation of 17 m above msl. The barrier abuts against cliffs affecting soft detrital and carbonate Cenozoic rocks and covers Quaternary beach-rock and consolidated aeolianite deposits (cf. Moura et al., 2007). The densely vegetated dune field occupies an area of approximately 0.85 km² and the profile of the foredunes roughly corresponds to an asymmetrical triangle, steeply sloping and sometimes scarped in the seaward direction (Pinto and Teixeira, 2002). The emerged sandy beach has an orientation varying from E-W to NW-SE and has a width of 50 to 110 m (Pinto and Teixeira, 2002) - Figure 63. Beach sediments are typically medium sands, although coarser and finer sand fractions can occur locally.

The Salgados lagoonal area has been subjected to anthropic action over recent years. Since the 1980's, with the construction of a golf course, app. half of the early 20th century lagoonal area has been landfilled. Moreover, over the last 3 years, small artificial sand islands have been created to facilitate the maintenance of the autochthonous bird population.



Figure 61. Oblique aerial view of Salgados lowland in March 2011 Photo by S.B. Teixeira, ARH-Algarve, APA I.P..

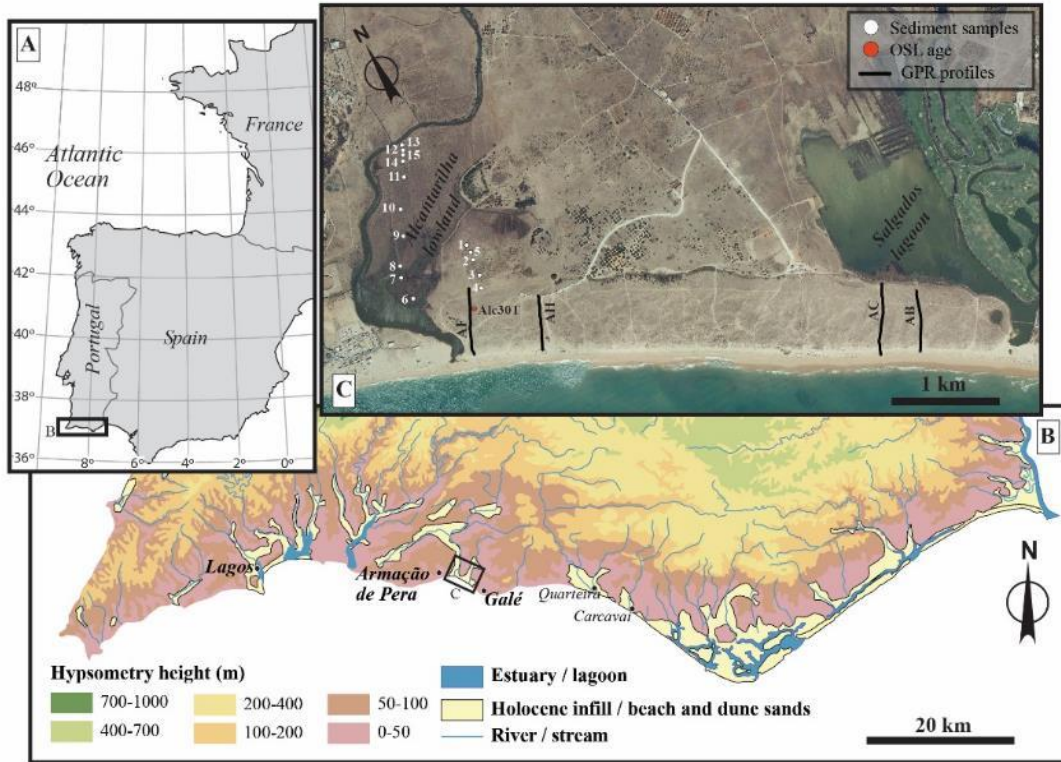


Figure 62. A and B - Geographical location of Salgados lagoon and Alcantarilha lowland. C – Aerial view of the lowlands and location of GPR profiles (AF, AH, AC and AB) – Costa et al., 2016b.



Figure 63. Points of observation (1, 2, 3 and 7) during the 5th ITFS Post-Meeting Field trip. Points 4, 5 and 6 are mentioned in text below and will be discussed in the field trip.

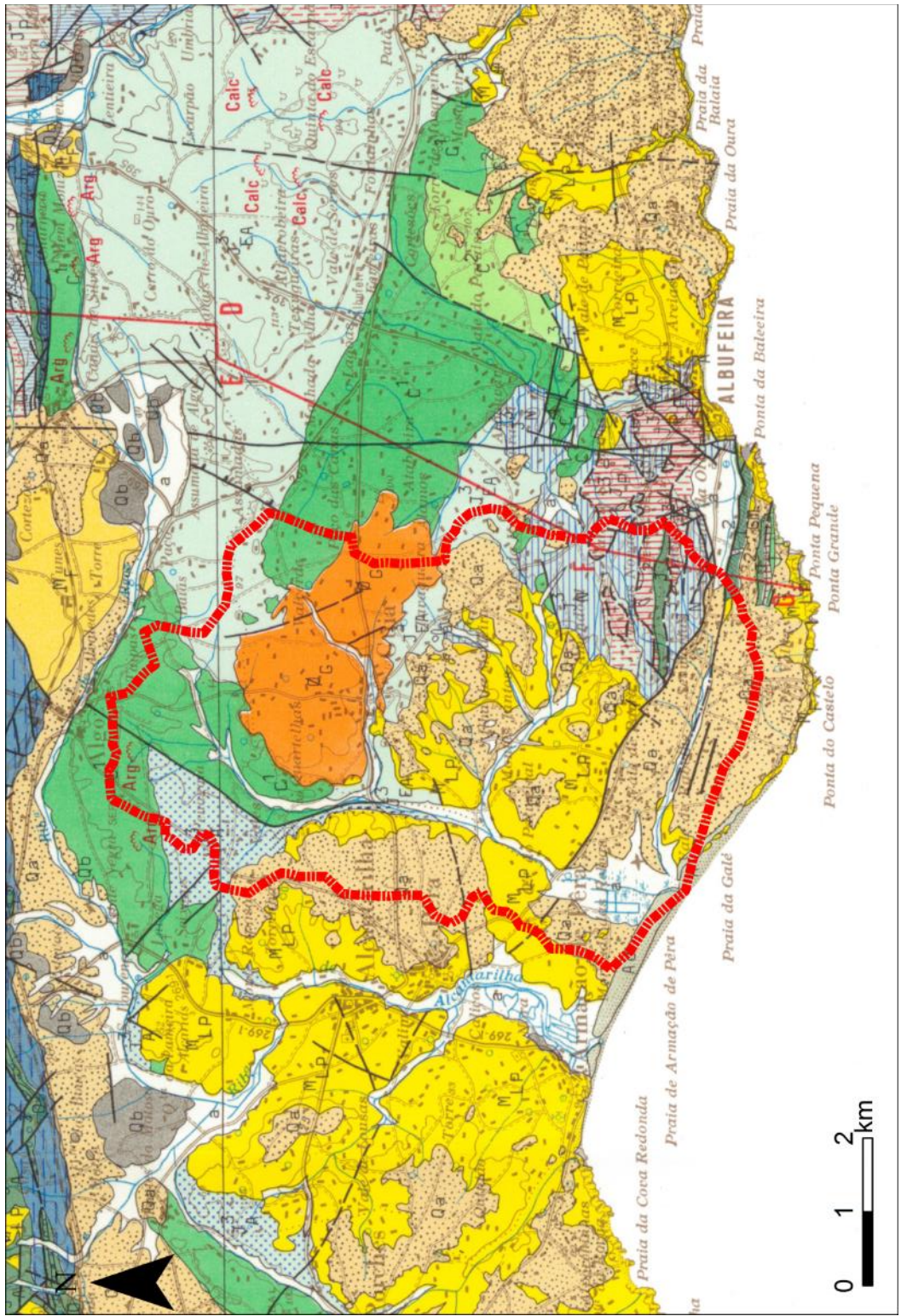


Figure 64. - Drainage basin of Ribeira de Espiche/Lagoa dos Salgados. Modified from Manuppella (1992). Legend is in Annex 1.

Late Holocene stratigraphy

Coring surveys of the Alcantarilha and Salgados lowlands were undertaken to understand their long-term evolutionary trajectory. The detailed age-models of the lowland sequences were summarized by Schneider et al. (2010), Dinis et al. (2010) and Costa et al. (2012) and Costa et al. (2016b). Here, we compile all available information from the literature to present the Holocene stratigraphic sequence (formed since approx. 7 ka cal yr BP) for both sites organized in 7 facies associations, which are described below (Figure 65 and Figure 66):

Facies F1 – Sandy lagoonal deposits – this facies association corresponds to (mostly) greyish sands with marine shell fragments and less abundant clay laminae. Most of the sediment showing facies F1 accumulated in an essentially shallow environment open to marine influence, preceding the drastic deceleration in the rate of sea-level rise around 6 to 7 ka cal yrs BP. The origin of this facies was associated with the Holocene transgression in the Algarve (see Schneider et al., 2010, Costa et al., 2016b for further details).

Facies F2 – Tidal flat deposits – F2 essentially consists of yellowish to greyish medium to fine sand containing marine shell (bivalves) fragments and exhibiting normal grading. Sand is intercalated with numerous muddy laminae. An age range of approximately 1.5 to 3 ka cal yrs BP was suggested for this facies by Costa et al. (2012).

Facies F3 – Alluvial plain/muddy lagoon deposits - this is the dominant facies association in the depositional record of both lowlands. F3 is composed of brownish silt and clay material of terrigenous source that becomes darker to the top/surface. It corresponds to recent and to the present-day sediments across most of the lowlands that are subjected to occasional flooding. Sediments of facies F3 show average thickness of approximately 0.8 m and have been deposited in progressively lower-energy conditions favored by the presence and increasing efficiency of the barrier.

Facies F4 – Transitional (pedogenetic) deposits - only identified at the Alcantarilha lowland and with a very limited inland extent (sampled in both cross-sections illustrated in Figure 65). This facies consists of brownish poorly sorted, sandy silt, with terrestrial gastropod shell fragments and abundant calcium carbonate precipitates (*caliche*) that form irregular concretions or accumulate in pores within the sediment, hardening and imprinting a whitish colour to the host materials. Occasionally, this facies overlies facies F5 (Figure 65 – cores 8 to 13) but it also develops in other stratigraphic positions. This pedogenic facies developed under dry weather conditions, favouring precipitation of calcium carbonate and the formation of *caliche* in relation with interstitial water.

Facies F5 – Tsunami deposits – this is a contrasting and peculiar facies, mostly consisting of a laterally extensive layer of (marine) shell-rich sand usually free of mud displaying an erosive base and a sharp upper boundary (Figure 67 and Figure 68). This facies has a marked marine signature, as shown by its foraminiferal and geochemical content (see Costa et al., 2012, Quintela et al., 2016, Costa et al., 2016b, Moreira et al., 2017). It is essentially composed of medium to fine sands. It extends around 850 m inland. The sediment becomes finer and its thickness decreases inland (from >0.60 m to a few mm) until it wedges out and can no longer be macroscopically identified in trenches and cores. Moreira et al. (2017) proved that the

geochemical marine signal extends beyond the macroscopic identification of this facies. The general altitude of the basal contact rises gradually inland (from ca. -0.05 m up to 1.28 m above msl) even though this facies varies laterally in terms of thickness and sedimentary characteristics. Several centimeter-sized mud clasts ripped from the underlying unit were identified in facies F5 sediments. They were more noticeable and abundant close to the base of the tsunami layer (Costa et al., 2012). Linear extrapolation of sedimentation rates obtained from vertical profiles of ^{210}Pb and ^{137}Cs in the sedimentary sequence coupled with radiocarbon dates from the underlying units allow association of this facies with the AD1755 tsunami (Costa et al., 2012).

Facies 6 – Wind-reworked sand – these deposits are confined to the eastern and seaward margin of Alcantarilha lowland, immediately adjacent to the leeward side of the dune. They formed after the emplacement of a sandy fan that forms a prominent (though spatially restricted) geomorphological feature extending into the alluvial plain (as described in Dinis et al., 2010). It is composed of fine to medium, well sorted, sand and its presence inland is limited to a few hundred meters. The association of this facies with the AD 1755 event was proposed by Dinis et al. (2010) based on the morphology and singularity of the washover fan in this coastal sector. The fan is roughly ellipsoidal, ~ 200 m wide and ~ 300 m elongated parallel to the shoreline, rising ~ 0.9-1.2 m above the surrounding floodplain with its boundaries visible in aerial photos. Its lower boundary is undulating and marked by the textural contrast between sand (fan) and underlying mud (alluvial).

Facies 7 – Channel deposits – Only present in very narrow sections of the lowlands. These facies occurs at the bottom of channels (either natural or anthropogenic) cutting through and disturbing some of the sediment facies presented above.

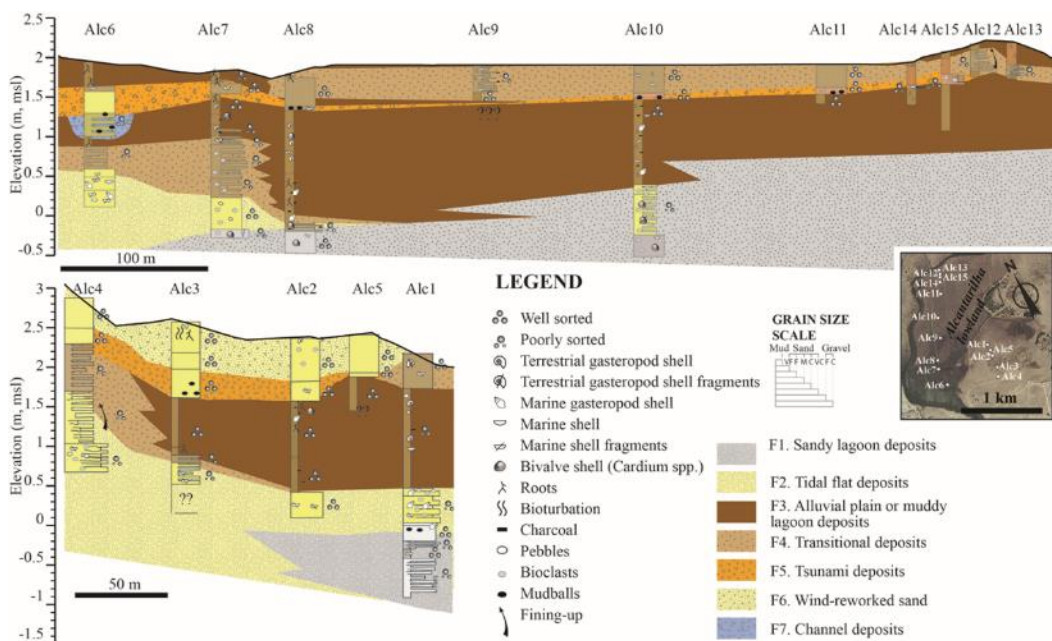


Figure 65. Schematic lithostratigraphic profile of Alcantarilha Lowland (Costa et al., 2016b).

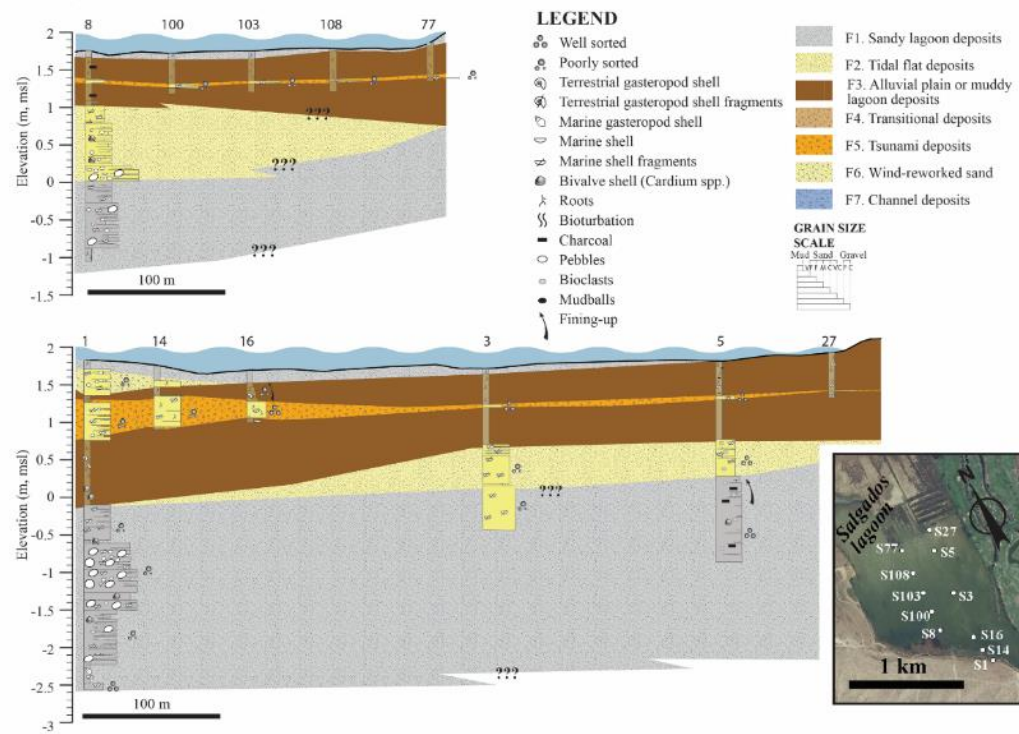


Figure 66. Schematic lithostratigraphic profiles of Salgados lagoon (Costa et al., 2016b).

The AD 1755 tsunami deposit

The AD 1755 tsunami inundation and associated deposits have been described in both the Alcantarilha and Salgados lowlands (cf. Lopes, 1841, Costa et al., 2009, 2012, 2015, 2016b, Dinis et al., 2010, Quintela et al., 2016, Moreira et al., 2017) - Figure 69 and Figure 70. The historical record describes the tsunami as follows: "*In...Armação (a 17th century fishing settlement immediately west of Alcantarilha lowland), located in the beach ¼ of league from another village named Pera (...) the sea left one house standing (...) it rushed more than ½ league (app. 3km) inland, flooding everything, leaving salt water lakes in the lowlands, creating islands and drowning 84 people (...)*", Lopes (1841, translation in Costa et al., 2012).

The tsunami sediment unit, corresponding to facies F5 above, is laterally variable in terms of its thickness and sedimentary characteristics. It is observed in its seaward section as a massive sandy deposit with no identifiable laminations or visible sedimentary structures (Figure 67 and Figure 68). However, further inland this unit is characterized by finer sediments. This is expressed in both the increasing percentage of mud inland and in a shift of the grain size curve of the >63µm spectrum towards finer sizes. Recent work (Quintela et al., 2016 and Moreira et al., 2017) were able to distinguish several inundation pulses based in the presence of estuarine foraminifera and in sub-centimetric grain-size variations.

Using heavy minerals and microtextural features it was possible to clearly establish provenance relationships between dune and tsunami deposits (similarity in abundances of staurolite, tourmaline and andalusite; degree of roundness and percussion marks on quartz grain surfaces of tsunami and dune sand - Figure 71 and Figure 72) (Costa, 2012, Costa et al., 2015).

Benthic foraminifera associations in the tsunami unit present a sharp contrast with under and overlying units. An abrupt increase in diversity and in the relative proportions of open marine/brackish forms and broken tests is observed in facies 5 (Costa et al., 2012, Quintela et al., 2016) - Figure 73 and Figure 74.

In Alcantarilha the tsunami deposit shares many similarities with the equivalent deposit in Salgados with two major exceptions: in Alcantarilha the tsunami deposit is located higher in the lithostratigraphical column and extends farther inland.



Figure 67. Contact between the tsunami unit and the under and overlying units identified in Lagoa dos Salgados. Photos by M. C. Freitas.



Figure 68. The AD 1755 tsunami deposit sandwiched in estuarine mud, Alcantarilha lowland. Photos by N. Hoska.

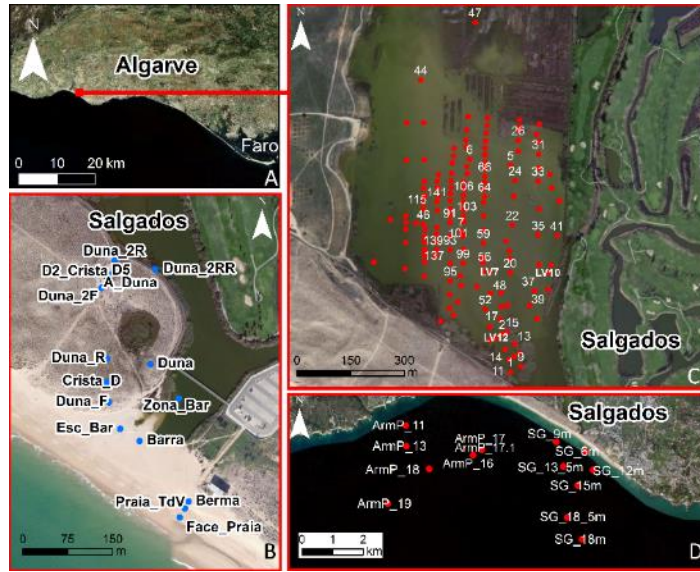


Figure 69. (A)- Location of Salgados lowland in the Armação de Pêra-Galé coastal ribbon; (B) - close up of the barrier showing location of the lowland and beach, dune and inlet samples; (C) - close up of the area reclaimed for the golf course and coring locations at the lowland and nearby alluvial plain; (D) nearshore samples – depths in metres below m.s.l. (Costa, 2012).

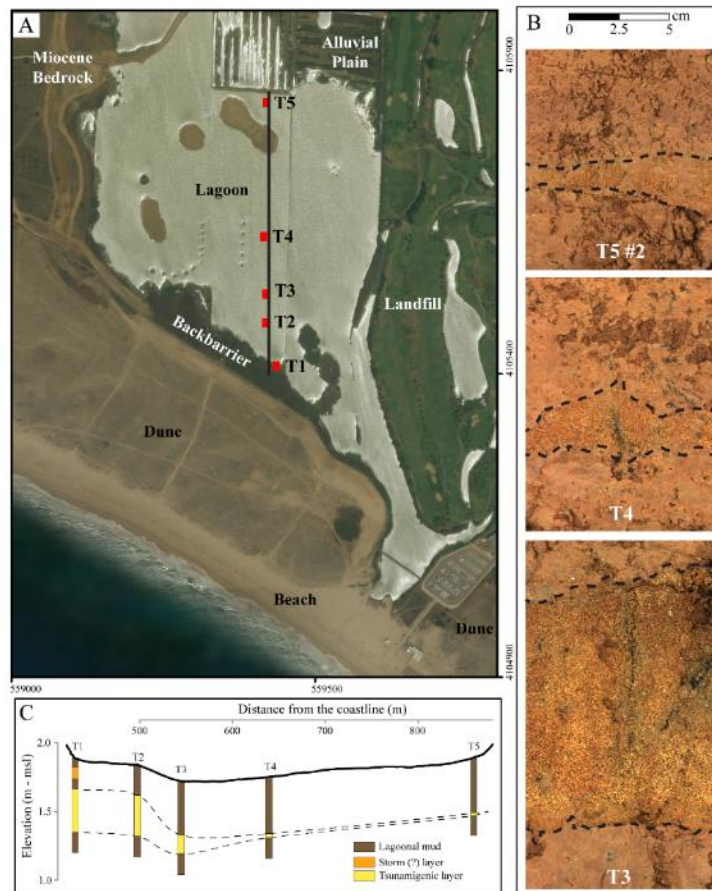


Figure 70. A and C. Cross-shore section showing the tsunami deposit (in Salgados) within lagoonal mud. B. High resolution photographs of box-cores, with delimitation of the sandy tsunami deposit (black dash line) (Moreira et al., 2017).

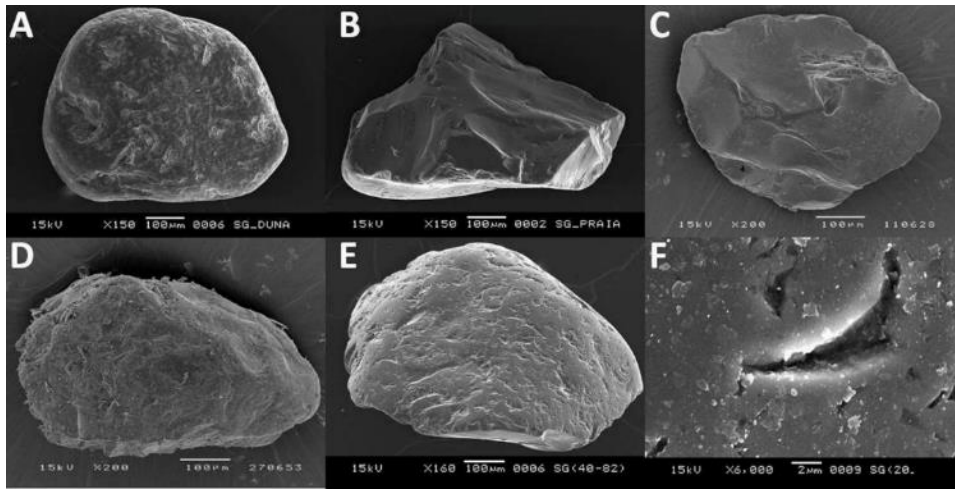


Figure 71. Microtextural images of quartz grains collected in Salgados. A – Dune. B- Beach. C- Nearshore. D- Offshore. E- Tsunami. F- Detail of percussion mark.

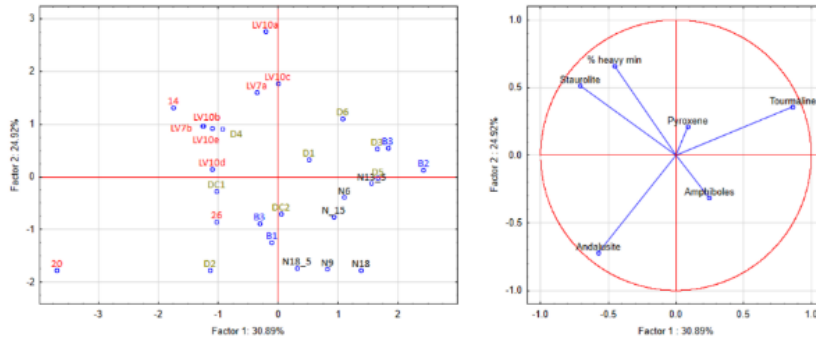


Figure 72. Principal component analysis of the heavy mineral assemblages of dune, beach, nearshore and tsunami sediments retrieved in Salgados. Left image – sample-plot along Component 1 and Component 2 (explaining 56% of total variance). Note the clustering of tsunami samples (in red) in the top left quadrant. Nearshore samples are in opposition, in the bottom right quadrant. Right image – variable-plot along the same components. Note parallel behavior of staurolite (densest heavy mineral among the common transparent assemblage) and percentage of heavy minerals. Both are characteristic of tsunami deposit in Salgados. B – beach; D – dune; N - nearshore; LV, 14 and 24 – Tsunami samples. LV7a and LV7b correspond to a depth of 46 and 41 cm below the surface, respectively. Samples LV10a, LV10b, LV10c, LV10d and LV10 correspond to a depth of 92, 81, 65, 57 and 47 cm below the surface, respectively.

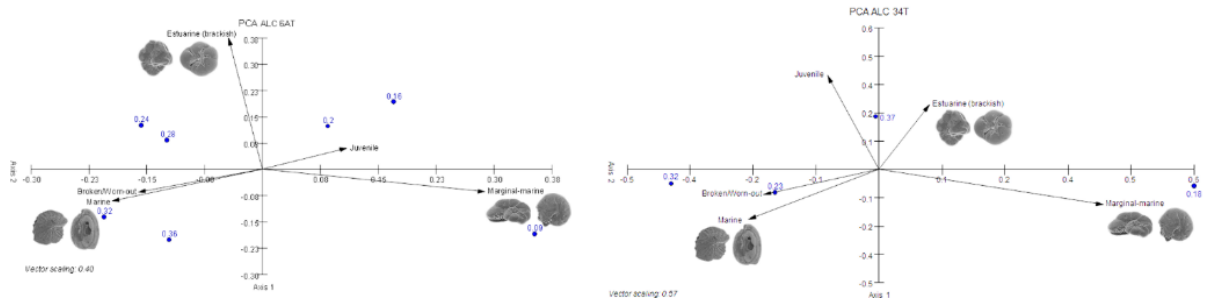


Figure 73. Principal Components Analysis results for samples retrieved in Alcantarilha (ALC 6AT and ALC 34T). Scanning Electron Microscope images of species representing the foraminiferal environmental groups are also displayed alongside the corresponding vectors. Marine: *E. macellum* and *Q. seminula*. Marginal-marine: *J. macrescens* and *H. germanica*. Estuarine: *H. wilberti* and *A. tepida*.

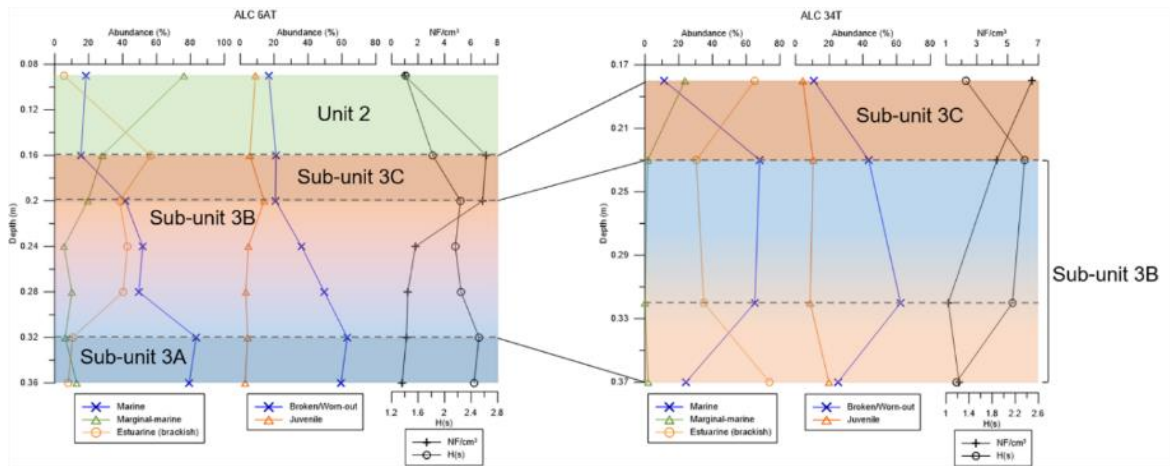


Figure 74. Interpretation of ALC 6AT and ALC 34T trenches' foraminiferal record. Variations in the proportion of foraminiferal environmental groups, broken/abraded tests, juvenile specimens, standing crop and Shannon-Wiener index (Hs) within the tsunami unit (Unit 3) (Quintela et al. 2016).

Geomorphological imprint

In the Alcantarilha lowland, Dinis et al. (2010) described a sandy overshaw fan attached to the leeward toe of the dune ridge just east of the present-day inlet. The fan thins and wedges out inland into the adjacent alluvial plain sediments (Figure 75). They attributed the fan's origin to localized overshaw and erosion of the dune by the AD 1755 tsunami and constrained the run-up height in this area to <10 m above msl.

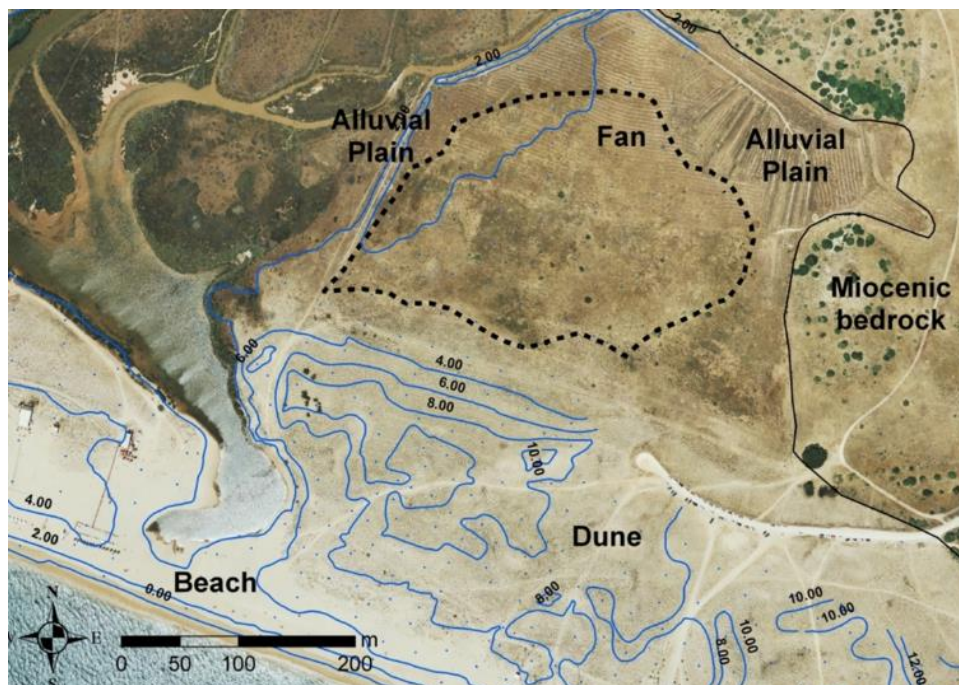


Figure 75. Geomorphological imprint (fan) in Alcantarilha (Dinis et al., 2010).

The historical record describes an extensive inundation of Alcantarilha lowland by the AD 1755 tsunami, which implies that it was most likely completely flooded. The morphology of the lowland and barrier indicates that the Alcantarilha inlet might have concentrated a significant part of the intruding tsunami flow, providing a preferred route for the massive inundation of the lowland. Moreover, even if the inlet was closed at the time of inundation, the overtopping should have occurred through the lower areas of the barrier, creating a depression in the dune field. Additionally, for a sufficiently high run-up at the coast, part of the incoming wave may have also overtopped low points of the dune crest.

GPR results in Alcantarilha barrier (for example Profile AF in Figure 76) are consistent with the interpretation by Dinis et al. (2010). Radargrams show an erosive surface at approx. 7 m msl that is most likely the remnant erosional contact marking the impact of the AD 1755 tsunami waves when they overtopped this region of the dune field (Figure 76). This estimation supports hydro- and morphodynamic modelling results that suggest minor erosion in the foredune and overtopping heights compatible with GPR results (Costa et al., 2016b). Indeed, the dune field reaches up to 17 m above msl and the limited extent and location of the fan in Alcantarilha suggests that the dunes were not overtopped in the central and higher sector of the dune field. Assuming that the morphologies contemporaneous with the overwash are similar to present-day forms, the elevation of the free surface of the ocean at the coast can be estimated to 7-10 m above msl (combining height of the erosive surfaces detected in the GPR profiles and geomorphological inferences).

In the dune barrier, aeolian sediment post-dating the inundation event and immediately overlying the erosive surface were OSL dated (Unit 6 - Figure 76) and yielded ages compatible with this interpretation (approx. 250 years old). In contrast, dune sediment underlying the erosive surface was dated to older ages (around 300 years old) (Costa et al., 2016b).

Similarly to Alcantarilha, GPR data obtained in Salgados (Figure 77) also indicates an erosive surface at app. 6 m above msl corresponding to the beheading of the top of the dune ridge up to a limited longshore distance from the inlet. On the other hand, the shape of the tsunami deposit in Salgados lagoonal area suggests a wide, thin and fan-shaped feature that thins landward before wedging-out within lagoonal mud, its apex pointing to the inlet. The plot of isopach lines of the tsunami deposit (Figure 78) shows a pronounced arcuate and concentric pattern rather than aligning parallel to the general trend of shoreline. An analogous pattern is obtained for lines of equal mean or median grain size and percentage of sand in sediment. Observation of present-day morphology and interpretation of the spatial distribution of the tsunami deposit features suggests that the tsunami waves overtopped a part of the barrier where dunes reached a maximum of 10 m above msl. Most of the intruding tsunami water was conveyed through the inlet gorge and the lower adjacent barrier tips before spreading radially inland.

Most of the results presented here suggest a relatively low impact of the tsunami over the coastal barrier mainly because of the likely high elevation of the dunes. However, it is important to highlight the fact that as a consequence of the inundation of the barrier, even if not complete, the impact seems to have been enough to destabilize the coastal dune and initiate the formation of scarps and pedestals and inland migration of parabolic dunes (Costa et al., 2016a). Likewise,

the integrated analysis of aerial imagery, GPR, maps and DTMs also revealed a number of pedestals within the dune sequence. The pedestals have not been reshaped since at least 1947 (earliest aerial photographic record). Considering that during the last century extreme storms that affected this coast (with wave heights above 5 m) were not capable of changing or eroding these pedestals, their origin is mostly likely attributed to a unique extreme event - the AD 1755 tsunami.

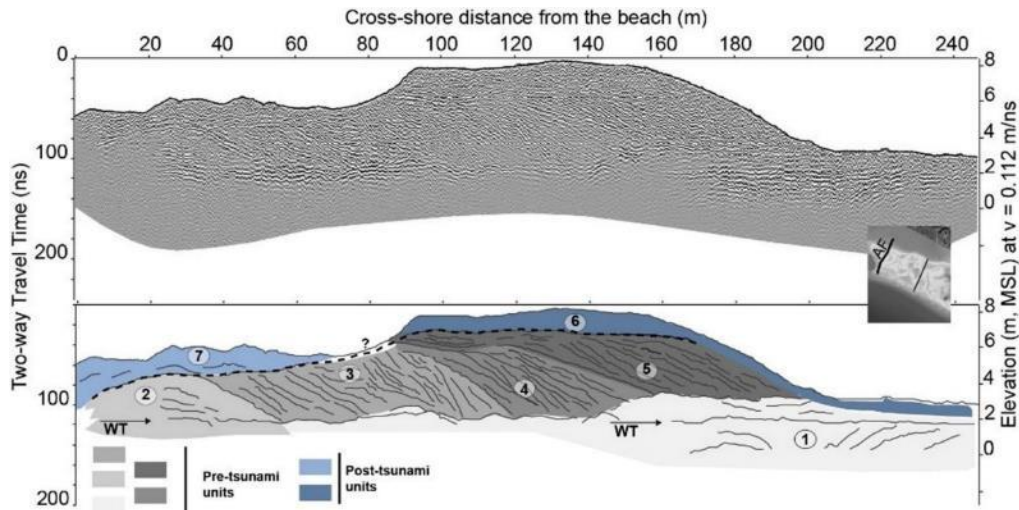


Figure 76. Ground Penetrating Radar Profile AF. Top image presents the raw data. Lower image presents the proposed stratigraphic interpretation based on the definition of major units (for details see Costa et al., 2016b). Dashed black line represents the erosive surface separating the pre- and post-tsunami units. The number labels indicate the chronological classification of the identified units labels.

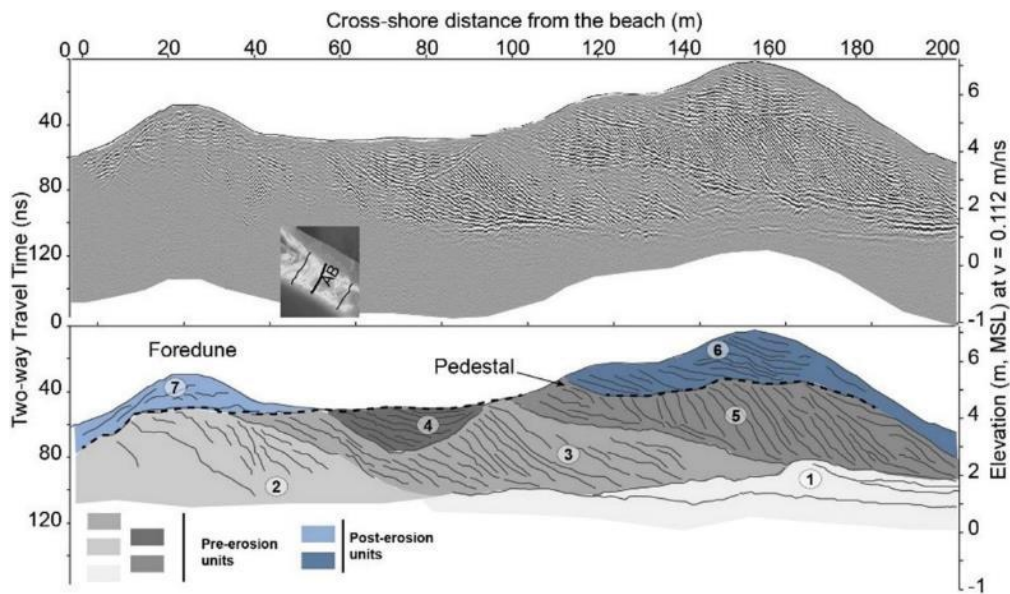


Figure 77. Ground Penetrating Radar Profile AB. Top image presents the raw data. Lower image presents the proposed stratigraphic interpretation based on the definition of major units (details see Costa et al., 2016b). Dashed black line represents the erosive surface separating the pre- and post-tsunami units. The number labels indicate the chronological classification of the identified units labels.

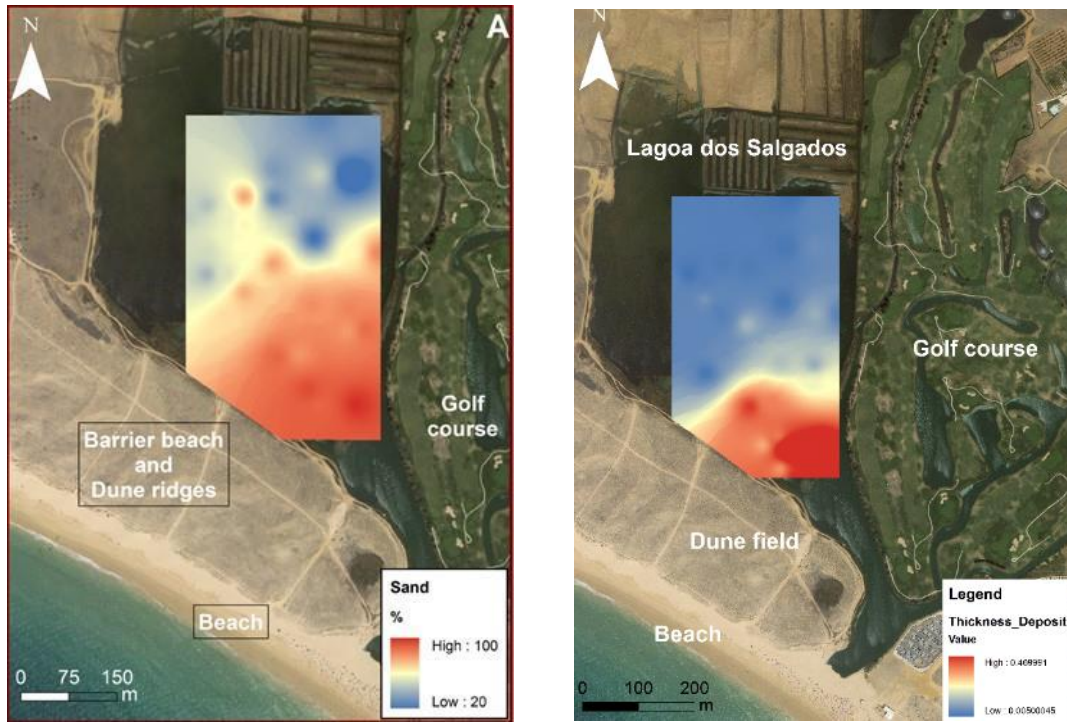


Figure 78. Spatial distribution of percentage of sand (left image) and thickness of the tsunami deposit – units in cm) in Salgados lowland (adapted from Costa, 2012).

STOP 4 – Ria Formosa

Ria Formosa is a multi-inlet barrier-island chain and lagoon extending for approximately 55 km in the eastern Algarve. Five sandy barrier islands and two spits form a roughly triangular chain, with maximum width of 6 km near Cape Santa Maria (Figure 79). Barriers are separated by 6 tidal inlets, and documentary sources from the 16th century onwards indicate the barrier chain included essentially five or six tidal inlets.

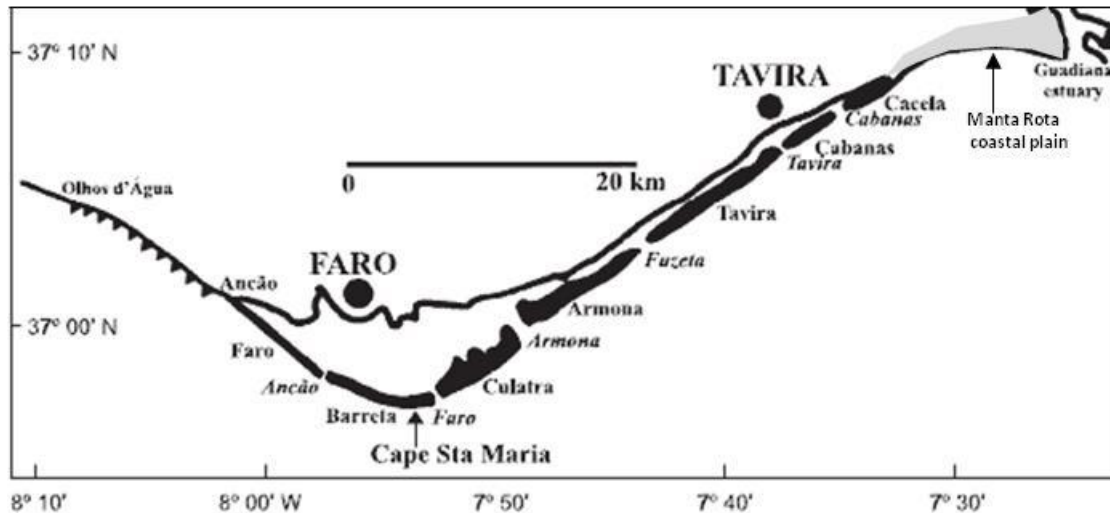


Figure 79. Ria Formosa barriers and inlets (italic). Erosion of the cliffs between Ancão and Olhos d'Água, updrift of the Ria Formosa barriers, constitute their main sediment source (modified after Andrade et al., 2004).

The lagoon is shallow, with average depth of 2 m (relative to msl). The flooded area in spring high tide is of 84 km² (76% of the total barred surface) and 80% of the lagoonal bottom emerges during spring low-water.

The main morphosedimentary features in the lagoon are sandy and muddy tidal flats, vegetated salt marshes, and channels - the intertidal forms representing 90% of the surface. Salinity of the lagoonal water is identical to the ocean due to high renewal rate (80% and 52% in spring and neap waters, respectively) combined with a semiarid precipitation regime and residual freshwater input. There are no significant coarse sediment fluvial inputs into the lagoon. Fine sand and mud delivered from the terrestrial margin are partly exported to the shelf and partly retained in intertidal flats and marshes, which accrete at rates of 0.4 – 4 mm·year⁻¹ (Andrade, 1990a, Neumeier et al., 2000). Coarse (sand to shingle) shell-rich sediment on channels and the lower domain of intertidal flats is of marine provenance, input via the tidal inlets and redistributed by strong tidal currents.

The morphology and morphodynamics of the barrier chain and inlets make this system atypical (cf. Andrade, 1990a for a comprehensive description). Atypical features include the backing by young bluffs instead of a wide coastal plain, development close to the upper mesotidal limit, morphology of most barriers more similar to barrier-island and spits in microtidal and wave-dominated coasts, size of flood tidal deltas dominating over ebb deltas

Erosion and accretion throughout the last 300 years have been, to a large extent, related with inlet drifting, closure and reopening, sand retention disclosed by groin and jetty emplacement,

and time-changes in hydraulic efficiency of interconnected inlets and associated sand-retention in flood and ebb tidal deltas. Landward recession affected Cacela and Ancão barriers at the very edges of the system, following natural closure of two terminal inlets. The westernmost inlet closed early in the 19th century while the eastern terminal inlet closed between 1923 and 1942 (Weinholtz, 1964, Andrade, 1990a). Starvation of the more central barriers activated pure erosive responses rather than rollover.

Most of the barriers (e.g. Ancão, western Barreta, eastern Tavira, Cabanas and Cacela) display a simple morphological framework, comprehending an ocean-facing beach backed by vegetated (single or multiple) dune ridges; further landward, the backbarrier flat is narrow and grades to intertidal flats or marshes, or slopes into a tidal channel. In western Culatra and eastern Barreta the backbarrier is wider due to seaward progradation of welded beach-ridges. The back barrier increases in morphological diversity and shoreline irregularity where rapid inlet drifting (and consequent barrier-tip extension and enlargement) allowed for incorporation of flood delta segments or terminal recurved spits, such as in eastern Culatra and eastern Armona.

Storm overwash of the barriers chain occurs on a regular basis. Time and space distribution of overwash, as well as the contribution of washovers to backbarrier changes and functional relations between overwash sand advection and aeolian processes and dunes, have been addressed in several studies (Andrade, 1990a,b, Matias, 2006, Matias et al., 2009 and references therein). Washovers are essentially represented by single and elongated drop-shaped features, similar to the breach-throat-fan splays quoted by Carter (1988). In most cases, they fail to cross the whole barrier width but localized barrier breaching has been documented, especially in poorly mature segments of narrow barriers, eventually inducing inlet relocation. Recently accreted barrier tips close to drifting inlets are more extensively overwashed and develop overwash platforms. Both the historical record and field evidences show that even the most damaging storms failed to extensively scalp the barrier dune ridges. Instead, storm waves cut a number of corridors across the dune and sculpture an ephemeral morphology roughly correspondent to types III and IV of Hesp's (1988) classification. Embryo dunes eventually reoccupy washovers and overwash corridors and grow and coalesce in few months to years until complete healing of the previous morphology.

Tavira barrier and the 1755 tsunami

Geomorphology

The middle section of Tavira barrier-island shows peculiar morphological features extending landward of the beach and foredune ridges, also present in the central section of Armona barrier. These features markedly contrast with every other barrier-island of Ria Formosa and their origin and significance has been addressed in the studies of Andrade (1990a, 1992), Andrade et al. (2004, 2016), where the morphodynamics of both barrier-islands and tidal inlets are investigated and discussed.

The field trip starts at the landward margin of the lagoon separating Tavira barrier from mainland (Figure 80). Here, the lagoon is elongated NE-SW and narrow, featuring an axial

channel (Tavira channel) that connects with the inlets of Fuzeta, to the southwest, and Tavira, further NW. Departing from this channel, meandering channels develop and ramificate over a muddy tidal flat that grades seaward into a channeled vegetated high marsh (with only a few expansions of fringing low marsh).

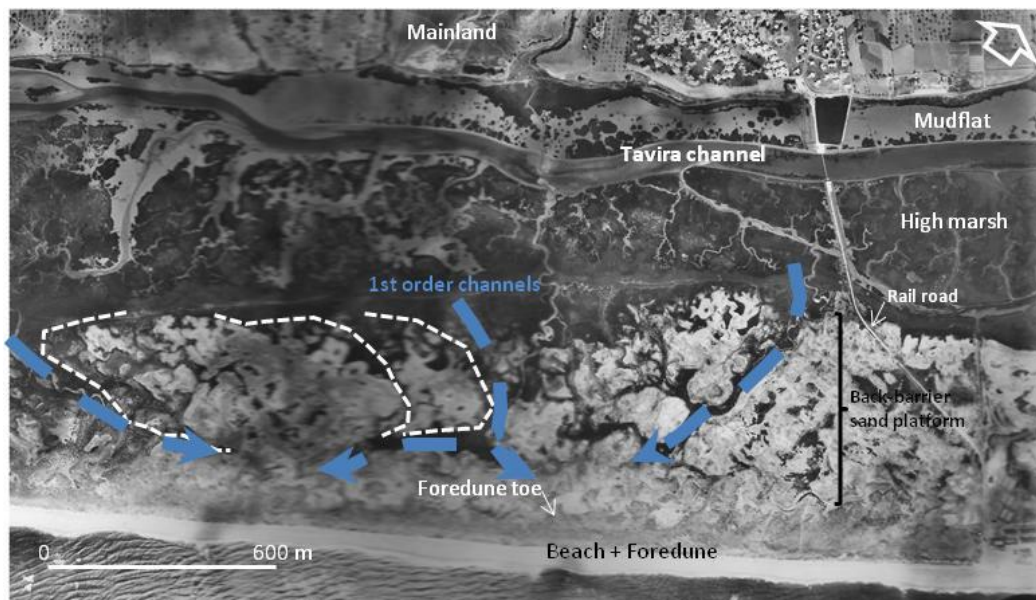


Figure 80. Aerial photo (FAP, 1984) showing mainland, lagoon and Tavira barrier island. Note the extension and morphology of the backbarrier domain, featuring a densely channeled sandy platform. First order channels (thick blue dashed arrows) limiting relict tidal deltas are indicated (see text for explanation).

The back barrier confining with the marsh consists of a sparsely vegetated sandy platform resting 2 - 2.5 m above msl. This surface is dissected by a poorly incised and labyrinthic second order channel network that outlines an apparently chaotic field of vegetated sand mounds (Figure 81). Second order channels are sandy and reactivated during spring flood tides, the sedimentary structures indicating flood-dominancy. The mounds are irregular in plan shape and look as randomly dispersed over the platform when viewed from a ground perspective. The plan shape and profiles of the mounds do not fit typical dune features, despite the sand showing similarity with both the nearby beach and foredune sand. Most mounds are isolated by channels whereas a few occur aligned in repetitive features defining “en echelon” pattern. Some show NE -elongated and recurved plan shapes and merge with the lee face of the foredune, whereas others, though adopting similar shape, are breached and separated from the present day foredune. Mound slopes are affected by carving induced by flood currents and wind-generated wavelets that also kill vegetation and locally trigger small scale avalanching. Together with aeolian deflation these processes degrade the backbarrier reliefs, nourish channel floors and allow for further redistribution of sand over the platform, without significant excavation of thalweg lines.



Figure 81. Ground perspective of the back barrier showing numerous sand mounds and second/order channels.



Figure 82. Oblique aerial photograph of Tavira barrier looking southeast (2009, www.siarl.igeo.pt/).

Viewed from the air, the apparently chaotic structure of the backbarrier gives place to a different pattern (Figure 80 and Figure 82). A number of repetitive first order channels radiate from the lagoon and embrace ovoid segments of the backbarrier that include sets of isolated sand mounds. If well preserved, a first order channel terminates by a dead end at the lee side of the foredune. Here, very coarse sand, shingle and large bivalve fragments may be found forming iron-stained lags, indicating strong current activity, scarcely compatible with the present-day hydrodynamic regime. Hydraulic connection between nearby first order channel is ensured in spring tides by the second order channel network.

First order channel heads may run along bended linear sand ridges emerging from the landward toe of the foredune. These linear bodies are interpreted as relict recurved spits. They are similar in shape, size and location to their active counterparts in Ria Formosa barriers, always related with a nearby tidal inlet and deltas. Both straight and recurved sand ridges trending oblique to the general elongation of the barriers may be found at present, either at the updrift barrier tip margining drifting tidal inlets, or corresponding to linear sand bars (ebb spits and channel margin linear bars – cf. Hayes, 1975 for nomenclature of tidal delta forms) of both flood and tidal deltas.

Inlet migration or deactivation allows for incorporation of these features following downdrift growth of the barrier.

Similarly, the ovoid segments of the backbarrier share striking similarities in shape and architecture with flood tidal deltas accumulating in relation with the small and eastward drifting inlets of Ancão and Fuzeta, though the size of the former is smaller than of the active deltas (Figure 83). The first order channels correspond to the ebb-dominated peripheral channel involving the active flood-shoals of these inlets. Active peripheral channels converge seaward and join to form the main inlet channel at the inlet gorge and this geometry is mirrored by first order channels in the barrier flat. Each ovoid segment is interpreted as corresponding to the sandy fan defining the broad geometry of a formerly active flood ramp, and sand mounds resting over and at the edge of this platform are taken as relicts of flood delta sand banks (e.g. former ebb-shields, linear ebb spits, swarms of large-scale hydraulic dunes).

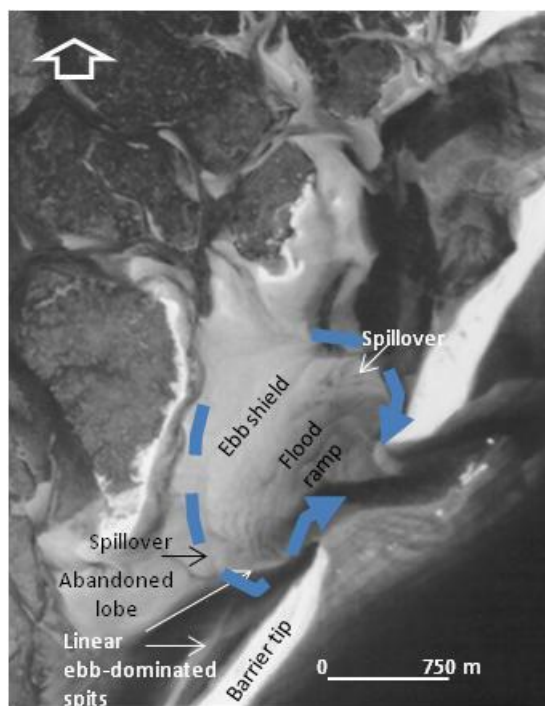


Figure 83. Vertical view of the eastward drifting Ancão inlet in September 1976 (aerial photo CGExercito). Note ebb dominated peripheral channels, large scale flood dominated sedimentary structures in flood ramp and stacked hydraulic dunes and mega ripples crowning the ebb shield indicating counterclockwise deviation of ebb flow over the shield

In addition, the preservation and morphological expression of sand mounds in some relict deltas is better preserved at their eastward section, the western domain showing only ill-defined and “ghostly” features. This is also apparent in present-day rapidly drifting flood deltas that accumulate most of the sand advected via the tidal channel and build up at their eastern (down drift) lobes. In contrast, the western lobes are subjected to progressive abandonment, starvation and reworking by tidal currents, leading to dilution of former morphologies and definition of staggered short and linear sand bars over abandoned lobes.

In summary, the data and interpretations above indicate that the backbarrier of Tavira barrier-island consists of numerous relict flood tidal deltas, the original morphologies having been degraded by tide and wind-related processes post-dating their emplacement.

The preservation level of the relict deltas is similar, suggesting that their emplacement was synchronous or delayed by a very small amount of time.

Data on tidal inlets locations since at least the 16th century show that the central section of both Tavira and Armona barrier-island were not affected by regular down drift migration of tidal inlets. On the contrary, they represent the only barriers that have not been extensively reworked by these processes on a regular basis. Thus, the setting of the relict features must correspond to an unusual and non-repeated process, characterized by the potential to affect a large expansion of the coastline. If similar features have developed at the same time and elsewhere along the same system, they have been obliterated and replaced by normal inlet drifting and barrier healing processes and features.

On the other hand, the existing body of knowledge on Ria Formosa inlet stability, and relations with tidal propagation parameters in the eastern domain of the lagoon, clearly excludes the possibility of numerous small and adjoining inlets persisting for long time-intervals in the central area of Tavira barrier-island (just as the central area of Armona barrier). This is especially true when considering that those inlets must have shared tidal prism with the multi-century persistent inlets of Fuzeta and Tavira.

The reasoning above strongly suggests that relict tidal deltas formed in consequence of an unusually intense episode of barrier overtopping, capable of disrupting and dismantling the whole sandy beach-foredune super-structure of these barriers in one single stroke and of pushing a vast amount of sand landward of the coeval shoreline to form the present-day barrier flat – the widest found in Ria Formosa barriers. Rather than the Algarve storms, the impact of an overwhelming tsunami inundation fits the required intensity level, low frequency and unique ability to obliterate a long and continuous healthy beach-dune system and accumulate scour fans landward of the shoreline that may eventually coalesce to form sand sheets landward of the coastline (see Goff et al., 2009 and references therein for examples of these processes and signatures related with contemporaneous tsunamis and paleotsunamis). In the case addressed here, the short distance to the landward margin may have potentiated the backflow of the tsunami and water receding to the ocean should have exploited breached segments between remnant dune knobs to incise inlet channels, their relicts corresponding to first order channel dead-ends.

However, the second-order channels and sand mounds populating the back barrier suggest that the newly formed washover sand sheets evolved in time, the sand having reorganized to form multiple and small (but surely ephemeral) flood tidal deltas and that at least part of those inlet-deltas drifted for a short distance eastwards. One map dated from 1762 and drawn by Carpinetti Lisbonense shows a unique, unexpected and enlightening representation of Tavira and Armona islands (Figure 84): both are represented as lying within the intertidal domain, a representation that is never found in documents either pre-dating 1755 or post-dating 1765. This makes the 1755 tsunami as the best candidate for the high magnitude single inundation event responsible

for the transfiguration of both the Tavira and Armona barrier-islands, and also that the barriers were not yet completely healed about 10 years after the impact. Historical accounts of the AD 1755 tsunami (Pereira de Sousa, 1919) indicate that several tsunami waves engulfed and submerged the whole of Ancão barrier, at the western region of Ria Formosa. This barrier island features the highest foredunes of Ria Formosa. Eyewitness accounts of this impact suggest that sea level has been raised to at least 9 m msl and this is compatible with the large-scale inundation of the whole length of both Armona and Tavira barriers at the eastern side of the barrier chain.



Figure 84. Fragment of C. Lisbonense map (1762) showing the eastern barriers of Ria Formosa (Armona and Tavira) as intertidal domain.

The following geomorphological-based model has been proposed to explain the unique morphological organization of both Tavira and Armona islands (cf. Andrade, 1990a, Andrade, 1992).

1. The initial situation corresponds to a geomorphological arrangement similar to every other barrier island of the same system: a sandy island featuring a beach and robust foredune ridge (eventually multiple and discontinuous) stranding landward into a muddy intertidal marsh surface separated from mainland by channeled mudflats and marshes.
2. The 1755 tsunami impacts the barrier, fully disrupting and dismantling the back-beach and dunes, and injecting a massive amount of sand landwards. This sand drowned the region at the pre-event lagoonal margin building a sandy platform over mudflat and marsh that consists of multiple and coalescent washovers. The size of these washovers largely exceeds that of storm induced sand fans. A series of potential tidal inlets was created at the locations where powerful backwash concentrated and channeled. Low-lying areas over the washovers (eventually at the boundaries between adjacent overwash fans) were further exploited by receding water delineating precursors of peripheral channels that eventually evolved into first-order channels.
3. Tidal prism in this section of the lagoon is too small to accommodate a large number of active inlets. Inefficient inlets rapidly closed and became locations of chronic overwash, while others started developing flood deltas at the cost of reworking pre-existing overwash sand. Active inlets and deltas drifted eastward for limited time and

distance, allowing for development of recurved spits and abandonment of their western delta lobes. On the lagoonal side, small tidal channels adapted to the morphology imposed by the sand accumulation at the newly formed backbarrier.

4. After about two decades the barrier healed and a second generation dune-system was formed. Former peripheral channels adapted and formed the first-order network, allowing for tidal water to continue reaching the backbarrier up to the landward toe of the foredune. Former flood deltas are now fossilized and lateral connection between first-order channels is ensured in spring tides by a dense network of second-order channels that exploit topographic lows between relict sand accumulations. Original morphology is etched and diluted by tidal currents and wavelets, and aeolian activity promotes thorough redistribution of sand that builds upon a backbone of tidal-dominated sand accumulations.

Stratigraphy

The model above has stratigraphical and chronological implications that were tested by examining sediment cores and Ground Penetration Radar profiles, together with chronological data obtained from radiocarbon dating of organic particulate material in lagoonal mud and OSL dating of quartz grains (cf. Andrade et al., 2016 for the internal architecture of Tavira barrier-island).

Figure 85 shows a cross-section illustrating main lithostratigraphic units revealed from a line of short cores retrieved from the backbarrier of Tavira island. The general setting is coherent with the chronostratigraphic and lithostratigraphic sequence characterizing the western region of Ria Formosa (cf. Andrade et al., 2004) and with the time-sequence of Holocene depositional episodes found in other Algarve lowlands and mentioned above.

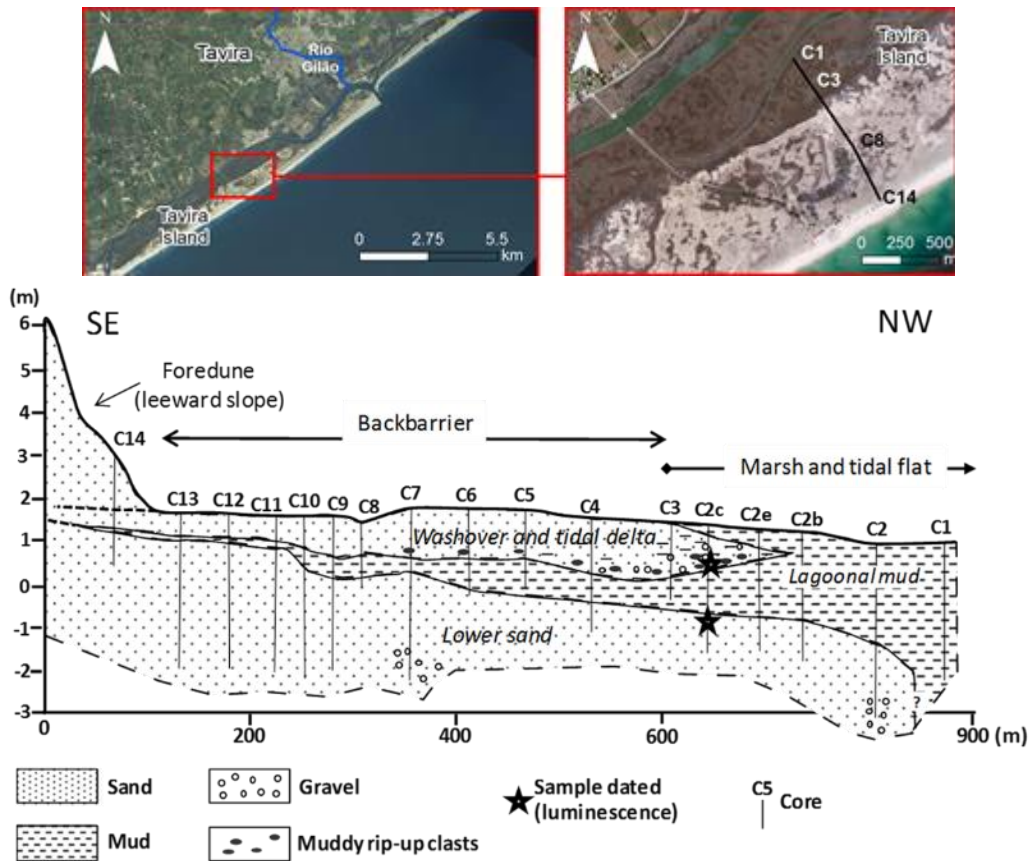


Figure 85. Upper panel – Tavira island indicating location of cores and cross-section shown in lower panel. Lower panel- cross-section of Tavira backbarrier showing main lithostratigraphic units and location of samples used for dating. Adapted from Andrade et al. (2016).

The lowest sediment unit reached by the cores corresponds to shelly open-marine facies sand to shingle. The top of the lower sand was OSL dated to 2400 ± 49 BC (cf. Andrade et al., 2016) and this result is compatible with considering the lower sand as pre-dating the formation of the barrier system. This unit is covered by organic-rich lagoonal mud with plant debris in diverse stages of fermentation and rootlets, the latter increasing in abundance towards the top. In addition to plant debris, remains of marine shells and foraminifera are also present in the mud. Transition from the lower sand to the mud is in general progressive.

The top of the muddy unit forms the present day lagoon bottom northward of the barrier but further south it is covered by a younger and laterally discontinuous sandy unit, corresponding to the backbarrier sandy platform that has been previously related with the 1755 tsunami. The top of the lagoonal mud has been radiocarbon dated to cal AD 1260 to 1430 (2σ range) where its vertical accretion has been stopped by the cap of washover sand (Figure 85).

This sand is also marine and shell-rich and was found sandwiched in the lagoonal mud at its northward limit, just before wedging out. It was dated using quartz luminescence methods to $AD 1743 \pm 49$ (Andrade et al., 2016). The dating results and lithostratigraphic data above converge to correlate both the event-sediments represented by the washover sand and the abrupt change in barrier morphology with the 1755 tsunami. The study of sediment cores taken

from the back barrier and adjacent marsh reveals that the emplacement of the tsunami sand, which eroded underlying soft lagoonal mud, transiently disturbed the low-energy sedimentation regime of the lagoon, dominated by organic silt and mud. Lagoonal sediments are ca. 2.5 m thick and quite homogeneous in texture and composition. Besides the 1755 event layer, no other high-energy sand lamina or layer disrupting the low-energy sediments was observed in this region.

As a final remark and food for thought we represent in Figure 86 the results of a Ground Penetrating Radar (GPR) survey line recently obtained from Tavira backbarrier. The line is broadly coincident with the cross section in Figure 85 and suggests that high-resolution analyses of stratigraphy and sediments, if supported by an adequate chronological framework, may provide further insights on the response of this barrier island to the impact of an extreme flooding event. Moreover, this approach may reveal how and when did the barrier respond in terms of healing and reconstructing in the aftermath of the 1755 tsunami.

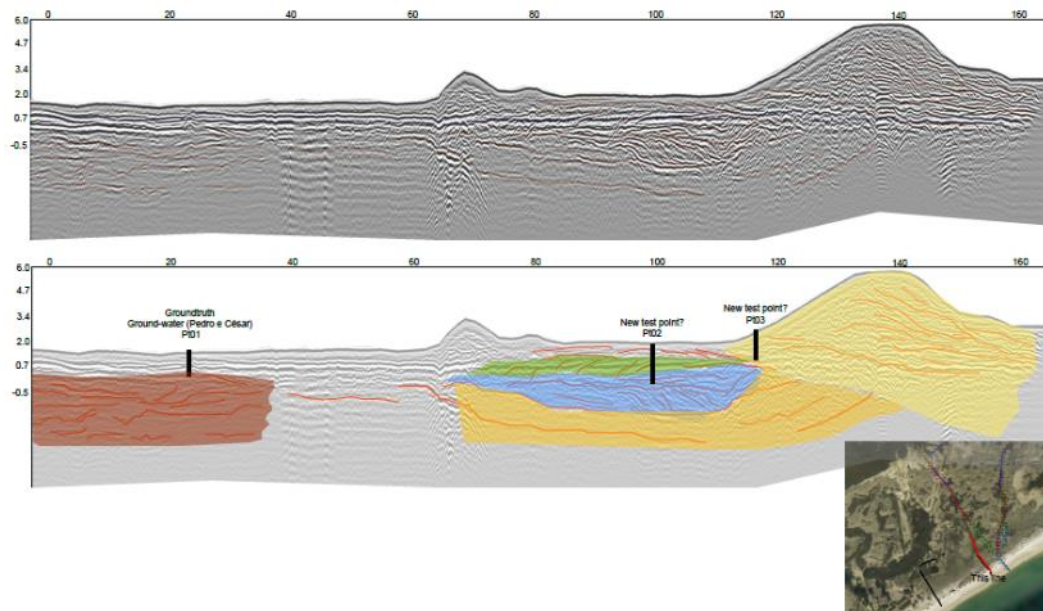


Figure 86. Ground penetrating radar results and preliminary interpretation of data obtained from profile line broadly coincident with lithostratigraphic cross-section above. Inedited results kindly forwarded by Rita Villanueva (U. Vigo), 2016.

References

- Allen, H. D. (2003) – A transient coastal wetland: from estuarine to supratidal conditions in less than 2000 years – Boca do Rio, Algarve, Portugal. *Land Degradation and Development*, 14: 265–283.
- Almeida, L., Voudoukas, M., Ferreira, Ó. (2009) - Review of climate change impacts on storm occurrence. MICORE project technical report, 118 p. <http://www.micore.eu/area.php?idarea=46>.
- Andrade, C. (1990a) – O ambiente de barreira da Ria Formosa. PhD dissertation, University of Lisbon, 645 p.
- Andrade, C. (1990b) – Estudo da susceptibilidade ao galgamento da Ria Formosa. *Geolis*, 4 (1,2): 69-76.
- Andrade, C. (1992) - Tsunami Generated forms in the Algarve Barrier Islands (South Portugal). *Science of Tsunami Hazards*, 10 (1): 21-34.
- Andrade, C., Andrade, A., Kortekaas, S., Dawson, A. (1997) - Sedimentological traces of tsunamigenic overwash of the Martinhal lowland (Western Algarve – Portugal). In: A. Eurocoast-Portugal (Ed.), *Seminário sobre a Zona Costeira do Algarve*, Faro, Portugal: 11-18 pp.
- Andrade, C., Freitas, M.C., Moreno, J., Craveiro, S. (2004) - Stratigraphical evidence of Late Holocene barrier breaching and extreme storms in lagoonal sediments of Ria Formosa, Algarve, Portugal. *Marine Geology*, 210: 339– 362.
- Andrade, C., Cunha, P. P., Freitas, M. C., Dinis, J., Martins, A. A., Costa, P. J. M., Oliveira, M. A (2010a) - Revisiting the sedimentary record of a high-energy marine-inundation at Martinhal (Algarve, Portugal). 18th Sedimentological Congress. September 2010. Mendoza, Argentina.
- Andrade, C., Freitas, M.C., Lario, J., Zazo, C., Cabero, A., Vigliotti, L. (2010b) - Onshore sedimentological evidence of tsunami records. Deliverable D21 project report (Task 6.1, WP 6 - Paleotsunami and Paleoseismic records). Technical report, Project EU 037110 – NEAREST: Integrated observations from NEAR shore sources of Tsunamis: towards an early warning system, 72p. + 8 Annexes.
- Andrade, C., Taborda, R., Oliveira, M., Alves, M., Marapuço, M. (2013) - Caracterização do clima de agitação ao largo. Relatório não publicado, Entregável 1.1.7.a. do projecto CISML, APA I.P. http://sniamb.apambiente.pt/infos/geoportaldocs/PoliticAs/Agua/Ordenamento/SistemasMonitorizacaoLitoral/E_1.1.7.a_Clima_agitacao_largo.pdf.
- Andrade, C., Freitas, M.C., Oliveira, M.A., Costa, P.J.M. (2016) - On the sedimentological and historical evidences of seismic-triggered tsunamis on the Algarve coast of Portugal. *AGU Books, Plate boundaries and natural hazards*. American Geophysical Union & Wiley, 370 p. ISBN: 978-1-119-05397-2.

Canelas, R., Oliveira, M.A., Crespo, A., Neves, R., Costa, P., Freitas, M.C., Andrade, C., Ferreira, R. (2014) – Mathematical simulation of boulder dislodgement by high-energy marine flows in the western coast of Portugal. EGU-2014, Geophysical Research Abstracts, Vol. 16: 16081.

Carter, R. (1988) - Coastal Environments. Academic Press, London, 617 p.

Costa, M. (1994) – Agitação marítima na costa portuguesa. Anais do Instituto Hidrográfico 13: 35-40.

Costa, M., Silva, R., Vitorino, J. (2001) - Contribuição para o estudo do clima de agitação marítima na costa portuguesa. Actas, 2^{as} Jornadas Portuguesas de Engenharia Costeira e Portuária, AIPCN/PIANC.

Costa, A., Andrade, C., Seabra, C., Matias, L., Baptista, M.A., Nunes, S. (2005) - 1755: terramoto no Algarve. Centro Ciência Viva do Algarve, 237 p. ISBN 9729977801.

Costa, P. J. M. (2006) - Geological recognition of abrupt marine invasions in two coastal areas of Portugal. Department of Geography and Earth Sciences, Brunel University, London, United Kingdom. MSc thesis: 139 pp.

Costa, P. J. M., (2012) - Sedimentological signatures of extreme marine inundations. Departamento de Geologia, University of Lisbon, Portugal. PhD thesis: 245 pp.

Costa, P. J. M., Andrade, C., Freitas, M. C., Oliveira, M. A. and Jouanneau, J. M. (2009) - Preliminary Results of Exoscopic Analysis of Quartz Grains Deposited by a Palaeotsunami in Salgados Lowland (Algarve, Portugal). Journal of Coastal Research, 39-43. issn: 0749-0208.

Costa, J.M.C., Andrade, C., Freitas, M.C., Oliveira, M.A., da Silva, C.M., Omira, R., Taborda, R., Baptista, M.A., Dawson, A.G. (2011) - Boulder deposition during major tsunami events. Earth Surface Processes and Landforms, 36: 2054–2068. doi: 10.1002/esp.2228.

Costa, P. J. M., Andrade, C., Freitas, M.C., Oliveira, M.A., Lopes, V., Dawson, A.G., Moreno, J., Fatela, F., Jouanneau, J.M. (2012) – A tsunami record in the sedimentary archive of the central Algarve coast, Portugal: Characterizing sediment, reconstructing sources and inundation paths, The Holocene, 22(8): 899–914.

Costa, P.J. M., Andrade, C., Cascalho, J., Dawson, A. G., Freitas, M. C., Paris, R. and Dawson, S. - (2015) - Onshore tsunami sediment transport mechanisms inferred from heavy mineral assemblages. The Holocene, Volume 25, no. 5: 795-809. doi: 10.1177/0959683615569322

Costa, P.J.M., Oliveira, M. A., González-Villanueva, R., Andrade, C. and Freitas, M. C. (2016a) - Imprints of the AD 1755 Tsunami in Algarve (South Portugal) Lowlands and Post-impact Recovery. In: V. Santiago-Fandiño, H. Tanaka, M. Spiske (Eds.), Tsunamis and Earthquakes in Coastal Environments: Significance and Restoration. Springer International Publishing: 17-30. doi: 10.1007/978-3-319-28528-3_2

Costa, P.J. M., Costas, S., Oliveira, M.A., González-Villanueva, R., Roelvink, D., Andrade, C., Freitas, M.C., Cunha, P.P., Martins, A., Buylaert, J.P. and Murray, A. (2016b) - How did the AD

1755 tsunami impact on sand barriers across the southern coast of Portugal? *Geomorphology*, 268: 296-311 <http://dx.doi.org/10.1016/j.geomorph.2016.06.019>

Cunha, P. P., Andrade, C., Freitas, M. C., Dinis, J., Martins, A. A., Costa, P. J. M., Oliveira, M. A., Buylaert, J.-P., Murray, A. S. and Marques, S. (2015a) - Characterization of the sedimentary record of the AD1755 tsunami in the Martinhal Holocene succession (Algarve, Portugal). MIA2015. VIII Symposium on the Atlantic Iberian Margin. September 2015. Malaga, Spain.

Cunha, P., Martins, A., Cabral, J., Gouveia, M., Buylaert, J.-P., Murray, A. (2015b) - Staircases of wave-cut platforms in western central Portugal (Cape Mondego to Cape Espichel) – relevance as indicators of crustal uplift. *Proceedings, VIII Simposio El Margen Ibérico Atlántico (MIA15)*, Málaga: 137 -144.

Daveau, S., Almeida, G., Feio, M., Rebelo, F., Silva, E., Sobrinho, A. (1978) - Os temporais de Fevereiro / Março de 1978. *Finisterra*, 13 (26): 236-260.

Dawson, A. G., Hindson, R., Andrade, C., Freitas, M.C., Parish, R., Bateman, M. (1995) – Tsunami sedimentation associated with the Lisbon earthquake of 1 November AD 1755: Boca do Rio, Algarve, Portugal, *The Holocene*, 5(2) : 209–215.

Dinis, J., Costa, P., Henriques, V, Freitas, M.C., Andrade, C. (2006) – Natural to anthropogenic forcing in the Holocenic evolution of three coastal lagoons (Caldas da Rainha Valley, western Portugal). *Quaternary International*, 150: 41–51.

Dinis, J., Andrade, C., Oliveira, M.A., Freitas, M.C., Cunha, P., Martins A., Costa, P. (2010) - Geomorphological constraining of tsunami(?) run-up in the Alcantarilha lowland (central Algarve, Portugal). *Proceedings, Coastal Hope 2010*. Lisbon, Portugal, 14–17 June 2010: 40–41.

Diogo, Z., Lira, C., Bastos, A., Silva, A., Carapuço, M., Taborda, R., Andrade, C., Freitas, C., (2014) - Impactos das tempestades extra-tropicais do inverno de 2014 nas praias da APA, I.P. / ARH TEJO. Relatório técnico, 118 p.

Duarte, J.C., Rosas, F., Terrinha, P., Gutscher, M.-A., Malavieille, J., Silva, S., Matias, L. (2011) - Thrust–wrench interference tectonics in the Gulf of Cadiz (Africa–Iberia plate boundary in the North-East Atlantic): Insights from analog models. *Marine Geology*, 289: 135–149.

Duarte, D., Volochay, K., Magalhães, R., Amaro, S., Cabral, J. (2014) – Caracterização de terraços marinhos entre Cascais e o Cabo da Roca com recurso a elementos cartográficos e de detecção remota. Implicações neotectónicas. *Geonovas, Rev. Assoc. Portuguesa de Geólogos*, 27: 39-46.

Esaguy, A. (1984) - Ria de Faro - Barra da Armona - Evolução 1873-1983. Direcção Geral de Portos, Lisboa.

Esteves, R., Sansana Silva, F., Pinto, J., Costa, M. (2010) - Caracterização de eventos extremos de agitação marítima em Portugal Continental. *Actas, 1as Jornadas de Engenharia Hidrográfica*, 21-22 de Junho, Lisboa: 205-208.

Filipe, A., Carvalho, M., Capitão, R. (2000) - Extreme sea waves off Faro. *Proceedings, 3rd Symposium on the Atlantic Iberian Continental Margin, CIACOMAR*, Faro, Portugal: 105– 106.

Freitas, J.G., Dias, J.A. (2013) – 1941 windstorm effects on the Portuguese coast. What lessons for the future? *Journal of Coastal Research*, SI65: 714-719.

Freitas, M. C., Andrade, C., Rocha, F., Tassinari, C., Munhá, J.M., Cruces, A., Vidinha, J., Silva, C.M. (2003a) – Lateglacial and Holocene environmental changes in Portuguese coastal lagoons: 1. The sedimentological and geochemical records of the Santo André coastal area (SW Portugal), *The Holocene*, 13(3): 433–446.

Freitas, M. C., Andrade, C., Cruces, A. (2003b) - Middle/Late Holocene alluviation of SW Portuguese lagoons – causes, sediments and rates. *Coastal Sediments'03 – The fifth International Symposium on Coastal Engineering and Science of Coastal Sediment Processes*, 18–23 May, Clearwater Beach, FL., CD-ROM, 14 p.

Freitas, M. C., Andrade, C., Ramos, R., Cruces, A., Henriques, V. (2010) – Evolução paleoambiental da planície litoral a sul da Nazaré desde o Tardiglacial. Integração no modelo de evolução do litoral ocidental português. *Proceedings, Iberian Coastal Holocene Paleoenvironmental Evolution, Coastal Hope 2010*, 14–17 June 2010, Lisboa: 48–58.

Goff, J., Lane, E., Arnold, J. (2009) - The tsunami geomorphology of coastal dunes. *Nat. Hazards Earth Syst. Science*, 9: 847–854.

Hayes, M. (1975) - Morphology of sand accumulation in estuaries: an introduction to the symposium. In: Cronin, L. (ed.) *Estuarine Research* (vol. 1), Academic Press: 3-22.

Hayes, M. (1979) - Barrier island morphology as a function of tidal and wave regime. In: Leatherman, S. (Ed.), *Barrier Islands*. Academic Press, London: 1 –29.

Hesp, P. (1988) - Morphology, dynamics and internal stratification of some established foredunes in southeast Australia. *Sedimentary Geology*, 55: 17– 41.

Hindson, R.A., Andrade, C. (1999) - Sedimentation and hydrodynamic processes associated with the tsunami generated by the 1755 Lisbon earthquake. *Quaternary International*, 56(1): 27-38.

Hindson, R.A., Andrade, C., Dawson, A.G. (1996) - Sedimentary processes associated with the tsunami generated by the 1755 Lisbon earthquake on the Algarve coast, Portugal. *Physics and Chemistry of the Earth*, 21(1-2): 57-63.

Kortekaas, S. (2002) - Tsunamis, storms and earthquakes: distinguishing coastal flooding events. Ph.D. Thesis. Coventry University. 171 pp.

Kortekaas, S., Dawson, A.G. (2007) - Distinguishing tsunami and storm deposits: An example from Martinhal, SW Portugal. *Sedimentary Geology*, 200 (3-4): 208-221.

Kullberg, M.C., Kullberg, J. C. (2000) – Tectónica da região de Sintra. In: *Tectónica das regiões de Sintra e Arrábida*. Mem. Geociências, Museu Nacional de História Natural da Universidade de Lisboa, 2: 35-84.

Lopes, J.B.L.S. (1841) - *Corografia ou Memória Económica, Estatística e Topográfica do Reino do Algarve*, Lisboa.

Manupella, G. (1992) - Carta Geológica da Região do Algarve (1: 100 000) - Folha Ocidental. Instituto Geológico e Mineiro, Lisboa.

Matias, A. (2006) - Overwash sedimentary dynamics in the Ria Formosa barrier islands. PhD thesis, University of Algarve.

Matias, A., Vila-Concejo, A., Ferreira, O., Morris, B., Dias, J.A. (2009) - Sediment dynamics of barriers with frequent overwash. *Journal of Coastal Research*, 25 (3): 768 – 780.

Matias, L., Cunha, T., Annunziato, A., Baptista, M.A., Carrilho, F. (2013) - Tsunamigenic earthquakes in the Gulf of Cadiz: fault model and recurrence. *Nat. Hazards Earth Syst. Science*, 13: 1–13. doi:10.5194/nhess-13-1-2013.

Moreira, S., Costa, P.J.M., Andrade, C., Ponte Lira, C., Freitas, M.C., Oliveira, M.A., Reichart, G-J., (2017) - High resolution geochemical and grain-size analysis of the AD 1755 tsunami deposit: Insights into the inland extent and inundation phases. *Marine Geology*, 390: 94-105. ISSN 0025-3227, <http://dx.doi.org/10.1016/j.margeo.2017.04.007>.

Moura, D., Veiga-Pires, C., Albardeiro, L., Boski, T., Rodrigues, A.L., Tareco, H. (2007) - Holocene sea level fluctuations and coastal evolution in the central Algarve (southern Portugal). *Marine Geology*, 237: 127-142.

Neumeier, U., Ciavola, P., Evarchi, C., Cabaço, S., Santos, R., Ferreira, O. (2000) - Environmental controls on intertidal sedimentation in the Ria Formosa (Algarve): preliminary results. *Proceedings, 3rd Symposium on the Iberian Continental Margin*, Faro: 25– 26.

Oliveira, M. A., Andrade, C., Freitas, M.C. and Costa, P. J. M. (2009) - Modeling Volume Transfer between Beach-Foredune and the Backshore by the 1755 Lisbon Tsunami at Boca Do Rio Lowland, Algarve (Portugal). *Journal of Coastal Research*, SI 56: 1547-1551.

Oliveira, M.A. (2011) - Caracterização de depósitos da Arrábida e da plataforma costeira do Guincho. Unpublished advanced training course report. Faculdade de Ciências da Universidade de Lisboa, 77 p.

Oliveira, M.A. (2017) - Boulder deposits related to extreme marine events in the western coast of Portugal. Provisional PhD thesis submitted for evaluation, Faculdade de Ciências da Universidade de Lisboa, 369 p.

Oliveira, M.A., Andrade, C., Freitas, M.C., Costa, P., Taborda, R., Janardo, C., Neves, R. (2011) - Transport of large boulders quarried from shore platforms of the Portuguese west coast. *Journal of Coastal Research*, SI64: 1871-1875.

Pereira de Sousa, F.L. (1919) - O terremoto do 1 de Novembro de 1755 em Portugal: um estudo demográfico, I, II, III and IV. *Serviços Geológicos*, Lisbon.

Pereira, A., Angelucci, D. (2004) - Formações dunares no litoral português, do final do Plistocénico e inícios do Holocénico, como indicadores paleoclimáticos e paleogeográficos. In: Tavares, A., Ferro Tavares, A., Cardoso, J. (eds.) - *Evolução geohistórica do litoral português e*

fenómenos correlativos. *Geologia, História, Arqueologia e Climatologia*, Universidade Aberta, Lisboa: 220-256.

Pereira, A., Trindade, J., Araújo-Gomes, J., Leandro, A. (2016) - Vestígios do tsunami de 1755: um indicador negligenciado no litoral de Portugal continental? In: Lourenço, L. and Santos, A. (eds.), *Terramoto de Lisboa de 1755: o que aprendemos 260 anos depois?* Imprensa da Universidade de Coimbra, Coimbra: 297-316. ISBN: 978-989-26-1098-6.

Pessanha, L., Pires, H.O. (1981) - Elementos sobre o clima de agitação marítima na costa sul do Algarve. Unpublished technical report. Instituto Nacional de Meteorologia e Geofísica, Lisbon.

Pinto, C., Teixeira, S.B. (2002) - Morphodynamics of the sandy barrier of Salgados coastal lagoon, Armação de Pêra Bay (Algarve - Portugal). In: E. Portugal (Ed.), *Eurocoast Littoral 2002, The Changing Coast*. Eurocoast/EUCC, Porto: 403-409 pp..

Prudêncio, I. Marques, R., Rebelo, L., Cook, G., Cardoso, G., Naysmith, P., Freeman, S., Franco, D., Brito, P., Dias, M. (2007) - Radiocarbon and Blue Optically Stimulated Luminescence chronologies of the Oitavos consolidated dune (Western Portugal). *Radiocarbon*, 49 (2): 1145-1151.

Quintela, M., Costa, P.J.M., Fatela, F., Drago, T., Hoska, N., Andrade, C., Freitas, M.C. (2016) - The AD 1755 tsunami deposits onshore and offshore of Algarve (south Portugal): Sediment transport interpretations based on the study of Foraminifera assemblages. *Quaternary International*, 408, Part A: 123-138.

Ramalho, M., Rey, J., Zbyszewski, G., Matos Alves, C., Palácios, T., Moitinho de Almeida, F., Costa, C., Kullberg, C. (2001) – Carta Geológica e Notícia Explicativa da Folha 34-C (Cascais) na escala 1: 50000. Instituto Geológico e Mineiro, Lisboa.

Rebêlo, L., Brito, P., Monteiro, J. (2002) - Monitoring the Cresmina dune evolution (Portugal) using differential GPS. *Journal of Coastal Research*, SI 36: 591-604.

Rey, J. (2007) - Stratigraphie séquentielle et séquences de dépôt dans le Crétacé inférieur du Bassin Lusitanien. *Ciências da Terra*, Vol. Esp. VI, Universidade Nova de Lisboa, Lisboa, 120p.

Rey, J., Gracinsky, P., Jacquin, T. (2003) - Les sequences de depot dans le Crétacé inférieur du Bassin Lusitanien. *Comunicações do Instituto Geológico e Mineiro*, Lisboa, 90: 15-42.

Rey, J., Caetano, P., Callapez, P., Dinis, J. (2009) – Le Crétacé du Bassin Lusitanien (Portugal). *Excursion du Groupe Français du Crétacé*, 100 p., <https://hal.archives-ouvertes.fr/hal-00452152>.

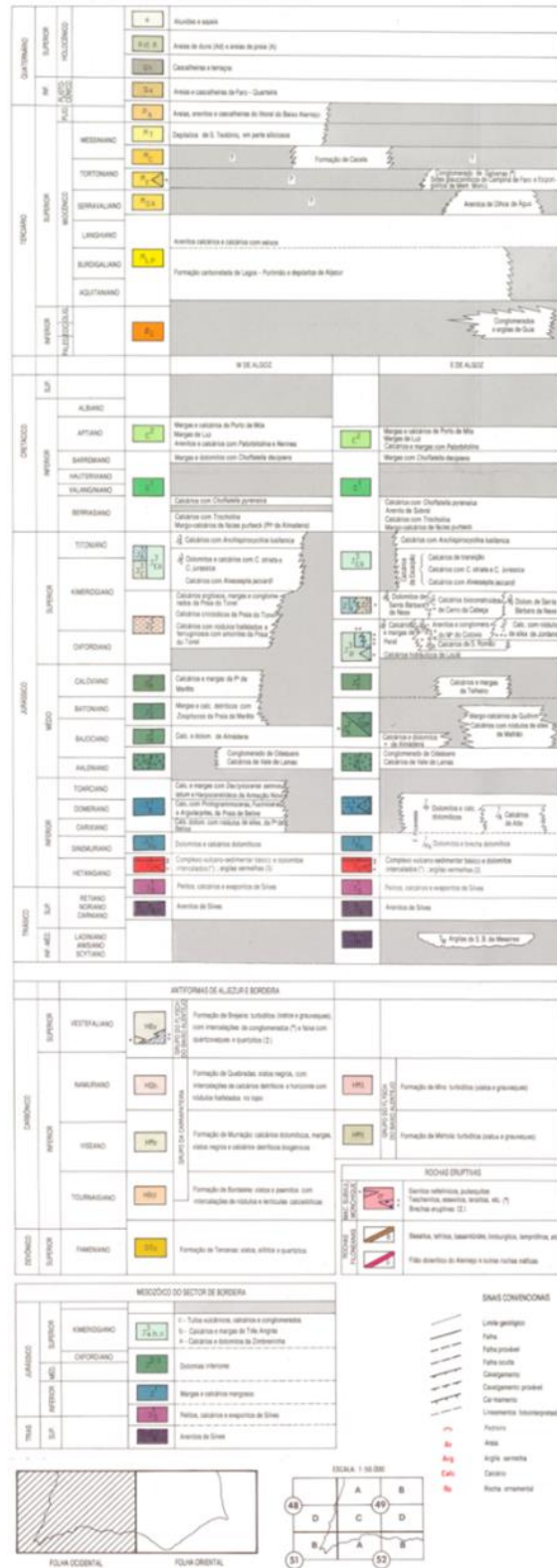
Ribeiro, M., Taborda, R., Rodrigues, A., Silveira, T. (2014) - Insights on sediment bypassing at headland-bay beaches: an example at the Portuguese west coast. *Proceedings, 3 Jornadas de Engenharia Hidrográfica*, Lisboa: 301-304.

Santos, M. (2006) – Caracterização e quantificação do transporte sólido eólico na duna da Cresmina. *Relatório de Estágio, Curso de Especialização Pós-graduada em Geologia Aplicada*, Departamento de Geologia, Faculdade de Ciências da Universidade de Lisboa, 55 p.

Scheffers, A., Kelletat, D. (2005) - Tsunami relics on the coastal landscape west of Lisbon, Portugal. *Science of Tsunami Hazards*, 23 (1): 3-16.

- Schneider, H., Höfer, D., Trog, C., Busch, S., Schneider, M., Baade, J., Daut, G. Mäusbacher, R. (2010) - Holocene estuary development in the Algarve Region (Southern Portugal) - A reconstruction of sedimentological and ecological evolution. *Quaternary International*, 221 (1-2): 141-158.
- Siddall, M., Chappell, J., Potter, E.-K. (2006) - Eustatic sea level during past Interglacials. In: Sirocko, F., Claussen, M., Litt, T., Sanchez-Goni, M. (eds.) - *The Climate of Past Interglacials*, vol. 7. *Developments in Quaternary Science*, Elsevier Science: 75-92. ISBN: 9780080468068.
- Soares, A., Moniz, C., Cabral, J. (2006) - A duna consolidada de Oitavos, a Oeste de Cascais, região de Lisboa : a sua datação pelo método do radiocarbono. *Comunicações Geológicas* 93, Laboratório Nacional de Engenharia e Geologia: 105-118. <http://hdl.handle.net/10400.9/886>
- Taborda, R., Dias, J. (1992) - Análise da sobrelevação do nível do mar de origem meteorológica durante os temporais de Fevereiro/Março de 1978 e Dezembro de 1981. *Geonovas* 1: 89-97.
- Taborda, R., Andrade, C., Marques, F., Freitas, M.C., Rodrigues, R., Antunes, C., Pólvora, C. (2010) - Plano estratégico do concelho de Cascais face às alterações climáticas. Relatório técnico não publicado, CeGUL, LATTEX, DEGGE, FCUL – C. M. Cascais.
- Teixeira, S.B., Gaspar, P., Rosa, M. (2005) - Holocene sea-level index points on the Quarteira coast (Algarve, Portugal). *Proceedings Coastal Hope 2005*, 24-29 July, Lisbon, Portugal,: 125-128.
- Trog, C., Höfer, D., Frenzel, P., Camacho, S., Schneider, H., Mäusbacher, R. (2013) - A multi-proxy reconstruction and comparison of Holocene palaeoenvironmental changes in the Alvor and Alcantarilha estuaries (southern Portugal). *Revue de Micropaleontologie*, 56: 131-158.
- Trog, C., Hempel, R., Frenzel, P., Mäusbacher, R. (2015) - Holocene palaeoenvironmental changes in three lagoons on the Algarve coast of Portugal. *Paleobio. Palaeoenv.* DOI: 10.1007/s12549-015-0185-0
- Weinholtz, M. (1964) - O cordão litoral da Ria de Faro e a sua utilização para fins turísticos e balneares-contribuição para o conhecimento da evolução das flechas de areia na costa sotavento do Algarve. *Boletim Trimestral de Informação, Direcção Geral dos Serviços Hidráulicos* 14, 46 p.
- Vis, G.-J., Kasse, C., Vanderberghe, J. (2008) - Late Pleistocene and Holocene paleogeography of the Lower Tagus valley (Portugal): effects of relative sea-level, valley morphology and sediment supply, *Quaternary Science Reviews*, 27(17–18): 1682–1709.
- Zbyszewski, G., Moitinho de Almeida, F., Torre de Assunção, C. (1955) – Notícia explicativa da Folha 30 – C (Torres Vedras) da Carta Geológica de Portugal na escala de 1: 50000. *Serviços Geológicos de Portugal*, Lisboa.

Annex 1 - Lithostratigraphy of the windward sector of the Algarve





5TH INTERNATIONAL TSUNAMI FIELD SYMPOSIUM

PARTNERS AND SPONSORS:

U

LISBOA

UNIVERSIDADE
DE LISBOA



Ciências
ULisboa



INSTITUTO
DOM LUIZ



Centro de Informação
geoespacial
do Exército



Município
Vila do
Bispo

CASCAIS



desde 1840
abreu®

ISBN 978-989-20-7817-5



9 789892 078175